

Spring 2006

Development of a high spatial selectivity tri-polar concentric ring electrode for Laplacian electroencephalography (LEEG) system

Kanthaiah Koka
Louisiana Tech University

Follow this and additional works at: <https://digitalcommons.latech.edu/dissertations>

 Part of the [Biological and Chemical Physics Commons](#), [Biophysics Commons](#), and the [Other Physics Commons](#)

Recommended Citation

Koka, Kanthaiah, "" (2006). *Dissertation*. 562.
<https://digitalcommons.latech.edu/dissertations/562>

This Dissertation is brought to you for free and open access by the Graduate School at Louisiana Tech Digital Commons. It has been accepted for inclusion in Doctoral Dissertations by an authorized administrator of Louisiana Tech Digital Commons. For more information, please contact digitalcommons@latech.edu.

**DEVELOPMENT OF A HIGH SPATIAL SELECTIVITY TRI-POLAR
CONCENTRIC RING ELECTRODE FOR LAPLACIAN
ELECTROENCEPHALOGRAPHY (LEEG) SYSTEM**

by

Kanthaiah Koka, B.E.

A Dissertation Presented in Partial Fulfillment
of the Requirements for the Degree
Doctor of Philosophy

COLLEGE OF ENGINEERING AND SCIENCE
LOUISIANA TECH UNIVERSITY

May 2006

UMI Number: 3218988

INFORMATION TO USERS

The quality of this reproduction is dependent upon the quality of the copy submitted. Broken or indistinct print, colored or poor quality illustrations and photographs, print bleed-through, substandard margins, and improper alignment can adversely affect reproduction.

In the unlikely event that the author did not send a complete manuscript and there are missing pages, these will be noted. Also, if unauthorized copyright material had to be removed, a note will indicate the deletion.

UMI[®]

UMI Microform 3218988

Copyright 2007 by ProQuest Information and Learning Company.

All rights reserved. This microform edition is protected against unauthorized copying under Title 17, United States Code.

ProQuest Information and Learning Company
300 North Zeeb Road
P.O. Box 1346
Ann Arbor, MI 48106-1346

LOUISIANA TECH UNIVERSITY

THE GRADUATE SCHOOL

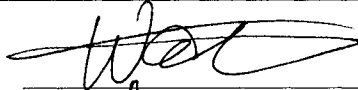
4-12-2006

Date

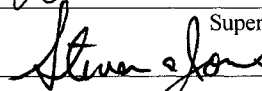
We hereby recommend that the dissertation prepared under our supervision by KANTHAIK KOKA

entitled DEVELOPMENT OF A HIGH SPATIAL SELECTIVITY TRI-POLAR CONCENTRIC RING ELECTRODES FOR LAPLACIAN ELECTROENCEPHALOGRAPHY (LEEG) SYSTEM

be accepted in partial fulfillment of the requirements for the Degree of DOCTOR OF PHILOSOPHY IN BIOMEDICAL ENGINEERING



Supervisor of Dissertation Research

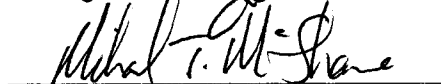


Head of Department

Biomedical Engineering

Department

Recommendation concurred in:



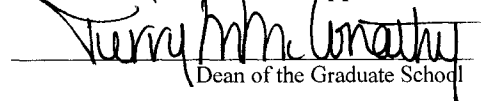
Advisory Committee

Approved:



Director of Graduate Studies

Approved:



Dean of the Graduate School



Dean of the College

ABSTRACT

Brain activity generates electrical potentials that are spatio-temporal in nature. Electroencephalography (EEG) is the least costly and most widely used non-invasive technique for diagnosing many brain problems. It has high temporal resolution but lacks high spatial resolution.

The surface Laplacian will enhance the spatial resolution of EEG as it performs the second spatial derivative of the surface potentials. In an attempt to increase the spatial selectivity, researchers introduced a bipolar electrode configuration using a five-point finite difference method (FPM) and others applied a quasi-bipolar (tri-polar with two elements shorted) concentric electrode configuration. To further increase the spatial resolution, the nine-point finite difference method (NPM) was generalized to tri-polar concentric ring electrodes.

A computer model was developed to evaluate and compare the properties of concentric bipolar, quasi-bipolar, and tri-polar electrode configurations, and the results were verified with tank experiments. The tri-polar configuration was found to have significantly improved spatial localization.

Movement-related potential (MRP) signals were recorded from the left pre-frontal lobes on the scalp of human subjects while they performed fast repetitive movements. Disc, bipolar, quasi-bipolar, and tri-polar electrodes were used. MRP signals were

plotted for all four electrode configurations. The SNR of four electrode configurations were studied and statistically analyzed using Bonferroni statistical tests.

MRP signals were recorded from an array of 5X7 on the left hemisphere of the head. The SNR, spatial selectivity, and mutual information (MI) were compared among conventional disc electrodes, bipolar and tri-polar concentric ring electrodes. The tri-polar concentric electrodes showed more significant improvement in SNR than the all other electrode systems tested. Tri-polar concentric electrodes also had significantly higher spatial selectivity and spatial attenuation for global signals. The increased spatial selectivity significantly decreased the MI in between different channels which will be useful in different BCI system.

The tri-polar and bipolar concentric ring electrode configuration was also shown to be appropriate for recording seizure electrographic activity. This higher spatial selectivity of tri-polar concentric electrodes may be useful for seizure foci detection and seizure stage determination.

APPROVAL FOR SCHOLARLY DISSEMINATION

The author grants to the Prescott Memorial Library of Louisiana Tech University the right to reproduce, by appropriate methods, upon request, any or all portions of this Dissertation. It is understood that "proper request" consists of the agreement, on the part of the requesting party, that said reproduction is for his personal use and that subsequent reproduction will not occur without written approval of the author of this Dissertation. Further, any portions of the Dissertation used in books, papers, and other works must be appropriately referenced to this Dissertation.

Finally, the author of this Dissertation reserves the right to publish freely, in the literature, at any time, any or all portions of this Dissertation.

Author Karsten K.

Date 5/5/06

DEDICATION

I would like to dedicate this dissertation to my parents Papaiah Koka and Venktravamma Koka for their support and patience during all my research. And also extend thanks to all my other family members.

TABLE OF CONTENTS

ABSTRACT.....	iii
LIST OF TABLES.....	ix
LIST OF FIGURES.....	x
ACKNOWLEDGMENTS.....	xv
CHAPTER 1. INTRODUCTION.....	1
CHAPTER 2. BACKGROUND THEORY.....	6
2.1 Finite Difference Five-Point-Method (FPM).....	7
2.2 Bipolar Electrode Method.....	8
2.3 Quasi-Bipolar Electrode Method.....	10
2.4 Nine-Point-Method (NPM).....	11
2.5 Applying NPM to the Tri-polar Electrode.....	12
CHAPTER 3. METHODS.....	15
3.1 Computer Models.....	15
3.1.1 Single Source Computer Model.....	15
3.1.2 Multiple Source Computer Model.....	17
3.2 Tank Experiments.....	19
3.3 Analyzing the Variation of Alpha Rhythms from Human LEEG.....	22
3.4 Movement-Related Potentials (MRP) from Fp1.....	25
3.5 Multi-Channel MRP Recording.....	30
3.5.1 MRP Recording with Conventional Disc Electrodes.....	31
3.5.2 MRP Recording with Concentric Ring Electrodes.....	32
3.5.3 Pre-processing of Multi-Channel MRP Recordings.....	33
3.5.4 Comparison of SNR.....	34
3.5.5 Comparison of Spatial Selectivity.....	34
3.5.6 Comparison of Mutual Information (MI).....	35
3.6 Animal Models for Seizure LEEG Recordings.....	37
3.6.1 Penicillin-G Model.....	37
3.6.2 Pilocarpine Seizure Model.....	39
3.6.2.1 Pilocarpine Protocol 1.....	39
3.6.2.2 Pilocarpine Protocol 2.....	41
3.7 Statistical Analysis.....	42
3.7.1 ANOVA.....	42

3.7.2 Bonferroni Statistical Test	43
CHAPTER 4. RESULTS	44
4.1 Calculation of Laplacian Potentials Using Computer Model.....	44
4.1.1 Calculation of Laplacian Potential for Single Source Computer Model	44
4.1.2 Calculation of Laplacian Potential for Multiple Source Computer Model	49
4.2 Tank Experimental Results	50
4.3 Verification of Single Source Computer Model with Tank Experiments.....	53
4.4 Human EEG Recording Using Tri-polar Laplacian Electrode.....	55
4.5 Recording of Movement-Related Potentials from Pre-frontal Lobes	56
4.6 Development of Laplacian EEG Amplifier System.....	62
4.6.1 Development of Two-Channel Pre-Amplifier System	62
4.6.2 Development of Three-Channel Amplifier System	65
4.6.3 Development of 15-channel LEEG System.....	68
4.7 Comparison of SNR of Multi-Channel MRP Recordings.....	75
4.8 Comparison of Spatial Selectivity.....	76
4.9 Comparison of Mutual Information	79
4.10 Seizure Recordings Using the Tri-polar Electrode	80
4.10.1 Penicillin-G Seizure Model.....	80
4.10.2 Pilocarpine Seizure Model.....	85
CHAPTER 5. DISCUSSION.....	91
CHAPTER 6. CONCLUSIONS	95
CHAPTER 7. FUTURE WORK	96
APPENDIX A.....	97
APPENDIX B	102
APPENDIX C	104
APPENDIX D	105
APPENDIX E	108
APPENDIX F.....	117
REFERENCES	118

LIST OF TABLES

Table 1 SNR for different electrodes at FP1 location.....	61
Table 2 SNR for Multi-channel MRP signals at location CZ.....	76
Table 3 Peak ratios of MRP signals for comparing spatial selectivity	79
Table 4 Mutual information values for three electrode systems.....	79

LIST OF FIGURES

Figure 1	Arrangement of FPM on a regular plane square grid.....	7
Figure 2	Bipolar concentric ring electrode.....	9
Figure 3	Quasi-bipolar concentric ring electrode.....	11
Figure 4	Nine-point arrangement for the NPM on a regular square grid.....	12
Figure 5	Tri-polar concentric ring electrode.....	13
Figure 6	Moving dipole computer simulation.....	15
Figure 7	Arrangement of random dipole computer simulation.....	19
Figure 8	Double inverter circuit for generating the dipole.....	20
Figure 9	Tank experimental setup.....	21
Figure 10	Typical EEG rhythms seen in healthy human EEG data.....	23
Figure 11	Placement of tri-polar concentric ring electrode for recording LEEG signals for analyzing alpha rhythm.....	24
Figure 12	Different areas of the brain.....	26
Figure 13	Custom made tri-polar concentric ring electrode.....	27
Figure 14	Conventional disc electrodes used for MRP signals.....	27
Figure 15	Position of electrode for recording MRP from pre-frontal area FP1 of the brain.....	28
Figure 16	Pre-amplifier used for recording movement-related potentials.....	28
Figure 17	The block diagram of the system used for recording the MRP signals.....	29
Figure 18	The position of electrodes for recording MRP signals.....	32

Figure 19 Custom arrangement of seven tri-polar electrodes with 1 cm spacing for recording MRP signals.	33
Figure 20 Typical electrode positions for recording LEEG during penicillin-G seizure model.....	39
Figure 21 Position of tri-polar electrodes on the rat head for pilocarpine seizure model.....	40
Figure 22 Laplacian potentials for bipolar concentric ring electrode.	45
Figure 23 Laplacian potentials for quasi-bipolar electrode.	45
Figure 24 Laplacian potentials for tri-polar electrode configuration.....	46
Figure 25 The Laplacian potentials for single unit dipole source computer model for 2 cm outer ring diameter electrode.	47
Figure 26 Attenuation of Laplacian signals for three electrode configurations from single unit dipole source computer model.....	47
Figure 27 Attenuation of Laplacian signals for three electrode configurations and conventional disc electrodes from single unit dipole source computer model.....	48
Figure 28 Normalized Laplacian potentials calculated from single constant unit dipole source and multiple random unit dipole source computer model.	49
Figure 29 Attenuation values for single constant unit dipole and multiple random unit dipole source computer model.	50
Figure 30 A typical recording from the three elements of tri-polar concentric electrodes during tank experiments.....	51
Figure 31 The voltages from each element of tri-polar concentric ring electrode. V _{disc} -potential on the disc, V _m ring-potential on middle ring, and V _o ring-potential on outer ring.....	51
Figure 32 Laplacian potentials recording during tank experiments for a 2.0 cm diameter (A) bipolar, (B) quasi-bipolar, and (C) tri-polar electrode configurations.....	52
Figure 33 Attenuation in dB calculated from tank experimental data for the three electrode configurations of a 2.0 cm diameter electrode due to radial distance from the center of the electrode.	52

Figure 34 Comparison of tank experimental results (measured) with computer simulation (simulated) of a single unit dipole source computer model.	54
Figure 35 Comparison of attenuation for three electrode configurations, quasi-bipolar, bipolar, and tri-polar electrode.....	54
Figure 36 Laplacian EEG recording from humans to verify the alpha rhythms with eyes closed position. (A) LEEG signal (B) Alpha rhythm (C) Beta rhythm (D) Delta rhythm and (E) Theta rhythm.	55
Figure 37 MRP signals recorded using conventional disc electrodes (B) and micro-switch state (A).....	56
Figure 38 MRP signals recorded using concentric ring electrodes. Trace (B) outer ring-disc, trace (C) middle ring-disc and trace (A) is reference from micro-switch.....	57
Figure 39 MRP signals recorded from conventional disc electrodes from the FP1 location.....	58
Figure 40 MRP signals recorded from bipolar concentric electrodes from the FP1 location.....	59
Figure 41 MRP signals recorded from quasi-bipolar concentric ring electrodes from the FP1 location.....	59
Figure 42 MRP signals recorded from tri-polar concentric ring electrodes from the FP1 location.....	60
Figure 43 MRP recordings using (A) conventional disc EEG electrodes, (B) bipolar concentric ring electrode, (C) quasi-bipolar concentric ring electrode, and (D) tri-polar concentric ring electrode.....	60
Figure 44 Two-channel pre-amplifier system.....	63
Figure 45 Regulated power supply using Max 664 and Max 663.	63
Figure 46 Three-channel pre-amplifier circuit drawn in Orcad Capture.	64
Figure 47 Three-channel pre-amplifier system used for recording LEEG from seizing animals.	65
Figure 48 Single channel LEEG system with Sallen-Key and MFB topology.....	66
Figure 49 Block diagram of three-channel amplifier system.....	67

Figure 50 Three-channel amplifier system built on the breadboard.	67
Figure 51 Block diagram of 15-channel amp board.	69
Figure 52 15-channel amp board circuit from Orcad Capture.	70
Figure 53 Front side of the 15-channel amp board.	71
Figure 54 Back side of the 15-channel amp board.	71
Figure 55 15-channel amp board with all the components.	71
Figure 56 Notch-Isolation board with only power supply and with out any components.	73
Figure 57 Notch-Isolation board with all the surface mount components.	73
Figure 58 Regulated power supply circuit used for 15-channel LEEG system.	74
Figure 59 The 15-channel LEEG amplifier system with custom-made seven electrode strap and DB37 cable to connect to the data acquisition system.	74
Figure 60 MRP signals recorded from the same subject at CZ location using three different electrode configurations. Positive peak was marked at 150 ms after rising edge of micro switch.	75
Figure 61 2-D map for the MRP signals recorded from conventional disc electrodes placed on the left hemisphere of the head for multi-channel MRP recordings.	76
Figure 62 2-D map of MRP signals recorded for bipolar electrode configuration from multi-channel MRP recordings.	77
Figure 63 2-D map of MRP signals recorded for bipolar electrode configuration from multi-channel MRP recordings.	78
Figure 64 A typical baseline LEEG recording taken during a rat experiment.	80
Figure 65 Tri-polar concentric electrode configuration LEEG during baseline recording.	81
Figure 66 Frequency spectrum of a typical rat LEEG signals taken during baseline recording for tri-polar concentric electrode configuration.	81
Figure 67 The LEEG signals recording during the seizure.	82

Figure 68 Spike and sharp wave activity during seizures with tri-polar electrode configuration.	83
Figure 69 Frequency spectrum of the spike and sharp wave activity during penicillin seizure model.....	83
Figure 70 Spike and sharp waves recorded from a penicillin seizure model animal experiment. Panel (A) conventional disc, Panel (B) bipolar concentric electrode, and (C) tri-polar concentric electrode.....	84
Figure 71 Baseline recording taken during the pilocarpine seizure experiments for rat3.	87
Figure 72 Onset of SE during the pilocarpine seizure experiments for rat3.....	87
Figure 73 Discrete seizures observed during pilocarpine seizure experiments for rat3. ..	87
Figure 74 Waxing-waning observed during pilocarpine seizure experiments for rat3.....	88
Figure 75 Continuous spiking activity observed during the pilocarpine seizure experiments for rat3.	88
Figure 76 Periodic epileptic discharges observed during the pilocarpine seizure experiments for rat3.	88
Figure 77 Percentage of rats showing different stages of pilocarpine induced seizures with Protocol 2 after the onset of SE.....	89
Figure 78 Spike and slow wave activity observed during pilocarpine seizure model.	90
Figure 79 Different stages of NREM sleep along with signals during awake.....	102
Figure 80 REM sleep stage signals along with EOG signals.....	103
Figure 81 Spike and sharp wave seen during seizure activity.	105
Figure 82 EEG signals showing spike waveforms.	105
Figure 83 Spike and slow wave form of seizure signals.....	106
Figure 84 Primary generalized seizures. 3 Hz spike and wave activity can be seen in all the channels.....	107
Figure 85 Focal sharp waves in the right anterior temporal lobes. The sharp activity is shown with arrow marks.....	107

ACKNOWLEDGMENTS

I am deeply indebted to my advisor Dr Walter Besio whose guidance and suggestions helped me for the duration of my research and pushed me ever so much to work harder and harder. He has been a constant source of encouragement and support all the way through.

I would like next to thank all my advisory committee members, Dr. McShane, Dr. Steven Jones, Dr. Weizhong Dai and Dr. Ravish Patwardhan for all their generous instructions and help during my research. In addition, I would like to thank Dr. Aijun Besio for helping in understanding the statistical terms used and statistical analysis of the data presented in my research. I also extend thanks to Dr. Mesut Sahin for his help and providing his lab equipment for doing the animal experiments and to thank Dr. James Spaulding for his help and instructions for handling the animals during animal experiments. I would like to thank all the members of my lab and supporting staff at CyBERS for their help.

Finally, I thank all those either directly or indirectly associated with me in bringing this dissertation to its logical end.

CHAPTER 1

INTRODUCTION

To the best of my knowledge Hans Berger recorded the first human Electroencephalograph (EEG) from a human scalp in 1924. Brain activity is a spatio-temporal phenomenon. It is distributed throughout the brain at different times while a command is being processed. Ions are associated with this activity, and their flow creates electrical activity that can be detected on the scalp surface with EEG equipment. Currently, EEG still is one of the most important non-invasive methods for investigation of neural activity of the brain [1]. Among the different methods used for recording brain activity, EEG is the cheapest and produces sufficient temporal resolution to enhance study of complex functioning of the brain.

Despite the development of other non-invasive brain imaging techniques, EEG is unsurpassed in terms of temporal resolution. Both functional magnetic resonance imaging (fMRI) and positron emission tomography (PET) have low temporal resolution taking hundreds of milliseconds to acquire necessary signals to form images. EEG and magneto encephalography (MEG) systems are much faster and take only tens of milliseconds. However, MEG is insensitive to deep or radial sources. According to Srinivasan [1], since the skull is such a poor conductor, current flow in the skull will mostly be radial, flowing from the inner to outer surface of the skull. This being the case, any magnetic system that detects tangential sources such as MEG will have problems

resolving sources in the brain. In addition, fMRI, PET and MEG are all costly and not portable for use every where.

Much advancement has come recently in the field of EEG, making it even more appealing for brain activity analysis. One such advancement is the application of the surface Laplacian to EEG. Surface Laplacian mapping has been shown to enhance the high spatial frequency components and spatial selectivity to the regional bioelectrical activity located close to the observation point [2-3]. These unique characteristics are based on the surface Laplacian being the second spatial derivative of the potential.

The application of Laplacian to EEG started with Hjorth [4] utilizing a five-point difference method (FPM). Many other approaches have revealed positive results as well, estimating the scalp Laplacian from the potential EEG measurements. Such approaches include the spline Laplacian algorithm by Perrin [5], and ellipsoidal spline Laplacian algorithm by Law [6] and realistic Laplacian estimation techniques by Babiloni *et al.* [7-8] and realistic geometry Laplacian algorithms [9]. Bin He [2-3] calculates the surface Laplacian with Hjorth's technique from an array of five disc electrodes measuring surface potentials, but these discs accept global signals and may be directionally dependent as suggested by Geselowitz and Ferrara [10].

Discussed above are the existing techniques for improving the spatial resolution of EEG without making assumptions about the quantity or distribution of the sources in the brain. However, all of them depend on post-processing. EEG electrode recordings are frequently contaminated with artefact such as electromyography (EMG) from eye movement; and the EEG signals are exposed to external interference such as A/C lines

prior to amplification. There is a need for a system with higher global signal rejection, localization, and improved signal to noise ratio.

The concept of mutual information (MI) was introduced by Shannon [11] and is a method of identifying advanced correlations in non-linear relationships. Many researchers have proposed MI as a test of independence between observed experimental variables. Information theory is playing an expanding role in interpreting data and in understanding the principles of representation and computation in the nervous system. MI is a measure of statistical dependence. The amount of useful or independent information gathered from EEG signals typically depends on the number of electrodes and the degree of MI or dependence between each electrode. The amount of information is the pooling of information from each channel, and Pooling of independent signals from individual sources can provide more reliable information than a single source [12-13].

Conventional disc electrodes have more MI between channels and therefore are more interdependent upon others and also seem to be more correlated. The MI between each electrode causes the total amount of information from the pooling of information to be less. The amount of information does not increase much when another electrode is added since the information is common to other electrodes. The total information depends on the number of electrodes used for recording and for more information we need to increase the number of electrodes. The number of electrodes is critical in many cases for recording EEG signals. Increasing the number of electrodes increases the number of channels, cost and complexity of the system. This is a considerable limitation of using the conventional disc electrodes for recording brainwaves. An increase in spatial

selectivity will decrease the MI and increase the total information content with less number of electrodes.

Another important aspect to consider in system design is noise-causes/sources, control, and susceptibility of the system. Conventional electrode systems commercially available for recording EEG have high input noise with inputs referenced to ground. The signals recorded with conventional EEG electrodes have higher amplitudes in the ranges of micro volts because they have higher surface area and greater distance separating them on the scalp relative to other electrode options. Tri-polar electrodes have smaller surface contact areas and the signals recorded range less than $0.1 \mu\text{V}$. The signal-to-noise ratio and input noise characteristics of the amplifier system must be more sensitive than conventional EEG amplifiers to record with tri-polar electrodes.

The main objective of this dissertation is to develop a unique, non-directional, surface Laplacian electrode and Laplacian EEG system which will improve the accuracy of the surface Laplacian by enhancing source localization and decreasing MI between electrodes in a recording system. This system should ensure more noise immunity than conventional systems.

The proposed tri-polar LEEG system will have a multi-channel amplifier system designed with lower input noise characteristics, high input impedance, higher common mode rejection ratio (CMRR) and higher signal-to-noise than the conventional amplifier systems available commercially for EEG. According to Bradshaw and Wikswo [14], if the signal-to-noise ratio is kept about the same as that of raw EEG, then a significant improvement in spatial resolution can be expected over other electrode systems. Besio [15-18] achieved an average signal-to-noise ratio of nearly 11 in his Laplacian ECG

work. Concentric ring electrodes automatically reject global signals, the outer ring acts like a guard for other electrode elements. The concentric ring electrodes can resolve the reference electrode problems as discussed by Nunez [6] and since concentric ring electrodes act like closely spaced bipolar recordings. Concentric ring electrodes are symmetrical [19] and alleviate electrode orientation problems as discussed by Geselowitz and Ferrara. They also act as spatial filters reducing the low spatial frequencies and increasing the spatial selectivity [19]. Due to this extremely localized sensing concentric electrodes automatically have an advantage in source localization which is useful for multiple clinical applications such as seizure localization, mapping motor activity, classification and independency of the signals recorded from each individual electrode. By directly obtaining the surface Laplacian it is possible to generate updated Laplacian EEG surface maps every few milliseconds, where an fMRI system needs several hundred milliseconds.

These substantial improvements in spatial selectivity and decrease in mutual information in between each channel make tri-polar concentric electrodes advantageous for acquiring EEG.

CHAPTER 2

BACKGROUND THEORY

The potentials on the scalp surface required for localization are prone to volume conductor smearing effects. The Laplacian of surface potentials reduces this smearing effect. Hjorth [4] used the FPM to calculate the surface Laplacian for EEG signals. Hjorth states that the equation for the source voltage in terms of the Laplacian operator is

$$V_{source} = i_{xy} \bullet r = -\left(\frac{\partial^2}{\partial x^2} + \frac{\partial^2}{\partial y^2}\right)V_{xy} \quad (2.1)$$

where V_{source} is the source voltage, i_{xy} is the orthogonal current entering the surface, V_{xy} is the potential on the surface and r is a constant having the dimension of resistance and being related to the conductivity of the actual medium.

Bin He [2-3] stated that “Although the Laplace operator in its general form is based on knowledge of the continuous potential distributor, it can also be represented by a central difference operator, based on a limited number of samples” [4]. Five surface electrodes were used in the arrangement as shown in Figure 1 to approximate the Laplacian operator. The second derivative terms are approximated using finite differences.

$$V_{source} \cong (V_0 - V_1) + (V_0 - V_2) + (V_0 - V_3) + (V_0 - V_4) \quad (2.2)$$

2.1 Finite Difference Five-Point-Method (FPM)

The electrodes for finite five-point-method (FPM) are shown in Figure 1. The potentials v_0 through v_4 correspond to the five points' p_0 through p_4 . Spacing between these points is r . The potentials at all these points can be expanded with Taylor's Series [20-21].

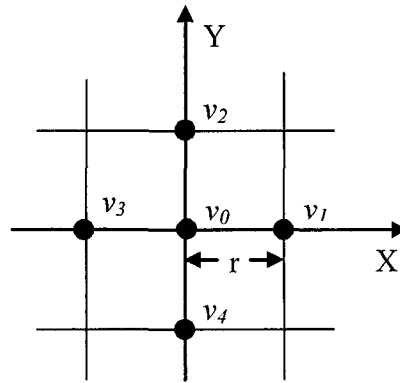


Figure 1 Arrangement of FPM on a regular plane square grid.

Expanding potential v_1 in Taylor's series along X coordinates

$$v_1 = v(r, 0) = v(0, 0) + r \frac{\partial v}{\partial x} \Big|_{p_0} + \frac{1}{2!} r^2 \frac{\partial^2 v}{\partial x^2} \Big|_{p_0} + \frac{1}{3!} r^3 \frac{\partial^3 v}{\partial x^3} \Big|_{p_0} + \dots \quad (2.3)$$

Expanding potentials v_2 , v_3 , and v_4 using Taylor's series and adding them together results in Equation (2.4).

$$v_1 + v_2 + v_3 + v_4 = 4v_0 + r^2 \left(\frac{\partial^2 v}{\partial x^2} + \frac{\partial^2 v}{\partial y^2} \right) \Big|_{p_0} + \dots \quad (2.4)$$

From Equation (2.4) the solution of the second derivative terms of the potential at p_0 , the Laplacian of potential v_0 is given by

$$\left(\frac{\partial^2 v}{\partial x^2} + \frac{\partial^2 v}{\partial y^2} \right) \Big|_{p_0} = \Delta v \Big|_{p_0} = \Delta v_0 = \frac{1}{r^2} \left(\sum_{i=1}^4 v_i - 4v_0 \right) + O(r^2) \quad (2.5)$$

where Δ represents the Laplacian operator $\left(\frac{\partial^2}{\partial x^2} + \frac{\partial^2}{\partial y^2} \right)$ and $O(r^2)$ represents the

truncation error, $O(r^2) = \frac{r^2}{4!} \left(\frac{\partial^4 v}{\partial x^4} + \frac{\partial^4 v}{\partial y^4} \right) + \dots$, which is neglected while considering the

solution for the Laplacian of the potential v_0 . Therefore the Laplacian of the potential v_0 is

$$\Delta v_0 \cong \frac{1}{r^2} \left(\sum_{i=1}^4 v_i - 4v_0 \right) \quad (2.6)$$

Equation (2.6) is the solution used by Hjorth to obtain the surface potentials after neglecting $1/r^2$, which is a proportional constant.

2.2 Bipolar Electrode Method

He *et al.* [2-3] developed a bipolar concentric Laplacian electrode based on Hjorth's FPM. The bipolar electrode shown in Figure 2 has a disc at the center and a concentric ring around the disc. Based on the concept "two-dimensional Laplacian of the potential should be independent of the coordinate system selected" [2-3], He *et al.* developed the bipolar concentric ring electrode by rotating the axes. Thus the Laplacian of potential v_0 at point p_0 can also be obtained by

$$\left(\frac{\partial^2 v}{\partial x'^2} + \frac{\partial^2 v}{\partial y'^2} \right) \Big|_{p_0} = \Delta v_0 = \frac{1}{r^2} \left(\sum_{i=1}^4 v_i - 4v_0 \right) + O(r^2) \quad (2.7)$$

Performing the integral of the potential Laplacian over the area results in Equation (2.8) for the Laplacian of potential at the center disc of the bipolar concentric ring electrode.

This radius r is the inter-point distance in FPM.

$$\Delta v_0 \approx \frac{4}{r^2} \left\{ \frac{1}{2\pi r} \int v dl - v_0 \right\} \quad (2.8)$$

Where r is the inter-electrode distance between the elements of a bipolar concentric electrode, $\frac{1}{2\pi r} \int v dl$ = the average voltage on the outer ring, v_0 is the voltage on the center disc.

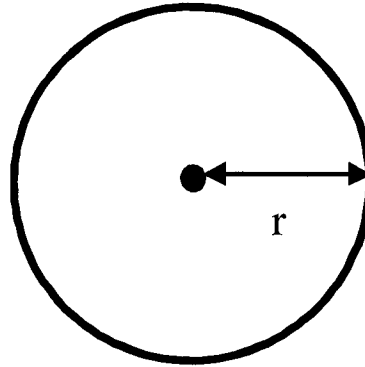


Figure 2 Bipolar concentric ring electrode.

The solution of Equation (2.8) for the bipolar electrode can be expressed by the mathematical explanation as shown in Equation (2.9) given by Huiskamp [22] to generalize a FPM Laplacian solution for a bipolar Laplacian electrode of radius r . Writing the Taylor's series expansion for a point which is at a distance of r from the center point p_0 and by defining $x=rcos\theta$, $y=rsin\theta$ and performing the integral over a radius of r results in

$$\begin{aligned}
\int_0^{2\pi} v(r \cos \theta, r \sin \theta) d\theta &= \int_0^{2\pi} v(0, 0) d\theta + r \int_0^{2\pi} \cos \theta d\theta \frac{\partial v}{\partial x} \Big|_{p_0} + r \int_0^{2\pi} \sin \theta d\theta \frac{\partial v}{\partial y} \Big|_{p_0} \\
&+ \frac{r^2}{2} \int_0^{2\pi} 2 \cos \theta \sin \theta d\theta \frac{\partial^2 v}{\partial x \partial y} \Big|_{p_0} + \frac{r^2}{2} \int_0^{2\pi} \cos^2 \theta d\theta \frac{\partial^2 v}{\partial x^2} \Big|_{p_0} \\
&+ \frac{r^2}{2} \int_0^{2\pi} \sin^2 \theta d\theta \frac{\partial^2 v}{\partial y^2} \Big|_{p_0} + \dots
\end{aligned} \tag{2.9}$$

Solving Equation (2.9) results in

$$\Delta v_0 \approx \frac{4}{r^2} \left(\frac{1}{2\pi} \int_0^{2\pi} (v(r \cos \theta, r \sin \theta)) d\theta - v_0 \right) = \frac{4}{r^2} (\bar{v} - v_0) \tag{2.10}$$

where \bar{v} is the average potential on the concentric ring and v_0 is the potential on the center point p_0 .

2.3 Quasi-Bipolar Electrode Method

Besio *et al.* [15-18] proposed another concentric ring Laplacian electrode, quasi-bipolar concentric ring electrode. The quasi-bipolar concentric ring electrode is as shown in Figure 3. In the quasi-bipolar configuration, the electrode has three elements (disc, middle ring and an outer ring). It is not a true bipolar configuration due to the disc and outer ring being shorted. This method was proposed to estimate the Laplacian potentials at the center disk based on the equation

$$\Delta v_o = \frac{(\bar{v} + v_0)}{2} - v_m \tag{2.11}$$

where v_0 = potential on the disc, \bar{v} = potential on the outer ring, and v_m = potential on the middle ring.

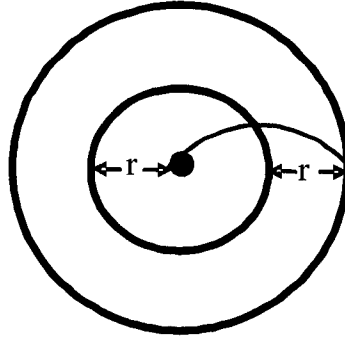


Figure 3 Quasi-bipolar concentric ring electrode.

2.4 Nine-Point-Method (NPM)

The nine-point-method (NPM) is considered to improve the approximation to the Laplacian over the FPM and quasi-bipolar method. The arrangement of the nine points p_1 to p_8 and p_0 is as shown in Figure 4. Where $v_1, v_2, v_3, v_4, v_5, v_6, v_7, v_8$ and v_0 are the potentials corresponding to the points p_1 to p_8 and p_0 . A Taylor series expansion for $v_1, v_2, v_3,$ and v_4 results in Equation (2.4). Similarly for potentials v_5, v_6, v_7, v_8 whose inter-point distance is $2r$ the Taylor series is given by

$$\frac{v_5 + v_6 + v_7 + v_8}{4} = v_0 + r^2 \left(\frac{\partial^2 v}{\partial x^2} + \frac{\partial^2 v}{\partial y^2} \right) + \frac{r^4}{3} \left(\frac{\partial^4 v}{\partial x^4} + \frac{\partial^4 v}{\partial y^4} \right) + \dots \quad (2.12)$$

To approximate the solution of the Laplacian potential v_0 , Equation (2.12) is subtracted from sixteen times Equation (2.4). This manipulation results in Equation (2.13)

$$\begin{aligned} 16(v_1 + v_2 + v_3 + v_4) - (v_5 + v_6 + v_7 + v_8) &= 60v_0 + 12r^2 \left(\frac{\partial^2 v}{\partial x^2} + \frac{\partial^2 v}{\partial y^2} \right) \Big|_{p_0} \\ &+ \frac{16r^6}{120} \left(\frac{\partial^6 v}{\partial x^6} + \frac{\partial^6 v}{\partial y^6} \right) + \dots \end{aligned} \quad (2.13)$$

The Laplacian of potential v_0 is

$$\left(\frac{\partial^2 v}{\partial x^2} + \frac{\partial^2 v}{\partial y^2} \right) = \Delta v_0 = \frac{1}{12r^2} \left\{ 16 \sum_{i=1}^4 v_i - 60v_0 - \sum_{i=5}^8 v_i \right\} + \mathcal{O}(r^4) \quad (2.14)$$

where $O(r^4) = \frac{r^4}{270} \left(\frac{\partial^6 v}{\partial x^6} + \frac{\partial^6 v}{\partial y^6} \right) + \dots$, is truncation error, which will be neglected while considering the solution for the Laplacian potential of v_0 . The truncation error of the NPM does not have 4th order terms as the FPM and quasi-bipolar method do.

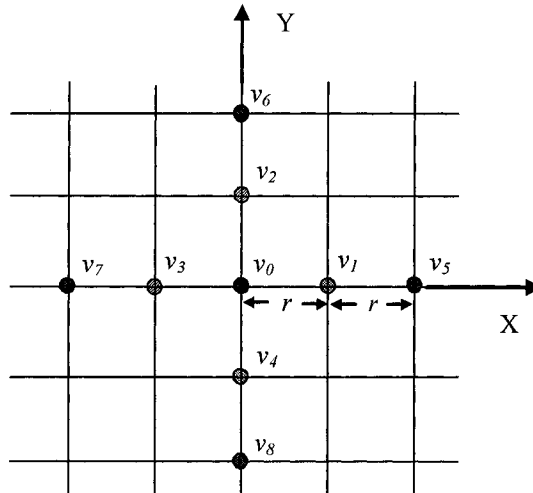


Figure 4 Nine-point arrangement for the NPM on a regular square grid.

2.5 Applying NPM to the Tri-polar Electrode

Aakula [23] developed a tri-polar electrode from the NPM based on Huiskamp's approximation. The tri-polar electrode shown in Figure 5 has three electrode elements. It has a disc surrounded by two concentric ring elements. The NPM is considered as two FPMs. Points p_1, p_2, p_3, p_4 and p_0 forming one FPM with inter-point distance of r and points p_5, p_6, p_7, p_8 and p_0 forming a second FPM with inter-point distance of $2r$. Potentials $v_1, v_2, v_3, v_4, v_5, v_6, v_7, v_8$ and v_0 are potentials at these corresponding points.

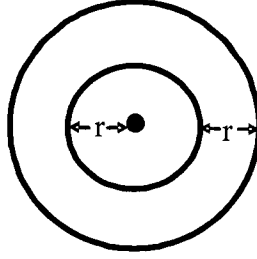


Figure 5 Tri-polar concentric ring electrode.

Applying the Taylor's series expansion along the circle of radius $2r$ and multiplying both sides by $1/2\pi$ results in

$$\begin{aligned}
 \frac{1}{2\pi} \int_0^{2\pi} v(2r \cos \theta, 2r \sin \theta) d\theta &= \frac{1}{2\pi} \int_0^{2\pi} v(0,0) d\theta + 2r \frac{1}{2\pi} \int_0^{2\pi} \cos \theta d\theta \frac{\partial v}{\partial x} \Big|_{p_0} \\
 &+ r \frac{1}{2\pi} \int_0^{2\pi} \sin \theta d\theta \frac{\partial v}{\partial y} \Big|_{p_0} + \frac{(2r)^2}{2} \frac{1}{2\pi} \int_0^{2\pi} 2 \cos \theta \sin \theta d\theta \frac{\partial^2 v}{\partial x \partial y} \Big|_{p_0} \\
 &+ \frac{(2r)^2}{2} \frac{1}{2\pi} \int_0^{2\pi} \cos^2 \theta d\theta \frac{\partial^2 v}{\partial x^2} \Big|_{p_0} + \frac{(2r)^2}{2} \frac{1}{2\pi} \int_0^{2\pi} \sin^2 \theta d\theta \frac{\partial^2 v}{\partial y^2} \Big|_{p_0} + \dots
 \end{aligned} \tag{2.15}$$

which is the average potential on the outer ring. To find the approximate solution for the Laplacian potential, Equation 2.15 is subtracted from 16 times Equation 2.10 to cancel the 4th order term and increase the accuracy of the Laplacian approximation [23], which results in

$$\begin{aligned}
 16 \frac{1}{2\pi} \int_0^{2\pi} (v(r \cos \theta, r \sin \theta)) d\theta - \frac{1}{2\pi} \int_0^{2\pi} (v(2r \cos \theta, 2r \sin \theta)) d\theta \\
 = 15v_0 + 3r^2 \left(\frac{\partial^2 v}{\partial x^2} + \frac{\partial^2 v}{\partial y^2} \right) \\
 + \frac{(2r)^6}{3} \int_0^{2\pi} \sum_{j=0}^6 (\sin \theta)^{6-j} (\cos \theta)^j \left(\frac{\partial^6 v}{\partial x^{6-j} \partial y^j} \right) + \dots
 \end{aligned} \tag{2.16}$$

The approximate solution to the Laplacian at a point p_0 is given as

$$\Delta v_0 \cong \frac{1}{3r^2} \left\{ \begin{array}{l} 16 \left(\frac{1}{2\pi} \int_0^{2\pi} v(r \cos \theta, r \sin \theta) d\theta - v_0 \right) \\ - \left(\frac{1}{2\pi} \int_0^{2\pi} v(2r \cos \theta, 2r \sin \theta) d\theta - v_0 \right) \end{array} \right\} \quad (2.17)$$

where

$$\text{Truncation error} = \frac{(2r)^6}{3} \int_0^{2\pi} \sum_{j=0}^6 (\sin \theta)^{6-j} (\cos \theta)^j \left(\frac{\partial^6 v}{\partial x^{6-j} \partial y^j} \right) + \dots$$

$$\frac{1}{2\pi} \int_0^{2\pi} v(r \cos \theta, r \sin \theta) d\theta = \text{Average potential on the middle ring.}$$

$$\frac{1}{2\pi} \int_0^{2\pi} v(2r \cos \theta, 2r \sin \theta) d\theta = \text{Average potential on the outer ring.}$$

Therefore (2.17) can be written as

$$\Delta v_0 = \frac{1}{3r^2} \{ 16(\text{middle ring potential} - \text{center disc potential}) \\ - (\text{outer ring potential} - \text{center disc potential}) \} \quad (2.18)$$

CHAPTER 3

METHODS

3.1 Computer Models

3.1.1 Single Source Computer Model

A mathematical model patterned after Figure 6 was designed in a custom Matlab (Mathworks, Natick, MA) program using the analytical solution to calculate the potential due to a moving unity dipole in an isotropic medium of conductivity σ is given as in Equation (3.1).

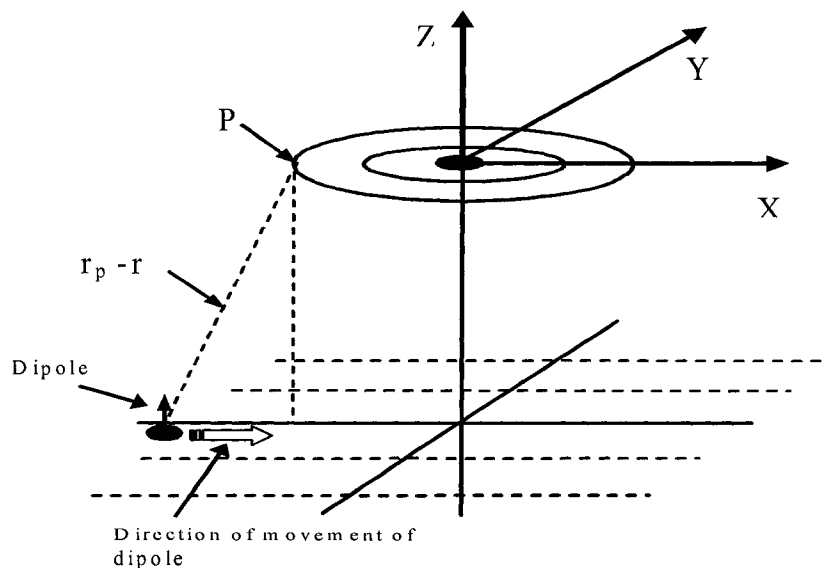


Figure 6 Moving dipole computer simulation.

$$V = \frac{1}{4\pi\sigma} \cdot \frac{(\bar{r}_p - \bar{r}) \cdot \bar{P}}{|\bar{r}_p - \bar{r}|^3} \quad (3.1)$$

Equation (3.1) can be rewritten as Equation (3.2).

$$V = \frac{1}{4\pi\sigma} \cdot \frac{\bar{P} \cos(\theta)}{|\bar{r}_p - \bar{r}|^2} \quad (3.2)$$

where θ is the angle made by the line joining the dipole and point P to the vertical line z .

In this mathematical model $(1/4\pi\sigma)$ is taken as a constant, using the values pertaining to the conductivity of saltwater and the permittivity of the printed circuit board (PCB) material used for the dipole preparation. These values are discussed further in the results section. Here \bar{r} is the position of the dipole and \bar{r}_p is the position of the point where the potential is calculated. \bar{P} is the dipole movement. The Equation (3.2) can be written in Cartesian coordinates as

$$V = \frac{1}{4\pi\sigma} \cdot \frac{dZ}{\left((X - dX)^2 + (Y - dY)^2 + (0 - dZ)^2\right)^{3/2}} \quad (3.3)$$

here (dX, dY, dZ) is the location of the dipole and $(X, Y, 0)$ is the location of the point P .

To test different size electrodes in this moving dipole single-source model, the outer concentric ring ranged from 5.0 to 36 mm in diameter with the disc and middle ring sized proportionally from 0.4 mm to 5 mm and 2.5 mm to 10 mm, respectively. An axial dipole, directed towards the positive Z -axis, was moved incrementally 1.0 cm at a time along the Z -axis from depths of -1.0 cm to -4.0 cm. The dipole traversed the X -axis from -5.0 cm to 5.0 cm and along the Y -axis from -5.0 cm to 5.0 cm. First, the depth of the dipole was kept constant while the dipole was moved along the X -axis and Y -axis. Then, the depth of the dipole was changed and was moved along the X -axis and Y -axis

again. From the simulated model of the moving dipole, the potentials on each electrode element were calculated using Equation (3.3). Calculating the potential on the disc was similar to calculating potential at a point due to a dipole. For calculating the potential on the ring, the ring was divided into 360 equal parts, and the potential at all 360 points was calculated and averaged to get the potential on the entire ring.

These potentials were then used to calculate the Laplacian of the bipolar electrode with Equation (2.10), quasi-bipolar electrode using Equation (2.11) and the tri-polar electrode with Equation (2.18). From the calculated Laplacian potentials for the bipolar, quasi-bipolar, and tri-polar electrode configurations, the attenuation in dB of the calculated potentials along the radial direction was calculated for each depth (1.0 cm to 4.0 cm in increments of 1.0 cm) for all the sizes of the electrode outer diameters from 5.0 mm, 10 mm, 20 mm and 36 mm with the disc and middle ring sized proportionally from 0.4 to 5 mm and 2.5 to 10 mm respectively.

The attenuation in dB was calculated using Equation (3.4).

$$A_{dB} = 20 \left(\log \left(\frac{v_1}{v_{\max}} \right) \right) \quad (3.4)$$

here A_{dB} is the attenuation at the position of the Laplacian potential v_1 and v_{\max} is the Laplacian potential at the origin. These attenuation values were compared in between the electrode systems and localization [24] capability was also using single-factor ANOVA and Bonferroni statistical tests and presented in the Results section.

3.1.2 Multiple Source Computer Model

To verify the spatial filter characteristics in the presence of noise, the single unity dipole computer model discussed in Section 3.1.1 was modified. A constant unity dipole directed towards the positive Z-axis representing the source of interest was modeled

directly below the concentric ring electrode and 20 noise source unit dipoles were placed at random locations. All the dipoles had the same orientation, directed towards the positive Z-axis. In this multiple source computer model, the outer concentric ring again was varied from 5.0 mm to 36 mm in diameter with the disc and middle ring sized proportionally from 0.4 mm to 5.0 mm and 2.5 mm to 10 mm respectively. The constant unity dipole was always active and only three or four random dipoles were kept active during the simulation. The arrangement for the multi-source computer model was shown in Figure 7. The noise dipoles were randomly selected. The potentials on the elements of the concentric ring electrodes were calculated using Equation (3.3). The Laplacian potentials for different electrode systems namely bipolar with Equation (2.10), quasi-bipolar with Equation (2.11) and tri-polar using Equation (2.18) were also calculated. The attenuation of the Laplacian potentials along the radial distance was calculated and localization [25] characteristics were determined.

The attenuation in dB for the calculated potentials from bipolar, quasi-bipolar and tri-polar concentric electrode configurations along the radial direction was calculated using Equation (3.4) for each depth (1.0 cm to 4.0 cm) for all the sizes of the electrode outer diameters ranging from 5.0 mm to 36 mm. These experiments were repeated 20 times. These attenuations along the radial distance were compared using single-factor ANOVA and Bonferroni statistical tests.

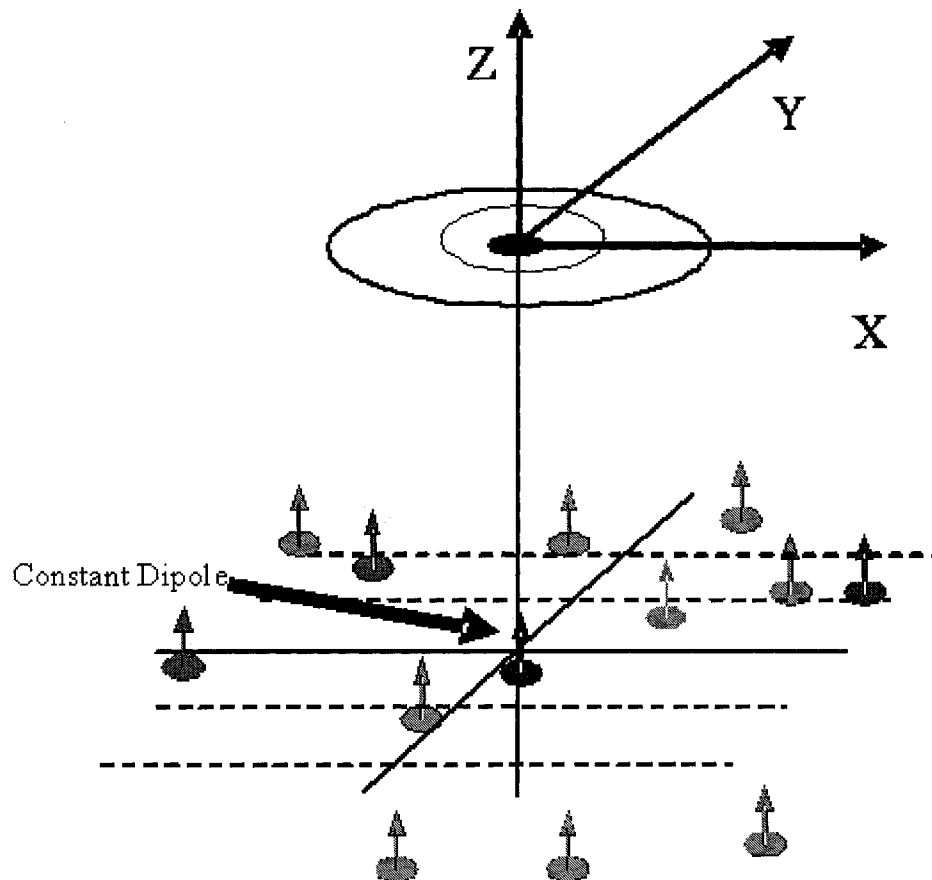


Figure 7 Arrangement of random dipole computer simulation.

3.2 Tank Experiments

Tank experiments were conducted in order to verify the results obtained by the single dipole computer model. A Plexi-Glass tank of size 50 cm x 26 cm x 30 cm was filled with a saltwater mixture of 9.0 gm/L concentration [26], providing a medium with conductivity similar to that of human intracellular fluid conductivity approximately 1.76 S/m. A dipole was constructed with two thin 1.0 mm radius copper discs, which were identically etched on both sides of a printed circuit board. Two 5.0 V pk-pk, 100 Hz AC square waves were then applied between the discs, the two discs were given alternating polarity square waves in order to limit the corrosion of the dipole discs.

The circuit used for generating alternating polarity square waves is given in Figure 8. In this circuit there were two inverting amplifiers were used. The outputs were giving two inverted 5.0 V pk-pk square waves as shown in the figure. This configuration was used to maintain the same output impedance after each inverting amplifier before connecting to each side of the dipole.

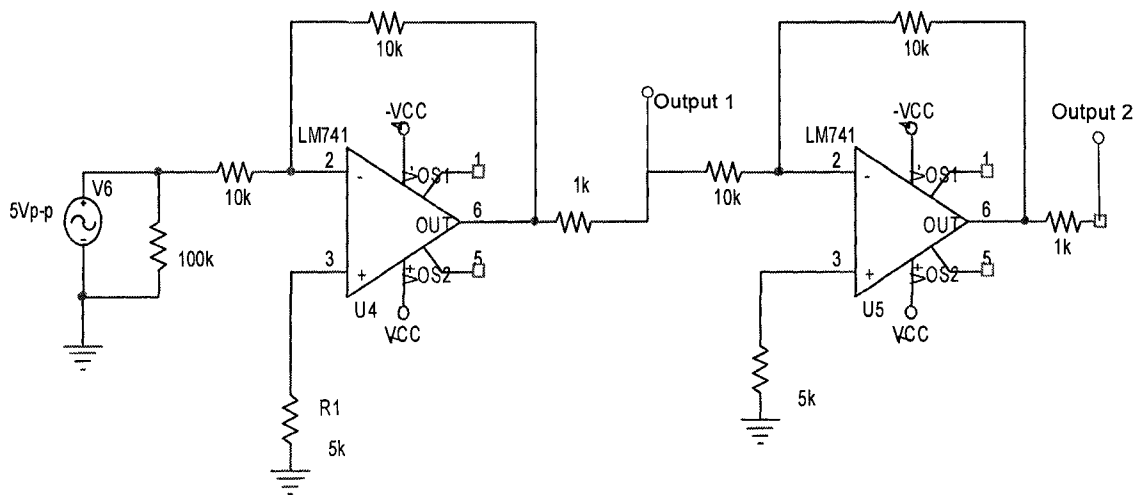


Figure 8 Double inverter circuit for generating the dipole.

At the bottom of the tank was marked with lines representing the X-Y plane. The dipole was kept at the origin. The concentric ring electrode was attached to the bottom of a vertically adjustable Plexi-Glass beam which could be adjusted in increments of 1.0 cm. The Plexi-Glass vertical beam was attached to a lead screw driven stage which moved along the X-axis at 1.8 cm/sec. The stage was driven with a 12VDC windshield wiper motor. The experimental setup used for the tank experiment is shown in Figure 9.

The concentric electrodes were designed with ORCAD (Cadence, San Jose, CA) software and prepared using an LPKF ProtoMat[®] C20 rapid prototype board plotter (LPKF Laser & Electronics, Wilsonville, OR). The experiment was repeated 20 times

with a constant dipole depth and the data were averaged to minimize variations due to the experimental setup. Then the depth was changed and the measurements were repeated until all four depths, 1.0, 2.0, 3.0, and 4.0 cm, were completed.

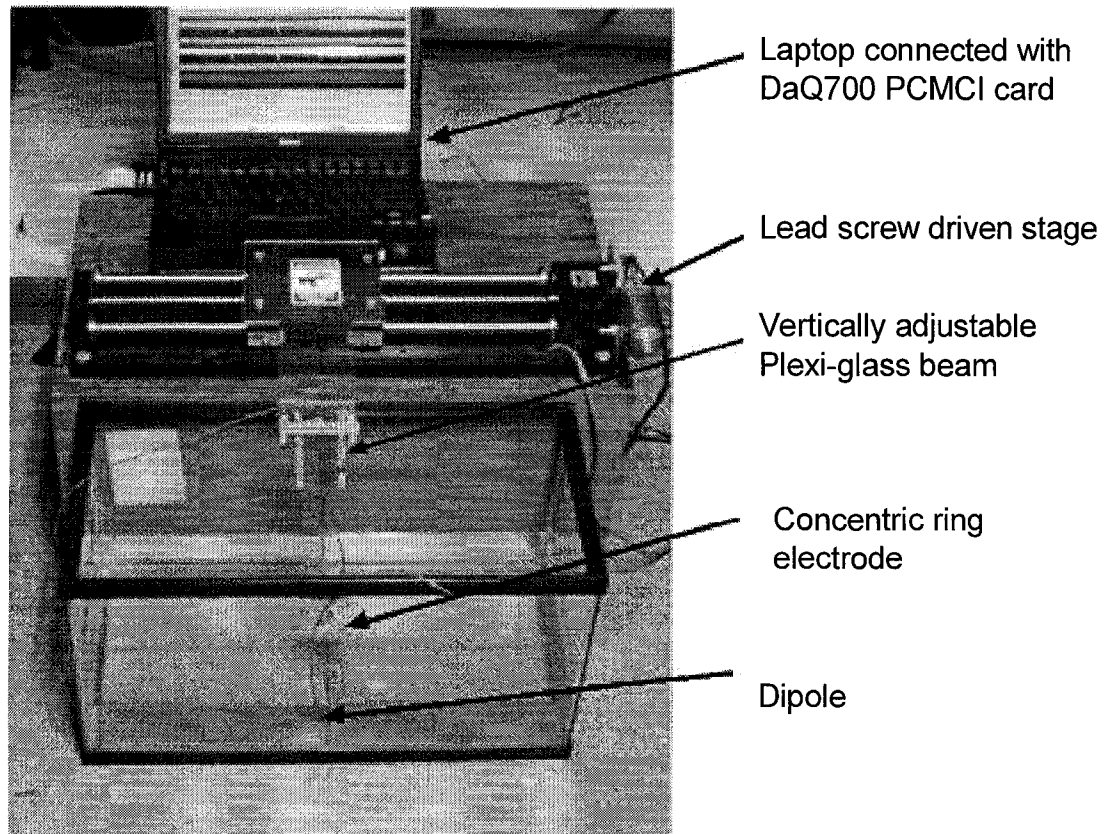


Figure 9 Tank experimental setup.

For appropriate comparison, the electrode elements in the tank experiments were matched with electrode dimensions used in the moving dipole computer model. The outer concentric ring ranged from 5.0 to 36 mm in diameter with the disc and middle ring sized proportionally from 0.4 to 5.0 mm and 2.5 to 10 mm, respectively. The widths of the outer and middle rings were both set at 0.03 cm and the radius of the disc was also set at 0.03 cm. The depth of the dipole was set at 1.0 cm to 4.0 cm below the surface of the

electrode. In the tank experiments, the electrode was moved in the direction of the positive X-axis on the surface of the saltwater solution while the dipole was set stationary at the location of $X = Y = 0.0$ cm, where as in the computer simulations the dipole was moved.

Potential measurements were taken from the three elements of the concentric ring electrodes using a custom LabView (National Instruments, Austin, TX-USA) program via a DaqCard 700 (National Instruments, Austin, TX-USA). The measurements were referenced by an exposed wire electrode between the dipole discs. The data were recorded at 1000 samples per second for 17 sec which covered a distance of 30.6 cm in the tank. The tank size was 10 times the larger 3.6 cm diameter electrode used. Post-processing was achieved with a custom Matlab program. Laplacian potentials were calculated for bipolar, quasi-bipolar and tri-polar electrode configurations, using Equation (2.10), Equation (2.11), and Equation (2.18), respectively. The attenuation of the signal due to the distance along the radial axis was calculated using Equation (3.4) and attenuation in dB was plotted for comparison between the three electrode configurations. The attenuation values were a measure of the localization [25] and global noise rejection abilities of the three electrode configurations. Single-factor ANOVA and Bonferroni statistical analysis were conducted on attenuation values to compare the performance of the three electrode configurations and are presented in the Results section.

3.3 Analyzing the Variation of Alpha Rhythms from Human LEEG

All data acquisitions were conducted in accordance with the Institutional Review Board (IRB) approved protocols submitted before the beginning of work. All

participants who participated were fully informed of the experimental protocol in accordance to the aforementioned IRB-approved protocol and signed Informed Consent forms. The human consent form is shown in Appendix-A.

A tri-polar concentric electrode (diameter of 20 mm for the outer ring, 10.6 mm for the middle ring, and 2.6 mm for the disc) was used for recording LEEG signals from humans. The single electrode LEEG signals were recorded from the occipital lobes to analyze the different frequency rhythms in the EEG. The EEG signals generally in healthy persons have four different frequency rhythms namely Delta (0.1 Hz - 3 Hz), Theta (4 Hz- 7 Hz), Alpha (8 Hz 13 Hz) and Beta (14 Hz- 40 Hz) rhythms [1]. These different rhythms are shown in Figure 10. Different rhythms of regular EEG are further fully described in Appendix-B.

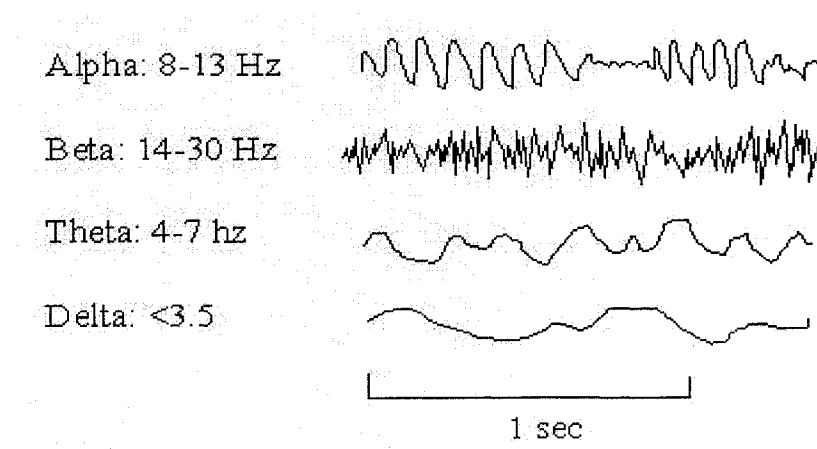


Figure 10 Typical EEG rhythms seen in healthy human EEG data.

Data were recorded from seven healthy adults (three females and four males) with an average age of 23 ± 1 years. The concentric ring electrodes were placed on the subject's left occipital lobes and a reference electrode was placed behind the left ear. The electrodes were attached using Ten20 (Grass Telefactor, RI) conductive paste. The

placement of electrodes is shown in Figure 11. The recordings were taken from the occipital lobes as they have stronger variation in alpha rhythms with the eyes closed and eyes open conditions. First, each subject was asked to close his/her eyes for 25 sec and be in a relaxed condition to generate more alpha waves. Then, the subject was instructed to open his/her eyes for another 25 sec while counting down from 100. The counting down will increase the mental activity and will decrease the alpha rhythms [27].

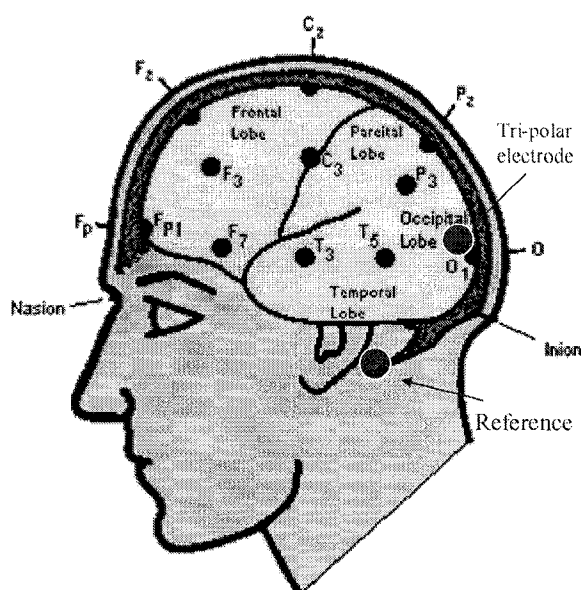


Figure 11 Placement of tri-polar concentric ring electrode for recording LEEG signals for analyzing alpha rhythm.

The signals were recorded using the Biopac MP35 amplifier (BIOPAC Systems, Inc, Goleta, CA). The signals were analyzed using the Biopac student EEG1 lesson programs. A custom Matlab program was used to filter the signals. The Matlab program was used to filter the LEEG signals in to four different frequency bands namely Delta (0.1 Hz-3 Hz), Theta (4 Hz- 7 Hz), Alpha (8 Hz- 13 Hz) and Beta (14 Hz- 40 Hz) rhythms as previously described [1]. The change in alpha rhythm in both the conditions

was plotted. The mean and standard deviation of the alpha rhythm in both eyes closed and eyes open condition were calculated.

3.4 Movement-Related Potentials (MRP) from Fp1

A correlation between a human body motion and EEG signals is a much sought-after task in current neurology. The knowledge about this correlation is in great demand as it would be a significant accomplishment towards the comprehension of human brain functions. The correlation of EEG to a body motion is very complicated, and finding a simplified method to determine this relationship would be very beneficial. Existing EEG systems can only resolve general volitional movements such as a hand movement. The primary area under study is the pre-motor area and pre-frontal lobes [30] which are shown in Figure 12.

All data acquisitions were conducted in accordance with the IRB approved protocols. All participants who participated were fully informed of the experimental protocol in accordance to the aforementioned IRB-approved protocol and signed Informed Consent forms. The human consent form is shown in Appendix-A. Movement-Related Potential (MRP) signals were recorded using concentric ring electrodes from 10 volunteers (aged in between 23-27, 3 female and 7 male). All volunteers gave their informed consent. The subjects were seated in a comfortable chair with their right hands kept on a table in front of the chair. The subjects were asked to keep their right index fingers on a micro-switch and to keep their eyes closed in hopes of minimizing eye movement artefacts. The subjects were asked to press the micro-switch cued a metronome at 1 Hz (i.e. they were asked to press the switch once per second). The experimental methods used for recoding MRP signals were adopted from the

methods described in the literature [28-29]. The recording was taken for five minutes on each subject.

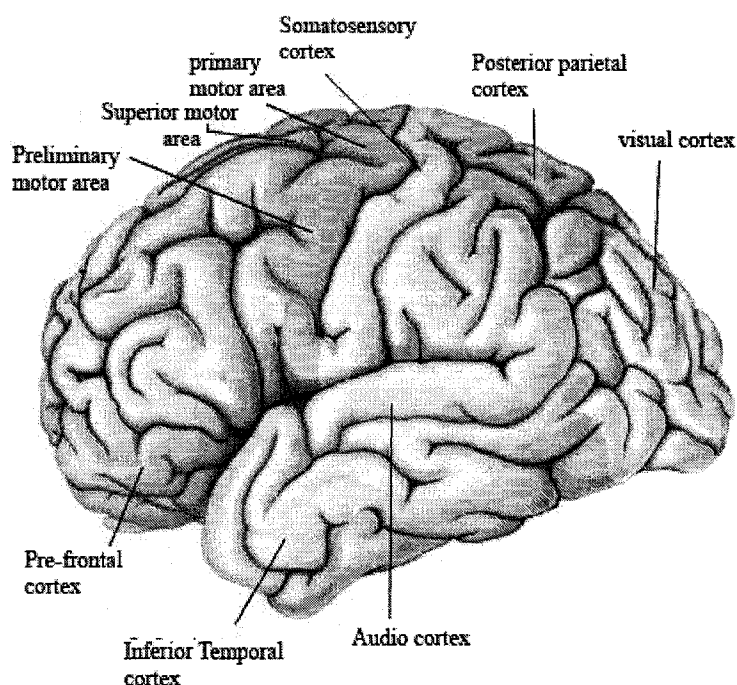


Figure 12 Different areas of the brain.

The concentric ring electrodes as shown in Figure 13 were used for recording MRP signals. The copper base and side walls of each element were painted with silver. The wells were filled with conductive 10/20 EEG paste. The conventional electrodes used for recording MRP were shown in Figure 14. The electrodes were kept on the left pre-frontal lobes according to 10/20 international system as shown in Figure 15. A custom-built pre-amplifier was kept in preceded the 15LT amplifier (Grass Telefactor, RI), was used to amplify the signals. The pre-amplifier was built with a differential amplifier and a high pass filter to remove the DC off set. The pre-amplifier is shown in

Figure 16. A DaqCard 6036E (National Instruments, Austin, TX-USA) was used to acquire the data through the custom LabView program.

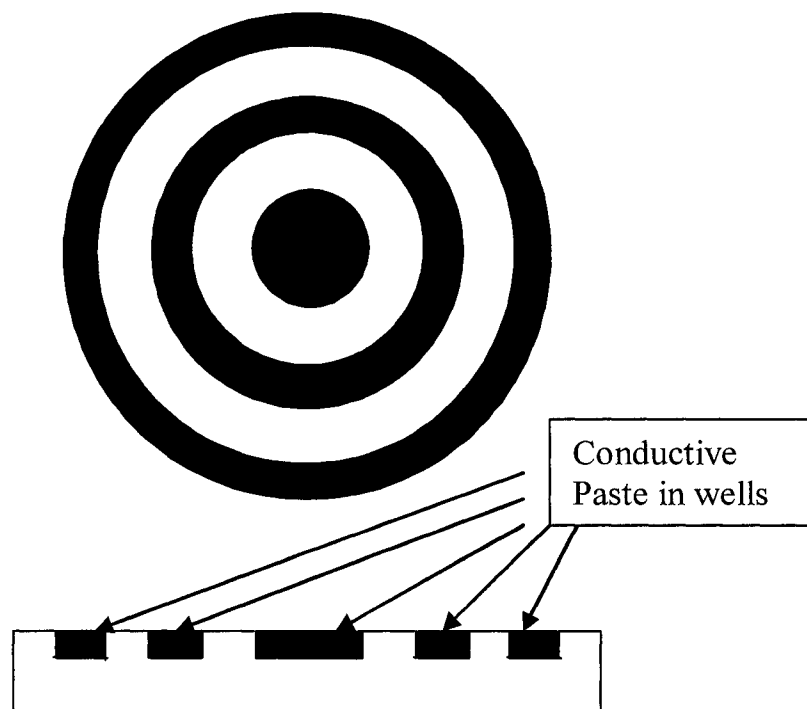


Figure 13 Custom made tri-polar concentric ring electrode.



Figure 14 Conventional disc electrodes used for MRP signals.

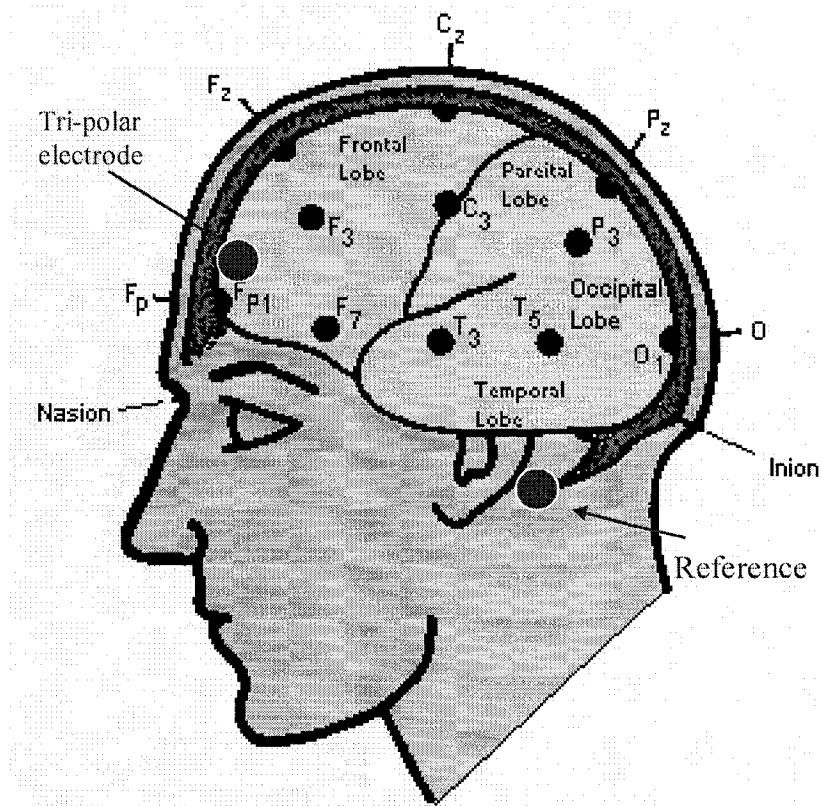


Figure 15 Position of electrode for recording MRP from pre-frontal area FP1 of the brain.

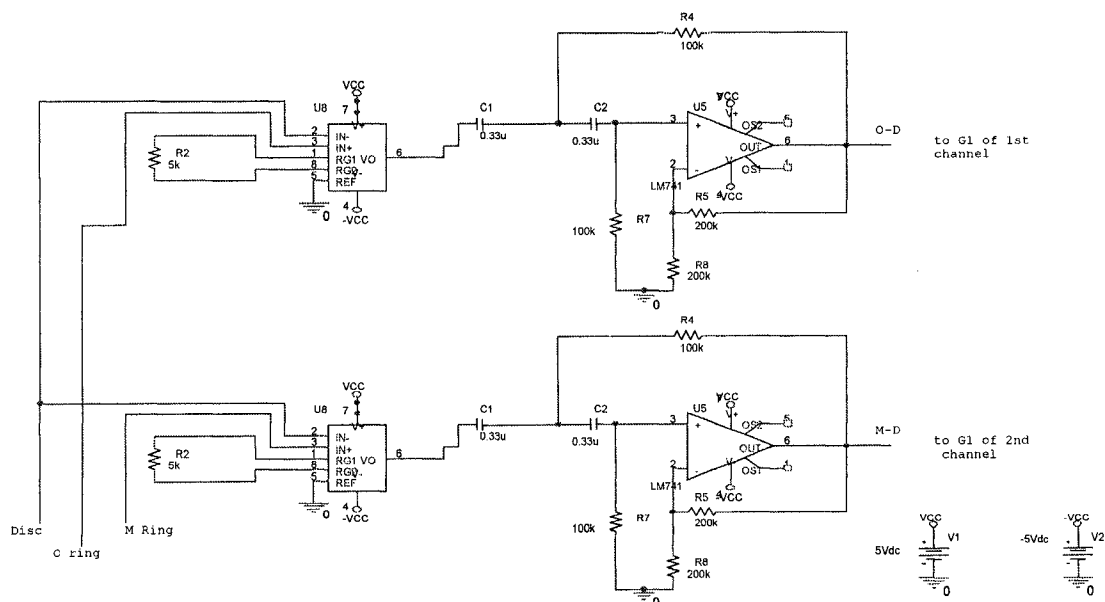


Figure 16 Pre-amplifier used for recording movement-related potentials.

The filter was set from 0.3 Hz to 30 Hz, and the sampling rate was kept at 250 samples per second. The gain of the amplifier was set to 40,000 for concentric ring electrode recordings and 10,000 for single ended recordings using conventional EEG disc (Grass F-E5GH, Grass Telefactor, RI, USA) electrodes. The electrode impedance was kept below 10 kOhms.

The concentric ring electrodes were prepared using LPKF ProtoMat[®] C20 rapid prototype board plotter of size 1.6 cm. The concentric ring electrode had the following sizes: (1) Disc of 2.0 mm diameter (2) Middle ring and Outer ring had 1.2 mm width and (3) The gap between each element was kept 2.0 mm. The concentric ring electrodes were prepared according to the schematic shown in Figure 13. The copper base and sidewalls were painted with silver paint (Spi2 products). The wells were filled with Ten20 conductive paste and the electrodes were repainted after each subject's recordings. For comparison conventional disc electrodes were also used to record EEG. The block diagram of the whole system used for recording LEEG signals from the pre-frontal areas of the brain is shown in Figure 17.

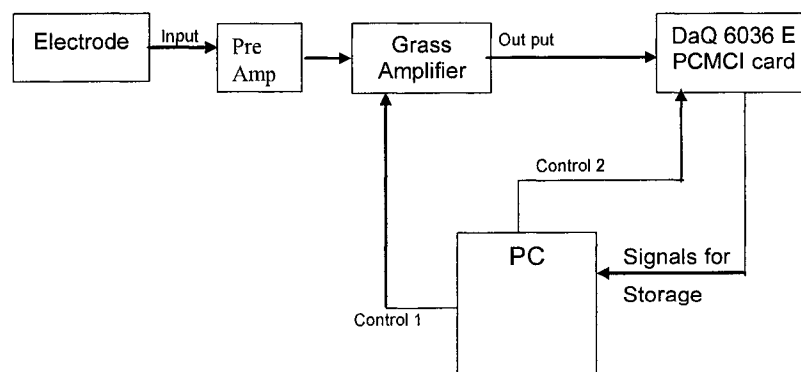


Figure 17 The block diagram of the system used for recording the MRP signals.

The acquired data were then processed with a custom Matlab program. The signal recorded from the micro-switch was used as a reference signal. The EEG and LEEG were divided in to one second windows size of 1 sec (500 ms before and 500 ms after the rising edge of the switch pulse). Approximately 150-200 artefact free windows were averaged. The trials contaminated with eye movements and head movements were removed. The Laplacian EEG was calculated of concentric bipolar, quasi-bipolar, and tri-polar electrode configurations using the respective formulae and plotted.

The MRP signals recorded with different electrode configurations were compared for peak signal to noise ratio. The peak signal to noise signal ratio or SNR [30] was calculated using (3.5) for each electrode configuration. The peak signal was taken as the length of the signal up to the second zero crossing prior to the positive peak and one zero crossing after the positive peak; the remainder of the window was taken as the noise signal.

$$SNR = \frac{E_{peak}}{E_{noise}} = \frac{\frac{1}{p} \sum_{i=1}^p x_i^2}{\frac{1}{n} \sum_{i=1}^n x_i^2} \quad (3.5)$$

where E is the energy, x_i is amplitude of the signal, p is the number of points in the peak, and n is the number points in the noise. The SNR for different electrode systems for each subject was calculated and shown in tabular form for the location FP1.

3.5 Multi-Channel MRP Recording

Movement-related potentials were recorded from multiple locations using a multi-channel amplifier. The multi-channel recording was taken to compare the SNR, spatial

selectivity and mutual information for three electrode systems namely conventional disc electrodes, bipolar electrodes and tri-polar electrodes.

3.5.1 MRP Recording with Conventional Disc Electrodes

Conventional gold disc electrodes of 1.0 cm diameter were used for recording MRP signals. The subjects were volunteers and gave an informed consent and the experiments abided by the IRB approved protocol as shown in Appendix-A. All five subjects involved in the experiment were male subjects and free of any known neurological disorders and their age ranged from 24-27 years and they were all right handed. Subjects were seated in a comfortable chair with armrests and their right index finger was placed on a micro-switch. The subjects were asked to press the micro-switch when cued, and EEG signals were recorded. A metronome was used as a cue every three seconds for subjects to press the micro-switch. The subjects were asked to close their eyes to reduce the electrooculogram (EOG) artefact. These MRP recording methods followed the methods previously used for recording MRP signals from FP1.

Thirty-five disc electrodes were placed on the left brain with the electrodes arranged in a 5x7 array around the area Fz-Cz-Pz-P3-T5-T3-F7-F3. The placement of the electrodes was based on a 10/20 system as shown in Figure 18. Due to the lack of instrumentation for recording 35 channels at a time, the recordings were taken seven channels at a time and synchronized later with the time reference from the micro-switch. The center of the array was positioned on the line joining P3 and F3, and the inter-electrode distance was 1.0 cm. The reference electrode was placed near the earlobe on the contra-lateral side.

The recordings were performed by referencing each electrode to the reference electrode. The skin-to-electrode impedance was checked before each experiment and kept below 10 KOhm. Custom-built pre-amplifiers (gain 100) along with a Grass 15LT amplifier were used for a total gain of 20,000. The filters were set from 0.3 Hz to 30 Hz. The data were acquired using a DI720 data acquisition (DataQ Instruments, Akron, Ohio, USA) system with a sampling rate of 250S/channel. One of the recording channels contained the micro-switch state so that a reference of movement instants could be kept.

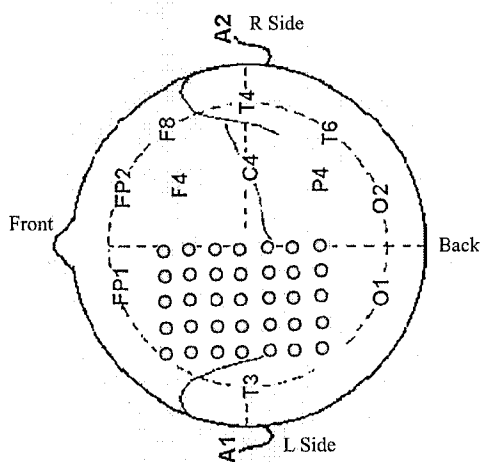


Figure 18 The position of electrodes for recording MRP signals.

3.5.2 MRP Recording with Concentric Ring Electrodes

The concentric ring electrodes were arranged at the same locations as the regular disc electrodes for direct comparison. The recordings were taken in differential mode, outer ring to disc and middle ring to disc. The recordings with concentric ring electrodes were also taken using seven electrodes at a time as conventional disc electrodes. The electrode setup used for recording with concentric ring electrodes is shown in Figure 19. Five transitions of the electrodes were necessary to record from the 35 locations. The

skin-to-electrode impedance was checked before each experiment and kept below 10 KOhm. The same custom-built pre-amplifiers and Grass 15LT amplifiers were used with the same filter settings as for the conventional disc electrodes.

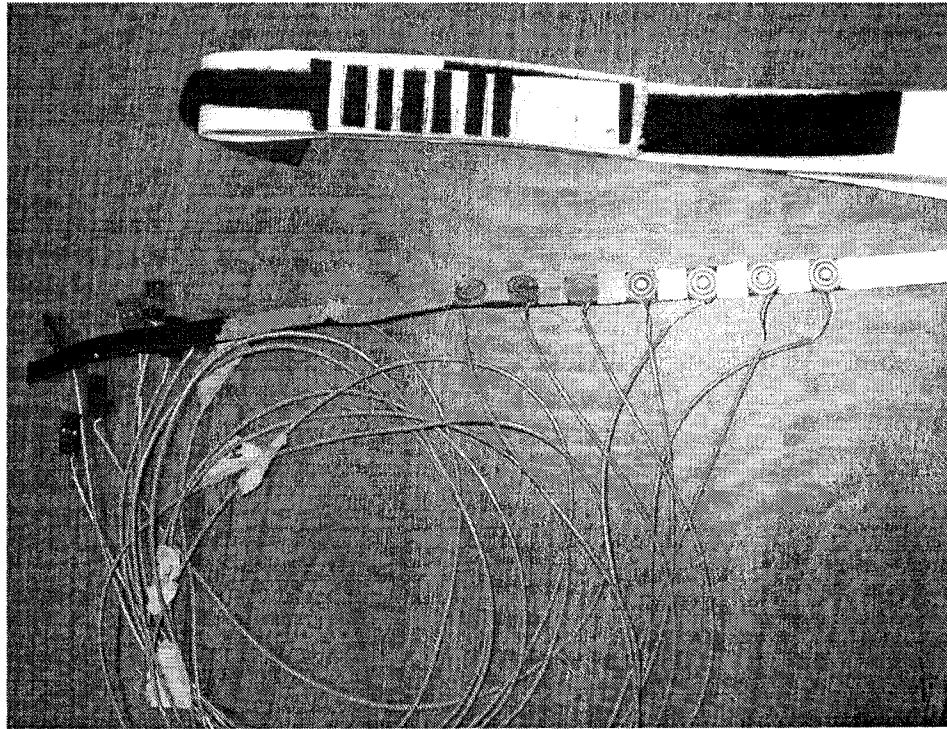


Figure 19 Custom arrangement of seven tri-polar electrodes with 1 cm spacing for recording MRP signals.

3.5.3 Pre-processing of Multi-Channel MRP Recordings

The MRP signals recorded with the different electrode systems were pre-processed using custom Matlab programs. The signals were pre-processed to remove 60 Hz even though no 60 Hz was evident. The EOG artefacts were removed with threshold detection. If the amplitude of the LEEG recording was more than absolute 0.5 V (after amplification), then that window was considered artefact and neglected. The micro-switch signal was used as a time reference of the movements. The time of movements

was detected using the threshold detector to determine the rising edge of switch signal. The signals recorded at different times were synchronized using the micro-switch pulse timing. The recordings from concentric ring electrodes were used to calculate the Laplacian potentials for the different concentric ring electrode systems using (1) and (2) with the custom Matlab programs. The EEG and LEEG were divided into windows of 1.0 sec (499 ms before and 500 ms after the movement). Approximately 150 artefact free trials were ensemble averaged for each electrode system for each subject to form the MRP.

3.5.4 Comparison of SNR

The peak signal to noise signal ratio or SNR [31] was calculated using (3) for each electrode configuration. The peak signal was taken as the length of the signal from a first zero crossing before the negative peak to first zero crossing after the positive peak; the remainder of the window was considered as the noise signal. The SNR of the three different electrode systems for each subject was calculated for all the locations but shown only for location CZ. A single-factor ANOVA and Bonferroni tests were conducted to compare the SNR of the three electrode systems and presented in the Results section.

3.5.5 Comparison of Spatial Selectivity

The averaged MRP signals from the three electrode systems were plotted in a 2-D map corresponding to their locations. The peak-to-peak potentials of the signal component at each location for each electrode were also calculated. To compare the spatial selectivity, the ratios of the peak-to-peak potentials from each electrode location to each adjacent electrode location were calculated. These peak ratios between adjacent locations were used as a measure of the spatial attenuation of the electrodes, the spatial selectivity. The peak ratios were averaged for all the subjects. A single-factor ANOVA

and Bonferroni tests were conducted to compare the spatial selectivity of the three electrode system.

3.5.6 Comparison of Mutual Information (MI)

For this research mutual information (MI) is used as a means for comparing the statistical independence of signals recorded from different locations using different electrode systems. MI is different from the linear correlation coefficient because it considers dependencies which are neglected while calculating the linear correlation coefficient. MI is zero if and only if the two random variables are strictly independent [32].

MI was calculated from the marginal densities of two individual channels recorded from two locations. For two channels recorded from locations X_i and X_j the marginal densities were given as $\mu_{x_i}(x_i)$, $\mu_{x_j}(x_j)$ and $\mu(x_i, x_j)$ was the cross marginal density between the two channels. The marginal densities were calculated using the following Equations.

$$\mu_{x_i}(x_i) = \int dx_j \mu(x_i, x_j) \quad (3.6)$$

$$\mu_{x_j}(x_j) = \int dx_i \mu(x_i, x_j) \quad (3.7)$$

MI was defined from the marginal densities as Equation (3.8)

$$I(X_i, X_j) = \iint dx_i dx_j \mu(x_i, x_j) \log \frac{\mu(x_i, x_j)}{\mu_{x_i}(x_i) \mu_{x_j}(x_j)} \quad (3.8)$$

The aim is to estimate $I(X_i, X_j)$, without knowing the densities $\mu(x_i, x_j)$, $\mu_{x_i}(x_i)$, and $\mu_{x_j}(x_j)$. Some rough approximations to MI based on cumulated expansions are very ease to use [32]. The problem with these rough approximations is that they are valid

only for distributions close to Gaussian and are best suited for ranking different distributions by interdependence, and not for estimating the actual dependences. The most straightforward and widespread approach for estimating MI is by partitioning X_i and X_j into bins of finite size, and approximating Equation (3.8) by the finite sum:

$$I(X_i, X_j) \approx I_{binned}(X_i, X_j) = \sum_{kl} p(k, l) \log \frac{p(k, l)}{p_{x_i}(k) \mu_{x_j}(l)} \quad (3.9)$$

where, $p_{x_i}(k) = \int_k dx_i \mu_{x_i}(x_i)$, $p_{x_j}(l) = \int dx_j \mu_{x_j}(x_j)$ and $p(k, l) = \int_k \int_l dx_i dx_j \mu(x_i, x_j)$ (\int_i means the integral over bin (i)). An estimator of $I_{binned}(X_i, X_j)$ is obtained by counting the numbers of points falling into the various bins. If $n_{x_i}(k)$ is the number of points falling into the i^{th} bin of X_i , and $n_{x_j}(l)$ is the number of points fall into j^{th} bin of X_j , and $n(k, l)$ is the number of points in their intersection. Then $p_{x_i}(k)$, $p_{x_j}(l)$ and $p(k, l)$ calculated as

$$p_{x_i}(k) = n_{x_i}(k) / N \quad (3.10)$$

$$p_{x_j}(l) = n_{x_j}(l) / N \quad (3.11)$$

$$p(k, l) = n(k, l) / N \quad (3.12)$$

Equation (3.9) converges to $I(X_i, X_j)$ if $N \rightarrow \infty$ and all bin sizes tend to zero, if all densities exist as proper functions.

First, the mutual information between the seven channels recorded at a time was calculated. This effort was performed five times since the 35 locations were recorded seven sites at a time. Then the grand MI average for each electrode system for each subject was calculated. The MI grand averages for each electrode system for each

subject were then tabulated. The method used for calculating the MI is given in Appendix-C. Finally MI of the three electrode systems were then compared using a single-factor ANOVA and Bonferroni tests.

3.6 Animal Models for Seizure LEEG Recordings

Seizures can be defined in neurological terms as episodes of sudden disturbances of consciousness, mental function, motor, sensory, autonomic activity. Seizures involve malfunction of neurons that produce an excessive discharge of synaptic and action potentials [33]. Seizures can be seen as regular brain activity where as the normal brain has abnormal activity. Seizures last for varying periods of time from a few seconds to hours. These are divided into convulsions, seizure disorder, epilepsy, status epilepticus, epilepsia partialis continua and reflex epilepsy. The EEG associated with seizure can be distinguished from general EEG by the pattern of the activity. EEG associated with seizures shows more spike and sharp waves and spike and sharp waves followed by a slow wave. These different forms of EEG signals during seizures and different types of seizures are further explained in Appendix-D. Animal experiments were conducted to record the electrographic seizure activity with tri-polar concentric ring electrodes to show the feasibility of using tri-polar electrodes for applications in general EEG diagnosis. Two animal seizure models were studied in this research.

3.6.1 Penicillin-G Model

All animal experiments were conducted in accordance with Louisiana Tech institutional animal care and use committee (IACUC) protocols as shown in Appendix-E. Tri-polar electrodes were used to record from the scalp of rats during seizure activity. Male Sprague-Dawley rats were tested in this research. Initially rats were given with α -

chlorolase (150 mg/Kg through i.p., Sigma, St. Louis, MO) a non-narcotic anesthesia that does not interfere with seizure activity. Once anesthetized the scalp was shaved for electrode placement. Rats were ventilated by tracheotomy and placed on a respirator. Respiration was monitored during the whole experiment. The head was stabilized by positioning it using ear bars and mouth piece attached to a stereotaxic frame (Kopf90, David KOPF Instruments). The rat scalp was prepared using NuPrep™ (D.O. Weaver & Co., Aurora, CO, USA) abrasive gel and three tri-polar electrodes were kept on the rat scalp using Ten20 conductive paste to record Laplacian EEG as shown in Figure 20. For some experiments four tri-polar electrodes were used. A reference electrode was kept behind the ears on the neck or on the tail. Custom-built pre-amplifiers along with Grass 15LT amplifier and DataQ DI720 data acquisition system was used to record the signals. The amplifier was set for a total gain of 20,000 and a band pass filter of 1 Hz to 30 Hz was used. The sampling rate was 2,000 samples per second per channel. The sampling rate was varied to 20,000 samples per second per channel during seizure activity for some recordings in an attempt to localize the origin of seizure activity. The rats were injected with the penicillin-G (250,000 units, Sigma, St. Louis, MO) after removing 0.25 CC of cerebro-spinal fluid as described by Patwardhan in an intracisternal rat seizure model [34]. Baseline LEEG recordings were performed before inducing the seizures. The recording was continued after injecting penicillin-G and during the seizure activity.

The rat EEG data were analyzed during the seizure activity to determine the ictal frequency. The recorded EEG signals were analyzed using a custom Matlab program. The EEG signals recorded before and during seizures were analyzed in the frequency domain to determine the seizure frequency content of seizure spikes.

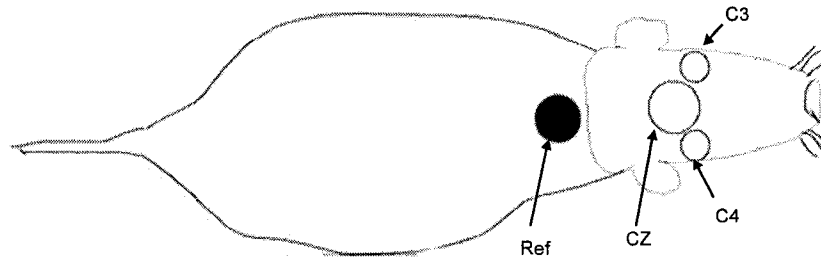


Figure 20 Typical electrode positions for recording LEEG during penicillin-G seizure model.

3.6.2 Pilocarpine Seizure Model

All experiments in this research were conducted in accordance with IACUC approved protocols from Louisiana Tech University. Male Sprague-Dawley rats weighing 250 gm-350 gm were used in this research. The rats were given food and water properly before the experiments, and the proper room temperatures and lighting were maintained. The pilocarpine seizure model was studied on rats with two different protocols.

3.6.2.1 Pilocarpine Protocol 1

Tri-polar concentric ring electrodes were used for recording. The animals were given a small dosage of ketamine (100 mg/Kg, Sigma, St. Louis, MO) through i.p. and the rat head was shaved and prepared with NuPrep™ abrasive gel. The rats were kept in an animal restrainer (BS4-52-0292, Harvard Apparatus, Holliston, MA). To stabilize the head it was fixed in position using a mouth piece attached to a stereotaxic table. The concentric ring electrodes along with reference electrode were attached on the scalp with Ten20 conductive gel. One of the electrodes was placed at location CZ and two others at C3 and C4 locations as shown in Figure 21. Scopolamine methylnitrate (2 mg/Kg i.p., Sigma, St. Louis, MO) was administered 30 min before the pilocarpine and

approximately 45 min after the ketamine injection. This waiting time after the ketamine was observed for several animals and in 30 to 45 min the animals were out of anesthesia and appeared to regain full facilities. Scopolamine was given to stop the peripheral cholinergic effects [35]. The skin-to-electrode impedance was measured with Biopac impedance meter 15 min after the scopolamine. Baseline LEEG recordings were taken 20 min after the scopolamine injection. Pilocarpine (300-400 mg/Kg, Sigma, St. Louis, MO) was administered to induce fast acting prolonged seizures [36-37]. The recordings were taken with custom-build pre-amplifiers along with a 15LT Grass amplifier. The pre-amplifier were described in the Results section while describing the development of Laplacian EEG instrumentation. The total gain was kept at 100,000; frequency pass band was set from 3 Hz to 30 Hz and the signals were digitized at 500 samples per second with a DI720 data acquisition system. The animal behavior was observed and noted during the entire experiment. The experiments were video monitored to verify the behavioral activity later. The signals recorded during this experiment were observed to determine the different stages of seizures [36-37].

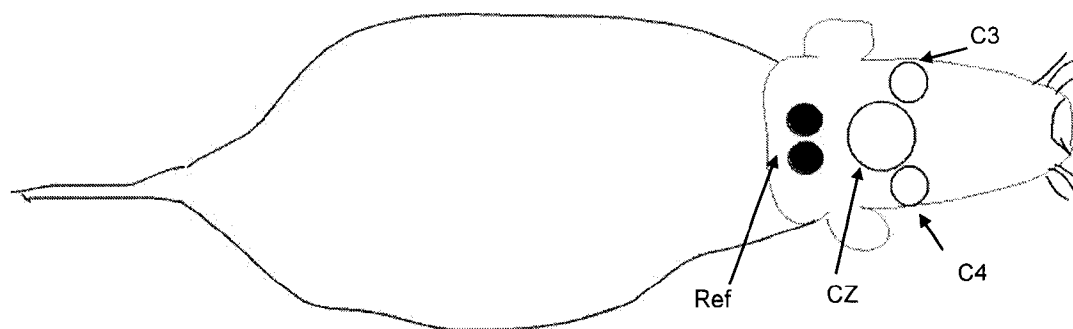


Figure 21 Position of tri-polar electrodes on the rat head for pilocarpine seizure model.

3.6.2.2 Pilocarpine Protocol 2

The animals were given a small dose of ketamine (100 mg/Kg) for preparation on the day before the experiment approximately 21 h before the experiment. The rat head was shaved and prepared with NuPrep™ abrasive gel and tri-polar concentric ring electrodes were placed on the scalp with a 0.5 mm thick layer of Ten20 conductive paste. One 1.0 cm outer diameter tri-polar electrode was placed at CZ and two 6.0 mm outer diameter tri-polar electrodes were placed at C3 and C4. These electrode positions were the same locations as in Protocol 1 shown in Figure 21. The tri-polar concentric ring electrodes had a small pigtail of approximately 7 cm long 3~4 conductor flexible shielded cable and a four pin connector attached to them. After placing the electrodes on the scalp with Ten20 conductive paste, the electrodes were fixed in place using dental acrylic (CO-ORA-LITE Dental Mfg Co., Diamond Springs, CA). The rats were returned to their standard living conditions. They were given food and water and monitored until the experiment.

Scopolamine methylnitrate (2 mg/Kg i.p.) was administered 30 min before the pilocarpine. Scopolamine was given to stop the peripheral cholinergic effects. Pilocarpine (310 mg/Kg) was administered via i.p. to induce the fast acting prolonged seizures [36-37]. The pilocarpine was injected approximately 21 h after the ketamine injection. The animals showed no signs of anesthesia before the pilocarpine injection.

In this model the animals were kept in their cage and allowed to move freely since the electrodes were fixed to their scalp and connected to a recording system through 60 cm cables and four pin connectors to small pigtail on the electrodes. The animals were behaviorally observed from the time of the scopolamine injection, and behavioral activity

and behavioral seizures were noted after the injection of pilocarpine. The recordings were taken using custom-built pre-amplifiers along with Grass 15LT amplifiers. The pre-amplifiers were described in Results section while describing the development of Laplacian EEG instrumentation. The total gain was 100,000; frequency band pass from 3 Hz to 30 Hz, digitized at 500 samples per second with a DI720 data acquisition system at 16 bit resolution. The recorded LEEG activity was analyzed for different stages of seizures of the pilocarpine seizure model [36-37]. The whole experiment was video monitored for later review.

3.7 Statistical Analysis

Statistical analysis is an important aspect of any part of research for understanding the results. In this research two statistical analysis procedures are mainly used.

3.7.1 ANOVA

A one-way ANOVA or single-factor ANOVA tests differences between groups that are classified with only one independent variable [38]. The advantage of using ANOVA rather than multiple t-tests is that it reduces the probability of a type-I error. One potential drawback to an ANOVA is that it cannot tell the difference specifically. ANOVA relates that there is a significant difference between groups, but not which groups are significantly different from each other [39]. A post-hoc comparison is necessary to find out where the differences and which groups are significantly different from each other and which are not. Single-factor ANOVA is performed using an inbuilt function in Microsoft[®] Excel (Microsoft Corporation, Redmond, WA) data analysis toolbox.

3.7.2 Bonferroni Statistical Test

ANOVA suggests that there is a significant difference between groups. Multiple comparison procedures are then used to determine which means are different from each other [38-39]. The Bonferroni [40] correction, a post-hoc comparison is a multiple-comparison correction used when several dependent or independent statistical tests are being performed simultaneously. Bonferroni correction sets the α value for the entire set of n comparisons equal to α by taking the alpha value for each comparison equal to α/n .

Bonferroni tests were performed using a custom program in SAS[®] (SAS Institute Inc., Cary, NC) analysis software or using a custom program in Matlab.

CHAPTER 4

RESULTS

4.1 Calculation of Laplacian Potentials Using Computer Model

4.1.1 Calculation of Laplacian Potential for Single Source Computer Model

Laplacian potentials simulated from a single-unit dipole source computer model for an electrode of outer diameter 2.0 cm and 1.0 cm depth were calculated for bipolar, quasi-bipolar and tri-polar concentric ring electrodes using Equations (2.10), (2.11) and (2.18) respectively. The Laplacian potentials were plotted for three electrode configurations namely bipolar, quasi-bipolar and tri-polar electrodes when the dipole traversed from -5.0 cm to 5.0 cm along the X-axis and -5.0 cm to 5.0 cm along the Y-axis for a depth 1.0 cm. These Laplacian potentials were shown in 3-D maps in Figures 22-24 for bipolar, quasi-bipolar and tri-polar electrode configurations, respectively. The Laplacian potentials calculated from tri-polar electrodes have sharper peaks than bipolar and quasi-bipolar electrodes which can be observed in Figure 24. The sharpness of peaks were calculated using the attenuation of Laplacian potentials along the radial distance and were given later in this section for all the concentric ring electrodes.

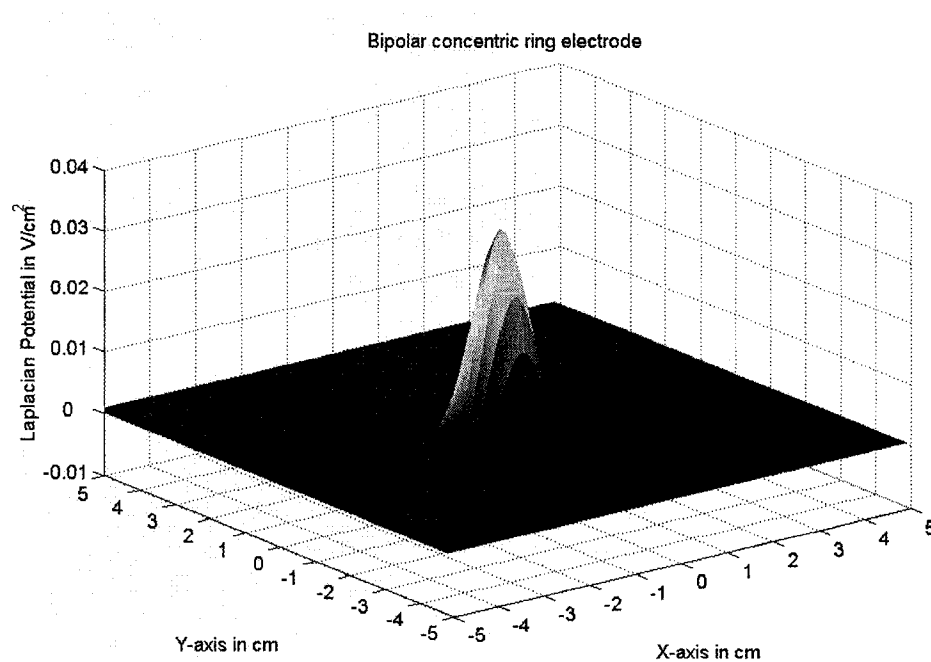


Figure 22 Laplacian potentials for bipolar concentric ring electrode.

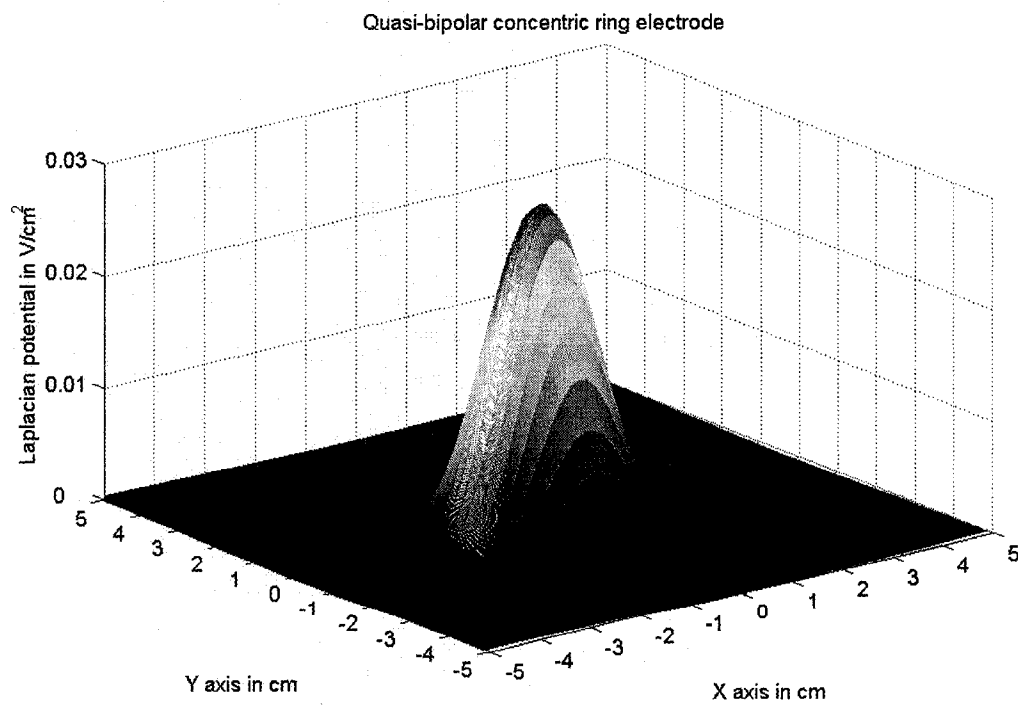


Figure 23 Laplacian potentials for quasi-bipolar electrode.

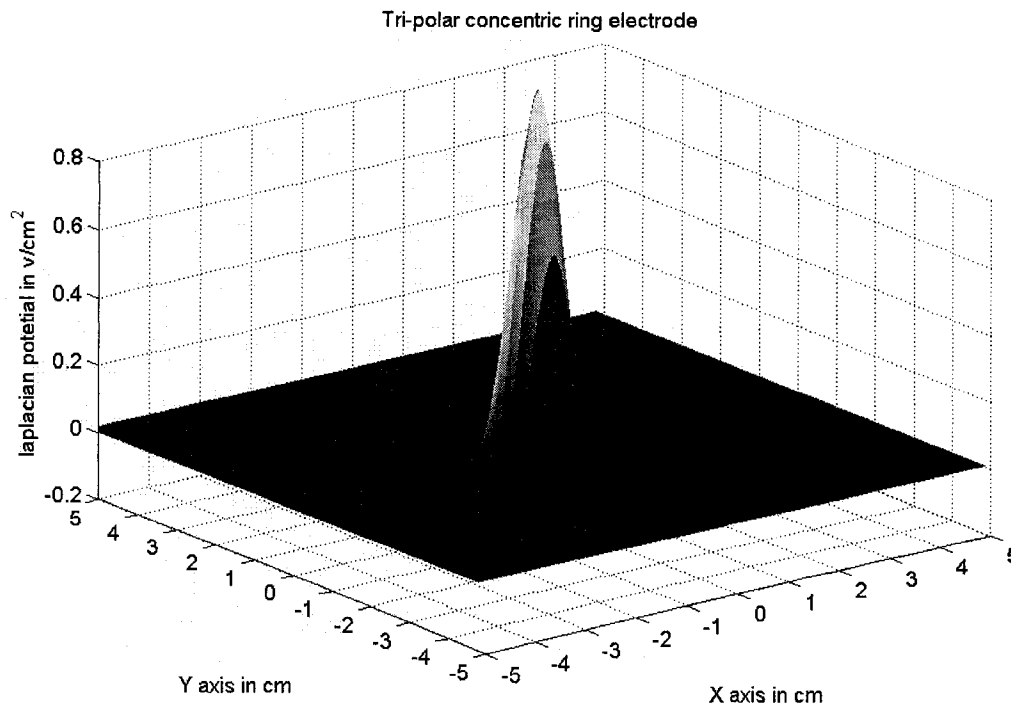


Figure 24 Laplacian potentials for tri-polar electrode configuration.

The Laplacian potentials calculated along the X-axis and $Y=0$ for different electrode configurations bipolar, quasi-bipolar and tri-polar were plotted in Figure 25 panels (A), (B), and (C) respectively. The electrode size and depth were kept the same as in the tank experiments to make the direct comparisons easier. The attenuation of the potentials due to distance along the radial axis was calculated using (3.4) for all three electrode configurations. The attenuation of Laplacian potential with the radial distance was plotted in Figure 26. The attenuation values were shown in dB units. The attenuation values were calculated for only one side as the concentric ring electrodes show symmetry on the other side, concentric electrodes are isometric electrodes. The radial distance for an attenuation of 20 dB can be compared as a measure of local sensitivity: bipolar electrode 0.65 cm, quasi-bipolar electrode 1.2 cm and tri-polar

electrode 0.5 cm which can be observed in Figure 26. The attenuation of the electrodes with radial distance is taken as a measure for electrode localization, sensitivity.

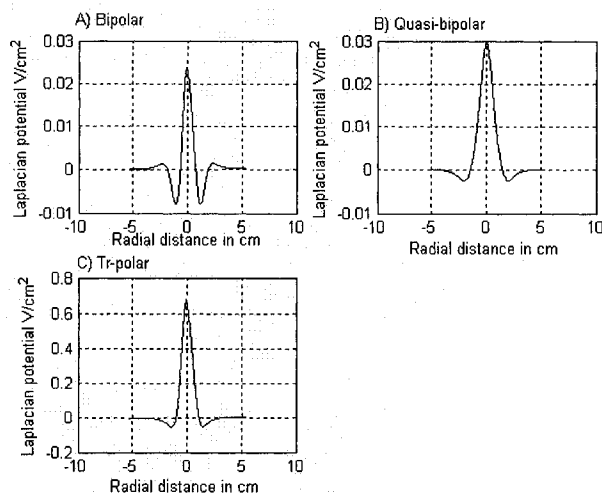


Figure 25 The Laplacian potentials for single unit dipole source computer model for 2 cm outer ring diameter electrode.

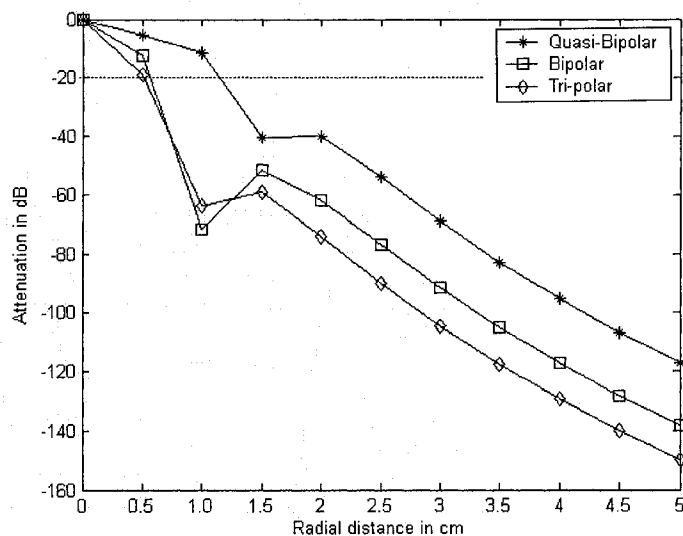


Figure 26 Attenuation of Laplacian signals for three electrode configurations from single unit dipole source computer model.

The attenuation of Laplacian potentials from all concentric ring electrode configurations were then compared with the attenuation of potentials from a disc

electrode of size 2.0 cm with a source dipole at depth 1.0 cm. These attenuation values from concentric and disc electrodes are shown in Figure 27.

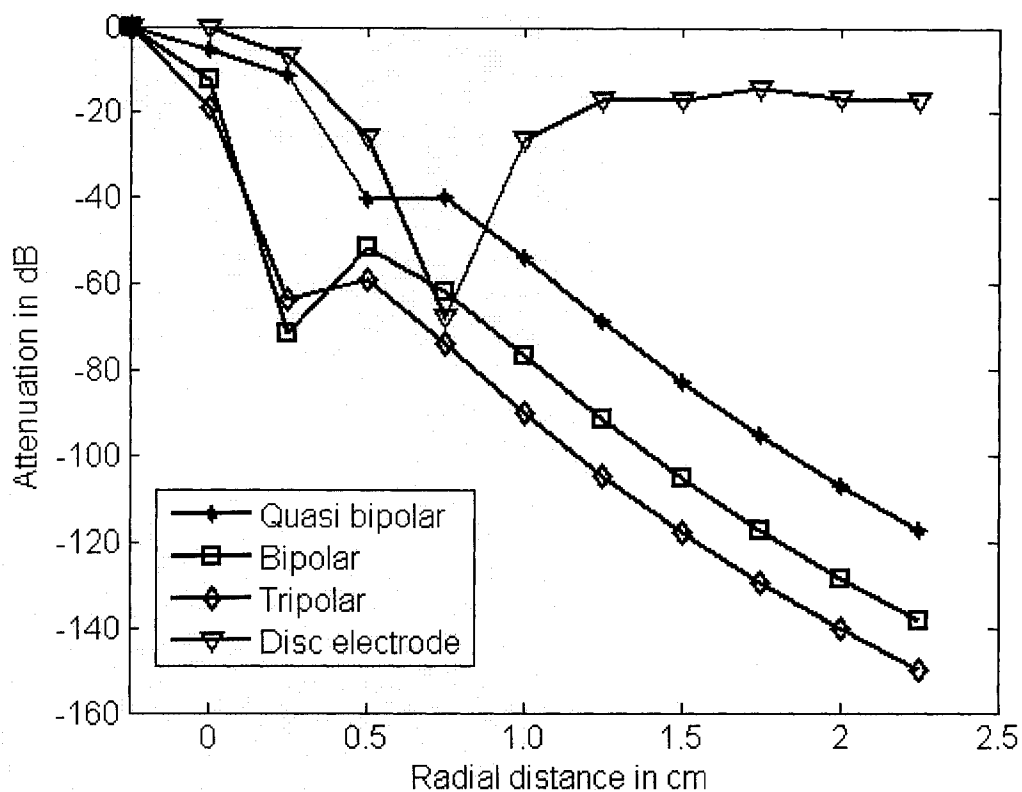


Figure 27 Attenuation of Laplacian signals for three electrode configurations and conventional disc electrodes from single unit dipole source computer model.

An ANOVA test ($p = 1 \times 10^{-4}$) also revealed that the tri-polar electrode had steeper attenuation and better global signal rejection compared with the other two configurations, bipolar and quasi-bipolar. The Bonferroni t-tests revealed that the tri-polar electrode had the highest attenuation over the bipolar and quasi-bipolar electrode configurations at the 1% significance level [41].

4.1.2 Calculation of Laplacian Potential for Multiple Source Computer Model

Figure 28 shows normalized Laplacian potentials for (A) bipolar, (B) quasi-bipolar, and (C) tri-polar electrode configurations. The traces in Figure 28 were derived from a computer model with a single constant unity dipole and multiple random unity dipole sources. The concentric ring electrode had an outer diameter of 2.0 cm and dipole plane was 1.0 cm below the concentric ring electrode location. The attenuation of the potentials due to distance along the radial axis was calculated using Equation (3.4) for the same three configurations. The attenuation of Laplacian potential with respect to radial distance was plotted in Figure 29. The attenuation values were shown in dB units.

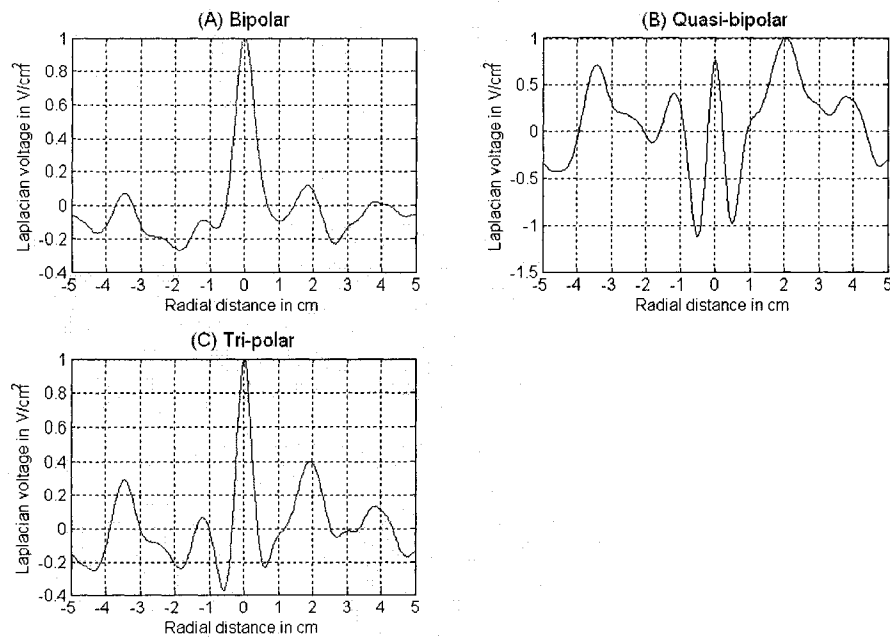


Figure 28 Normalized Laplacian potentials calculated from single constant unit dipole source and multiple random unit dipole source computer model.

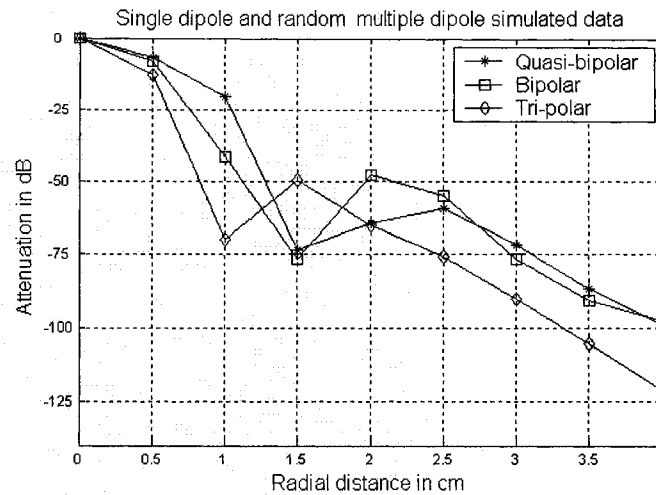


Figure 29 Attenuation values for single constant unit dipole and multiple random unit dipole source computer model.

As with the single source computer models an ANOVA tests ($p=3 \times 10^{-5}$) also revealed that the tri-polar electrode had the steeper attenuation and best global signal rejection compared with the other two configurations, bipolar and quasi-bipolar in the noisy environment. The Bonferroni t-tests revealed that the tri-polar electrode had significantly higher attenuation over bipolar and quasi-bipolar electrode configurations at the 1% significance level.

4.2 Tank Experimental Results

Signals from all three elements of concentric ring electrodes were recorded using the DaqCard 700 via a custom LabView program. The potentials recorded for a concentric ring electrode of 2.0 cm outer ring diameter, 1.06 cm middle ring diameter and 2.8 mm diameter disc are shown in Figure 30.

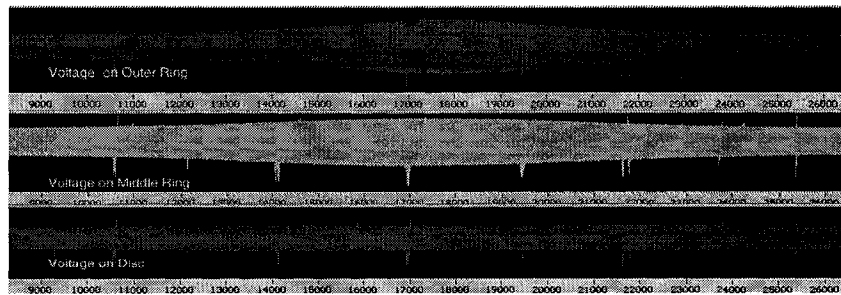


Figure 30 A typical recording from the three elements of tri-polar concentric electrodes during tank experiments.

The data were further processed with a custom Matlab program. The envelope of the signal was found to determine the voltages on each element of the tri-polar electrode. The processed voltages from each electrode element for one experiment are shown in Figure 31.

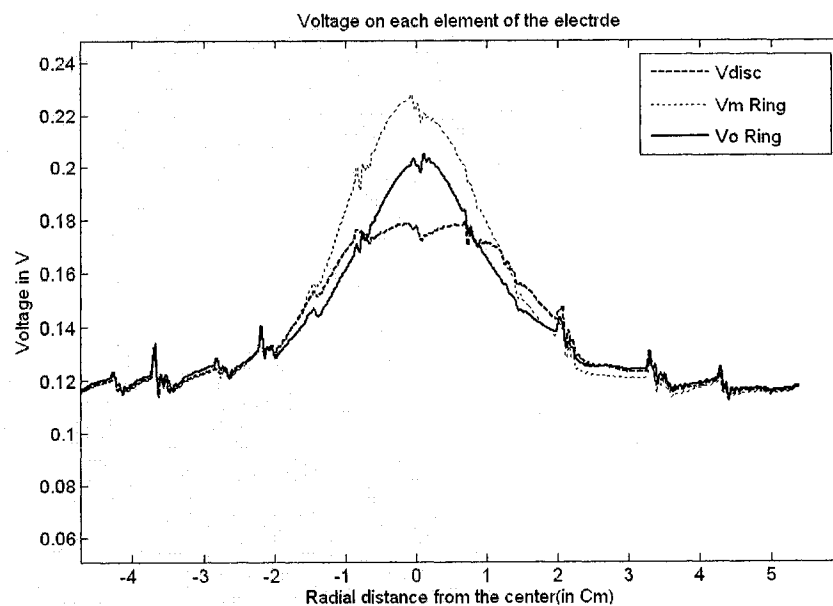


Figure 31 The voltages from each element of tri-polar concentric ring electrode. V_{disc} - potential on the disc, V_m ring - potential on middle ring, and V_o ring - potential on outer ring.

The Laplacian potentials were calculated using the Equations (2.10), (2.11), and (2.18) for bipolar, quasi-bipolar, and tri-polar electrode configurations and are shown in Figure 32 panels (A), (B), and (C) respectively. The Laplacian potentials are plotted with different vertical scales. The attenuation values in dB for the data displayed in Figure 32 were calculated using Equation (3.4) and plotted in Figure 33.

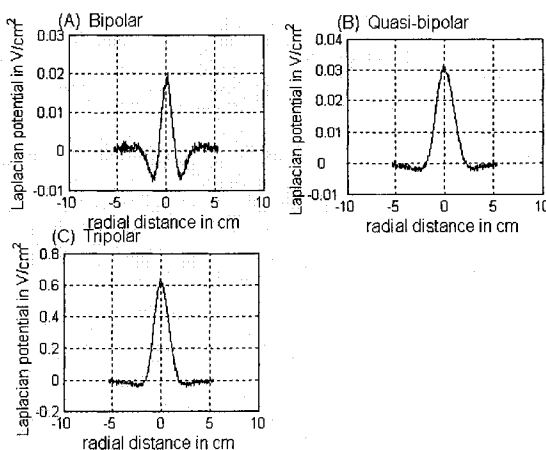


Figure 32 Laplacian potentials recording during tank experiments for a 2.0 cm diameter (A) bipolar, (B) quasi-bipolar, and (C) tri-polar electrode configurations.

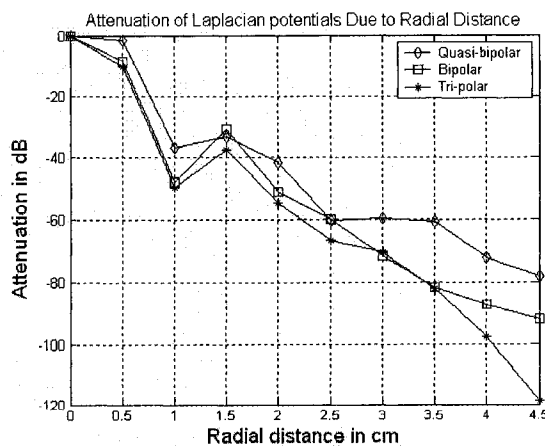


Figure 33 Attenuation in dB calculated from tank experimental data for the three electrode configurations of a 2.0 cm diameter electrode due to radial distance from the center of the electrode.

A single-factor ANOVA ($p=1.07 \times 10^{-4}$) revealed that the tri-polar configuration was significantly superior, with steeper attenuation compared with the other two electrode configurations. The results from Bonferroni t- tests also showed that the tri-polar electrode had significantly sharper attenuation than the bipolar and quasi-bipolar electrode configurations.

4.3 Verification of Single Source Computer Model with Tank Experiments

For comparison of the computer modeling and tank experiments, an electrode size of 2.0 cm outer diameter was used both in the simulations and tank experiments. In Figure 34, a comparison of attenuation in dB was shown between the computer model and measured tank experimental data for each of the three configurations, bipolar, quasi-bipolar, and tri-polar, panels (A), (B), and (C) respectively. Attenuation vs. radial distance was plotted in each of the three panels with the tri-polar configuration showing the greatest attenuation for all electrode configurations tested. A cross correlation was performed between the attenuation data of the closed form moving dipole computer model and tank experiment data. The cross-correlation coefficient was 0.82 ± 0.1 . In Figure 35, the comparison of localization for the three configurations was plotted for the closed form moving dipole computer model and measured potentials from the tank experiment.

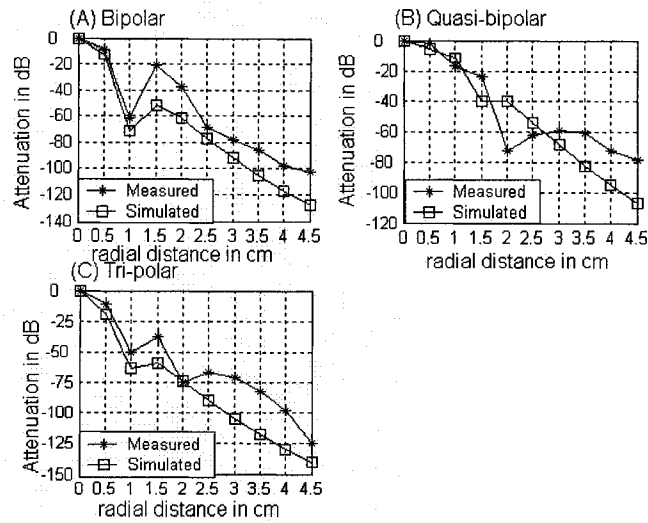


Figure 34 Comparison of tank experimental results (measured) with computer simulation (simulated) of a single unit dipole source computer model.

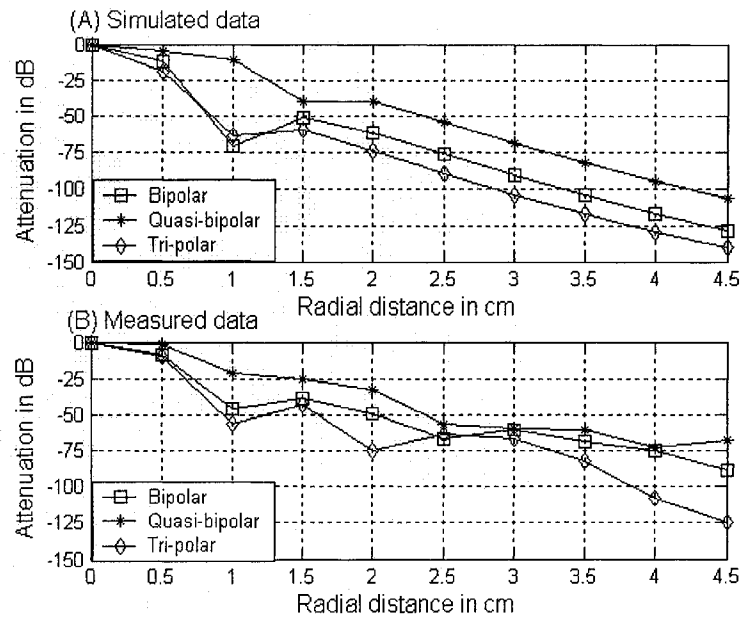


Figure 35 Comparison of attenuation for three electrode configurations, quasi-bipolar, bipolar, and tri-polar electrode.

4.4 Human EEG Recording Using Tri-polar Laplacian Electrode

Figure 36 Panel (A) shows LEEG recordings from subject 3 which is similar to other recordings. All the EEG rhythms were plotted using a custom Matlab program and the rhythms are shown in Panel (B) Alpha, Panel (C) Beta, Panel (D) Delta, and Panel (E) Theta. It was observed that the LEEG signal had more Alpha rhythm when the eyes were closed. The mean Alpha rhythm was $15\mu\text{V}$ during the initial 25 sec when the eyes were closed but only $7\mu\text{V}$ during the following 25 sec when the eyes were open. The Alpha rhythm shows up best in Panel (B) of Figure 36 during first 25 sec of the trace when the eyes were closed.

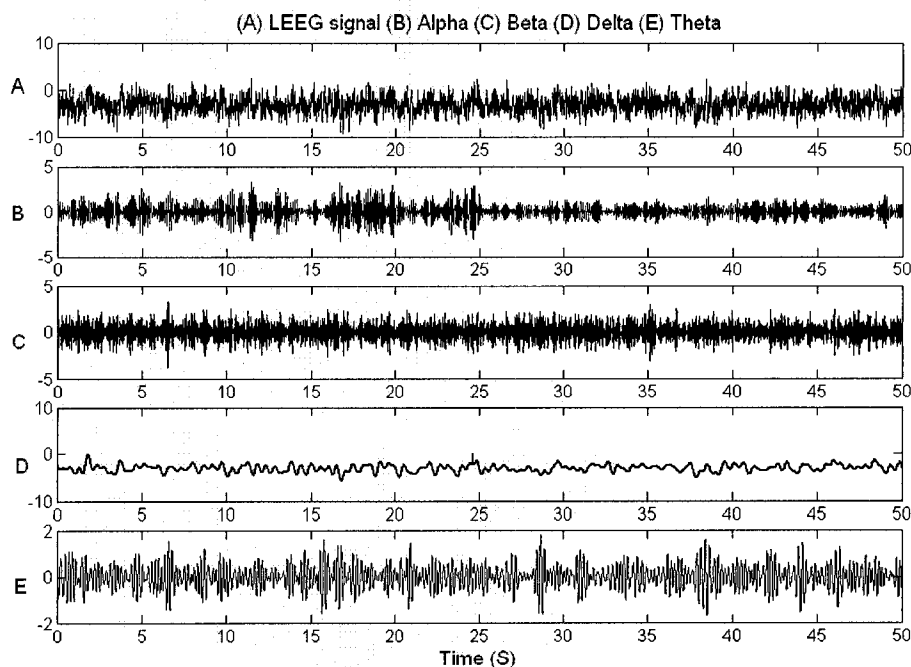


Figure 36 Laplacian EEG recording from humans to verify the alpha rhythms with eyes closed position. (A) LEEG signal (B) Alpha rhythm (C) Beta rhythm (D) Delta rhythm and (E) Theta rhythm.

4.5 Recording of Movement-Related Potentials from Pre-frontal Lobes

The MRP signals recorded from the FP1 location using a conventional disc electrode is shown in Figure 37, trace (B) along with the state of the micro-switch in trace (A). The data recorded from tri-polar concentric ring electrodes at the same FP1 location is shown in Figure 38. The signals from a concentric ring electrode were recorded in differential mode, outer ring to disc trace (B) and middle ring to disc trace (C) along with the state of the micro-switch trace (A).

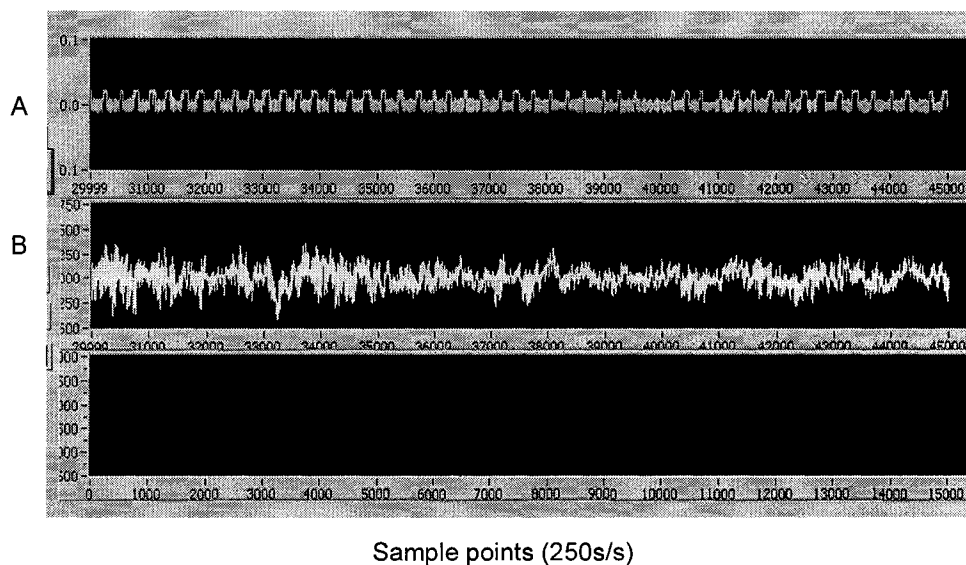


Figure 37 MRP signals recorded using conventional disc electrodes (B) and micro-switch state (A).

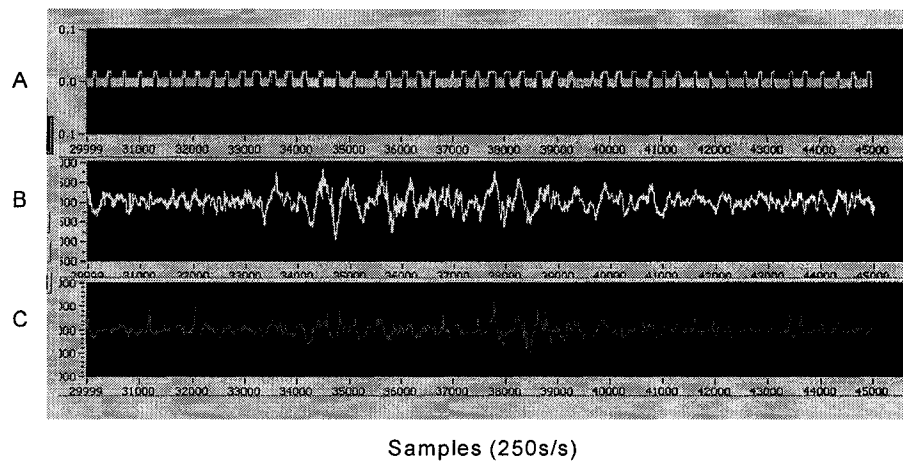


Figure 38 MRP signals recorded using concentric ring electrodes. Trace (B) outer ring-disc, trace (C) middle ring-disc and trace (A) is reference from micro-switch.

The MRP signals recorded with the different electrode systems were pre-processed using custom Matlab programs. The signals were pre-processed to remove 60 Hz. The EOG artefacts were removed with threshold detection. If the EEG or LEEG recordings were greater than absolute 0.5 V (after amplification), then that window was neglected considering it as an artefact. The micro-switch signal was used as a time reference of the movements. Threshold detection was used to find the time of movements using the rising edge of the micro-switch signal. The recordings from concentric ring electrodes were used to calculate the Laplacian potentials for the different concentric ring electrode systems using Equations (2.10), (2.10) and (2.18) for bipolar, quasi-bipolar and tri-polar concentric ring electrode respectively. The EEG and LEEG were divided into windows of one sec (499 ms before and 500 ms after the movement). For each subject and electrode system, approximately 150 artefact free trials were ensemble averaged for each location to form the MRPs. Time zero was the rising edge of the micro-switch state signal.

The MRP signals recorded from subject 2 are shown in Figure 39 from the conventional disc electrodes. Figure 40 shows the MRP signals recorded from a bipolar concentric ring electrode, Figure 41 from a quasi-bipolar concentric ring electrode, and Figure 42 from a tri-polar concentric ring electrode. The MRP signals recorded from all the electrodes are again shown Figure 43 to ease the comparison. The signals from the quasi-bipolar electrodes are very small and they are shown in inset form. The signals recorded from conventional disc electrodes have an 8 Hz signal evident on them. MRP signals recorded from all the electrode configurations under test have a post-movement negative peak around 100 ms and a positive peak [31] at 275 ms on average for all the subjects.

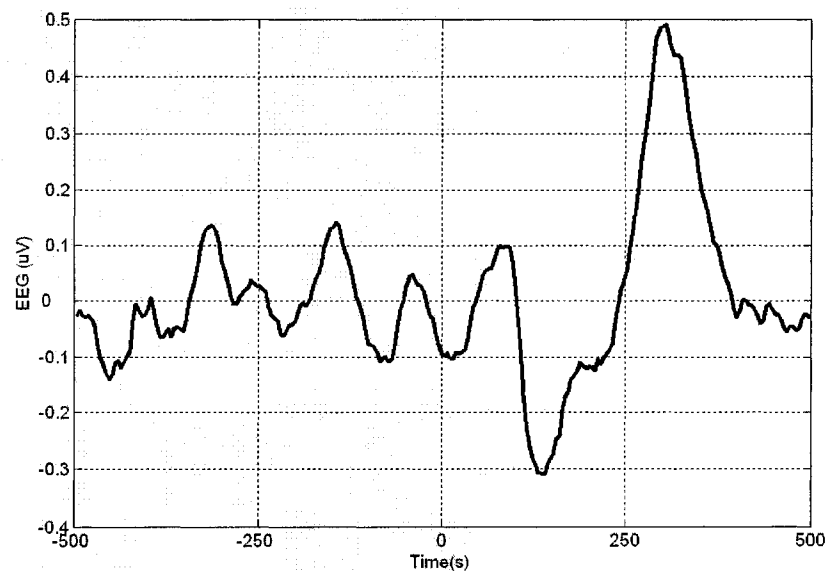


Figure 39 MRP signals recorded from conventional disc electrodes from the FP1 location.

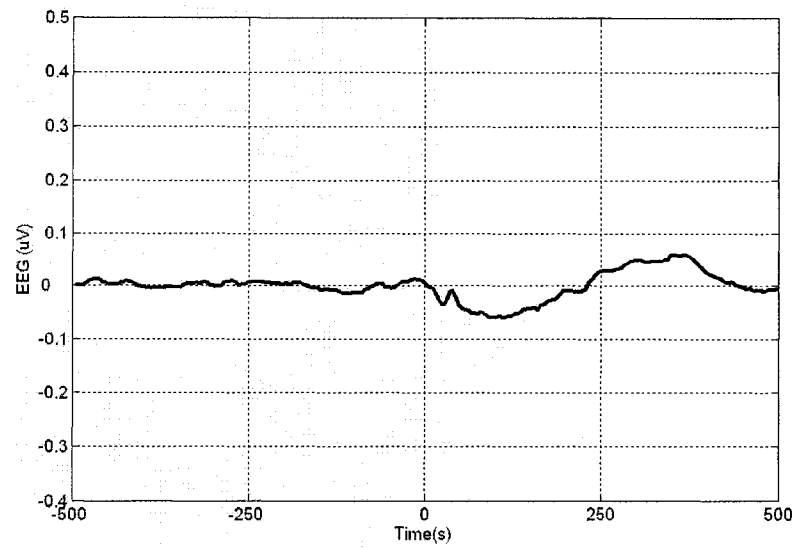


Figure 40 MRP signals recorded from bipolar concentric electrodes from the FP1 location.

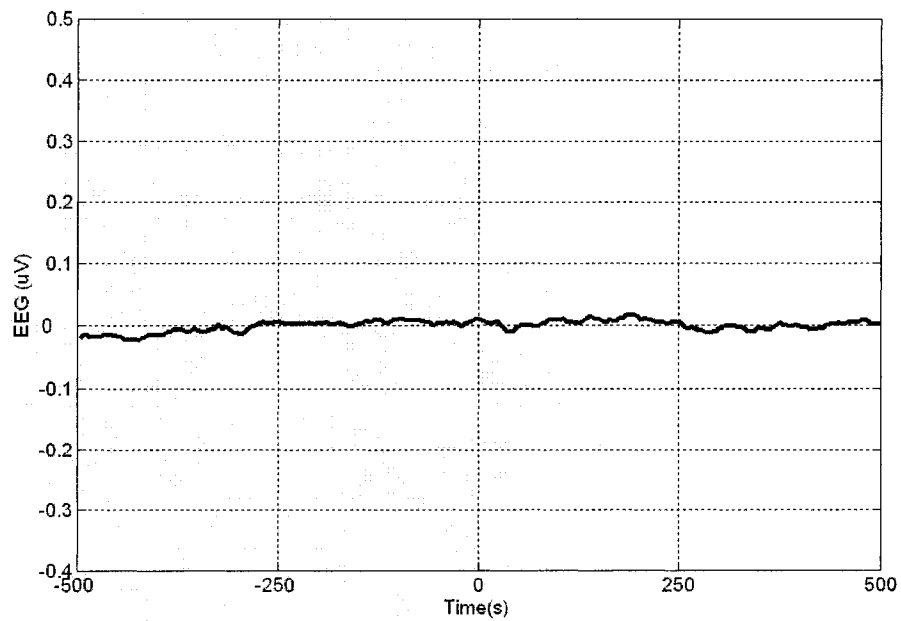


Figure 41 MRP signals recorded from quasi-bipolar concentric ring electrodes from the FP1 location.

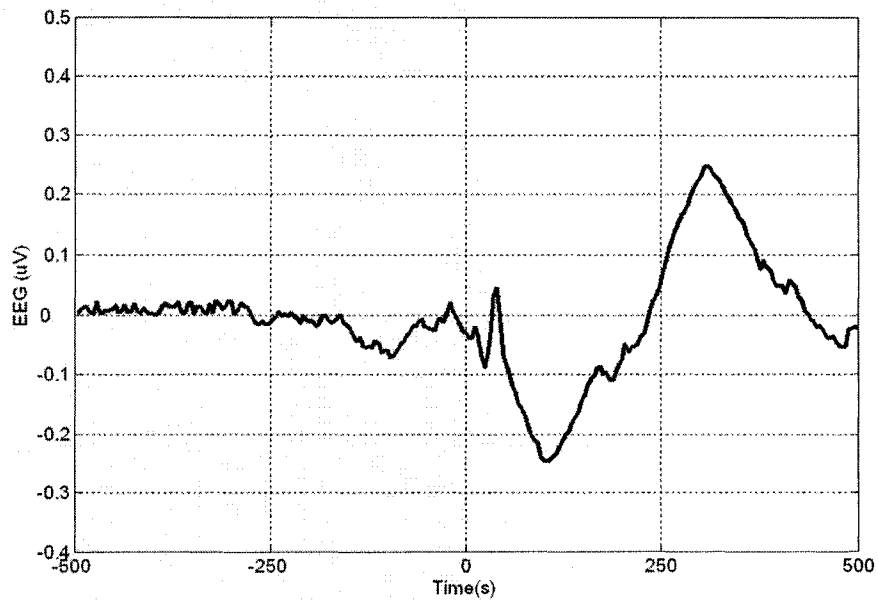


Figure 42 MRP signals recorded from tri-polar concentric ring electrodes from the FP1 location.

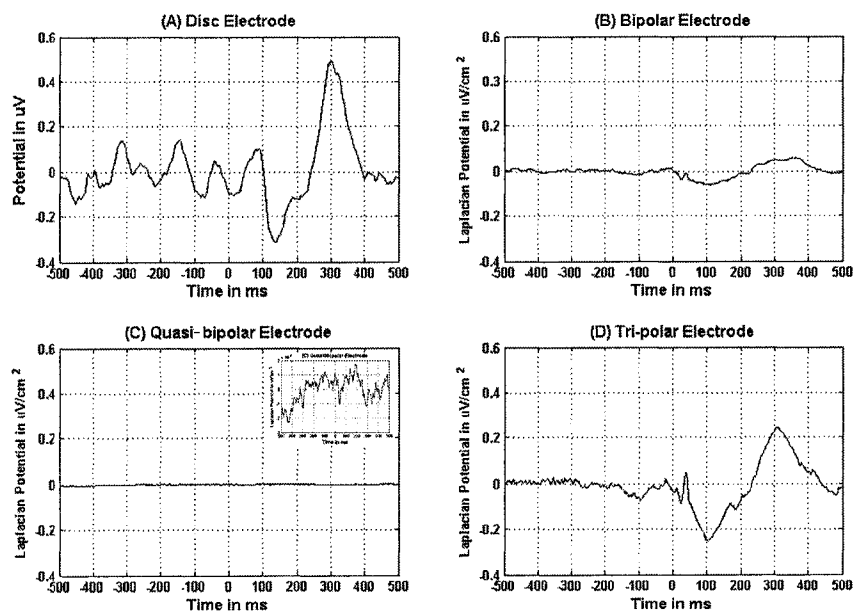


Figure 43 MRP recordings using (A) conventional disc EEG electrodes, (B) bipolar concentric ring electrode, (C) quasi-bipolar concentric ring electrode, and (D) tri-polar concentric ring electrode.

The SNR was calculated for different electrode systems according to Equation (3.5) based on the peak signal-to-noise signal ratio defined by Klug [31]. The SNR for different electrode systems for MRP signals recorded from the FP1 location are shown in Table 1. The average SNR for conventional disc electrodes is 7.36, 18.96 for bipolar concentric electrodes, 1.4 for quasi-bipolar concentric electrodes and 30.77 for tri-polar concentric electrodes. The quasi-bipolar electrodes have very low SNR which is evident from Figure 46 Panel (C). The post-movement peaks are not clearly visible in the quasi-bipolar electrode recording. As the clear peaks not observed with quasi-bipolar, the peak timing is taken same as the others to make the comparison simple. The signals recorded with tri-polar electrodes showed higher SNR than the other electrode systems tested. The SNR data were analyzed using a single-factor ANOVA and Bonferroni tests. The SNR of the tri-polar concentric ring electrode signals showed significant improvement ($p=1.58 \times 10^{-6}$) over the SNR of bipolar concentric ring electrodes, quasi-bipolar concentric ring electrodes and conventional disc electrodes.

Table 1 SNR for different electrodes at FP1 location

	Disc	Bipolar	Quasi-bipolar	Tri-polar
Subject1	5.78	23.384	1	31.998
Subject2	7.85	18.9424	1.736	29.4806
Subject3	4.7803	20.657	2.0885	30.3197
Subject4	6.486	18.9501	1.2311	30.6068
Subject5	11.94	19.8913	0.981	31.4565
Average	7.36726	18.96294	1.40732	30.77232

4.6 Development of Laplacian EEG Amplifier System

4.6.1 Development of Two-Channel Pre-Amplifier System

The two-channel pre-amplifier system was developed out of necessity due to the magnitude of our signals from small concentric electrodes. The two-channel pre-amplifier was used to acquire LEEG signals from a single tri-polar concentric ring electrode at location FP1 and the output of the pre-amplifier was connected to the Grass 15LT physiological amplifier system to further amplify and reduce the 60 Hz noise through a built in notch filter of 15LT amplifier. These pre-amplifiers have two stages as shown in Figure 44. The two-channel pre-amplifier consists of (i) differential amplifier with a gain of 5, (ii) high pass filter with a gain of 2 in the inverted Sallen-Key topology. This Sallen-Key topology is a second order high pass filter. The advantage of using Sallen-Key topology is it is the best design for low gain amplification, for accurate gain and it uses fewer of components than other topologies. The lower cutoff for the high pass filter was set at 0.3 Hz to reduce the DC offset without reducing the components of LEEG. These same pre-amplifiers were used to record from the conventional disc electrodes as well. The circuit was first tested on a breadboard. Then the circuit was laid out in Cadence ORCAD Layout software. This circuit was then made using LPKF C-20 computer controlled router circuit prototype machine. The power supply circuit was designed using the Max 663 and Max 664 (Dallas Semiconductors/Maxim, Dallas, Texas USA) regulators. The regulated power supply circuit is shown in Figure 45. The regulated power supply was powered using two 9V batteries.

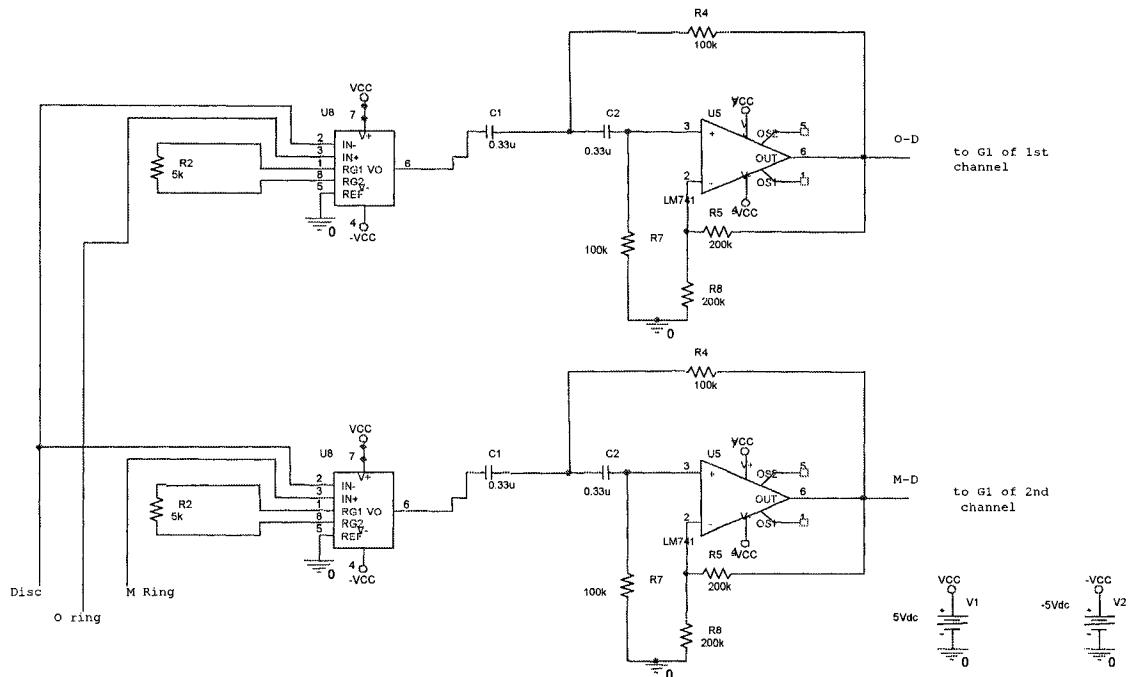


Figure 44 Two channel pre-amplifier system.

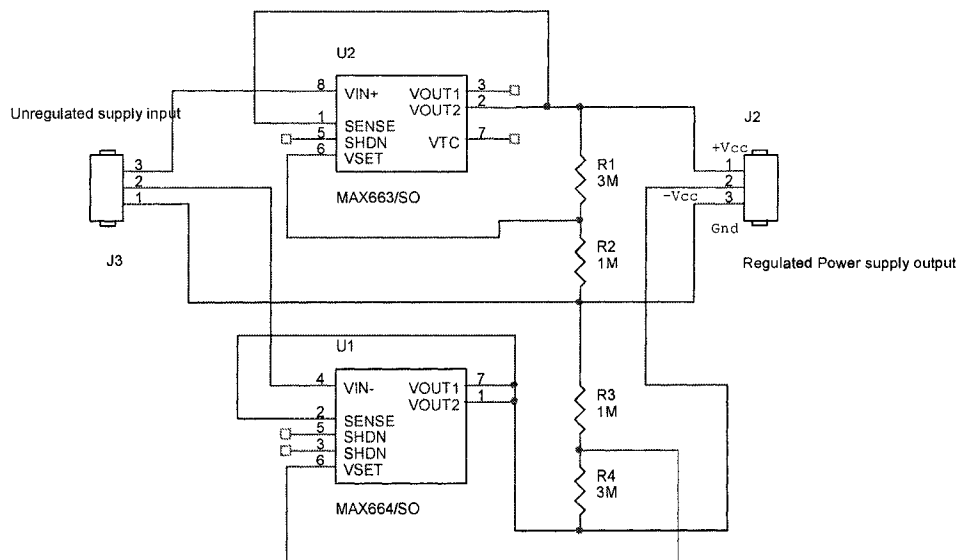


Figure 45 Regulated power supply using Max 664 and Max 663.

The two-channel pre-amplifier circuit developed for recording LEEG from FP1 was further modified to accommodate three channels. The three-channel pre-amplifier

system was developed to record LEEG signals from the seizing animals during the penicillin model seizure experiments. The three-channel pre-amplifier system is shown in Figure 46. Decoupling capacitors and connectors were included to reduce the noise. The three-channel amplifier circuit was drawn with ORCAD Cadence capture and laid out. The three channel pre-amplifier system was also built with the LPKF C-20, a computer controlled router circuit prototype machine and surface mount components were used to assemble the circuit. Figure 47 is an image of the final three-channel pre-amplifier system. The same power supply circuit as shown in Figure 45 was used for the three-channel pre-amplifier system as well.

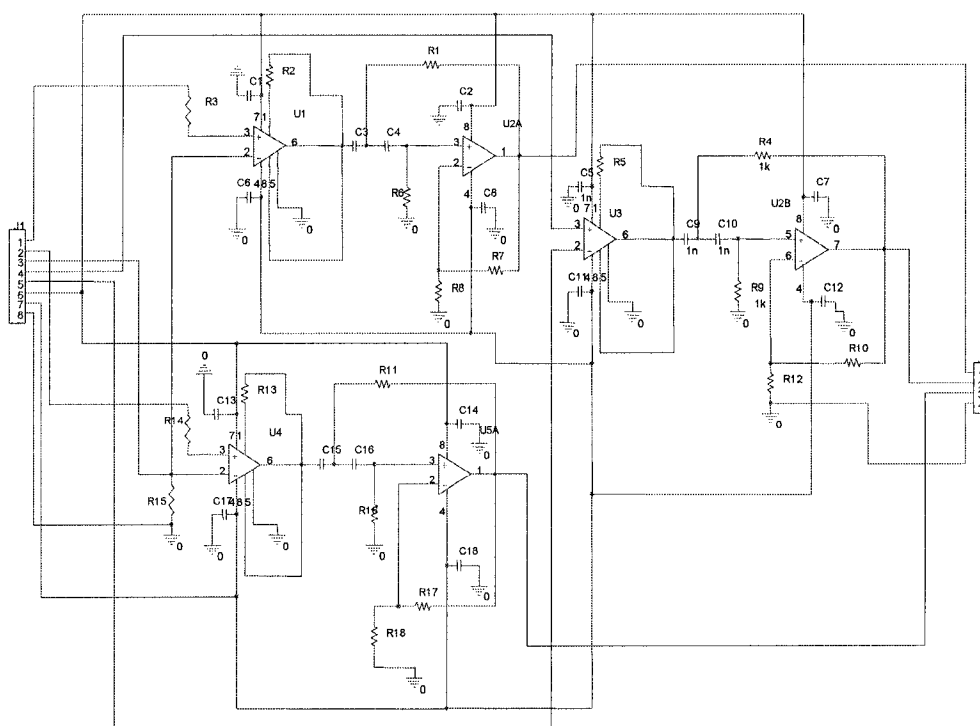


Figure 46 Three-channel pre-amplifier circuit drawn in Orcad Capture.

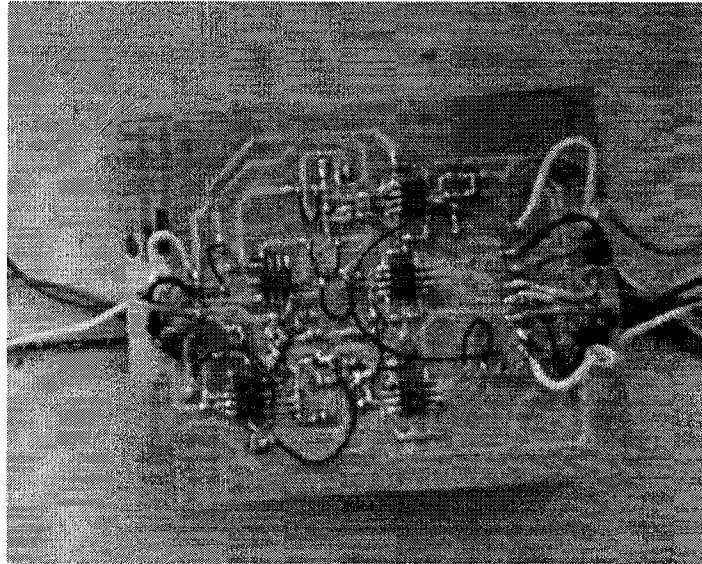


Figure 47 Three-channel pre-amplifier system used for recording LEEG from seizing animals.

4.6.2 Development of Three-Channel Amplifier System

Based upon the pre-amplifiers developed and discussed in section 4.6.1, a three-channel amplifier was developed. The amplifier had four stages for each channel. They were (i) Differential amplifier stage (ii) High-pass filter stage (iii) Third-stage low-pass filter (iv) Fourth-stage low-pass filter. The three-channel amplifier was developed to record one channel of ECG and two channels of differential LEEG from the (outer ring-disc) potential and the (middle ring-disc) potentials. The ECG channel only had three stages as it requires less gain compared with the LEEG channels. The single channel LEEG amplifier circuit is shown in Figure 48. This circuit has a differential amplifier with a gain of 5. The high-pass filter cut off was set to 0.3 Hz with a gain of two. This high-pass circuit is having same topology as second order Sallen-Key topology. As the LEEG system requires higher gain, a second order multi-feedback (MFB) low-pass amplifier topology was used. To further increase the stability and achieve higher gain,

this low pass filter stage was again divided into two different stages with a gain of 50 for one stage and 10 for other. The combination of Sallen-Key along with MFB results in the best possible stable design for the amplifier system. This single channel amplifier system was modified for recording LECG for the seizure animal experiments. The LECG channel had just three stages and a total gain of 10,000. The LEEG with two-channels and a LECG channel was built on a bread board. The block diagram of the three-channel amplifier system is shown in Figure 49. The three-channel amplifier system on the bread board is shown in Figure 50. The three-channel system was later modified to accommodate 15-channels of LEEG.

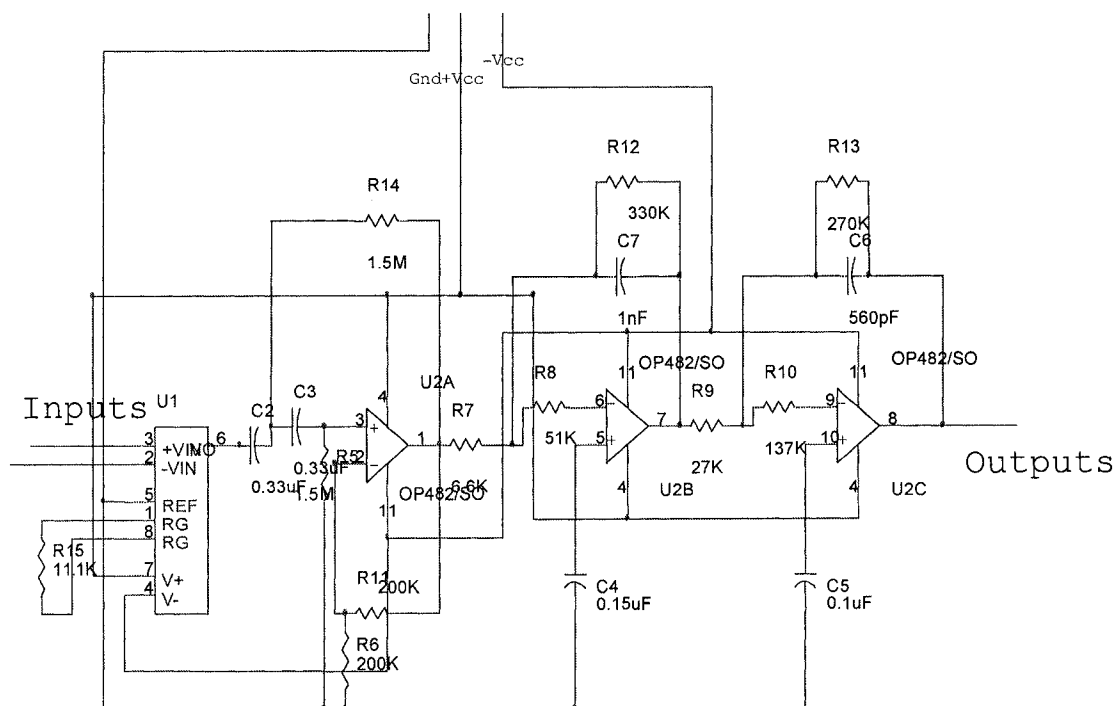


Figure 48 Single channel LEEG system with Sallen-Key and MFB topology.

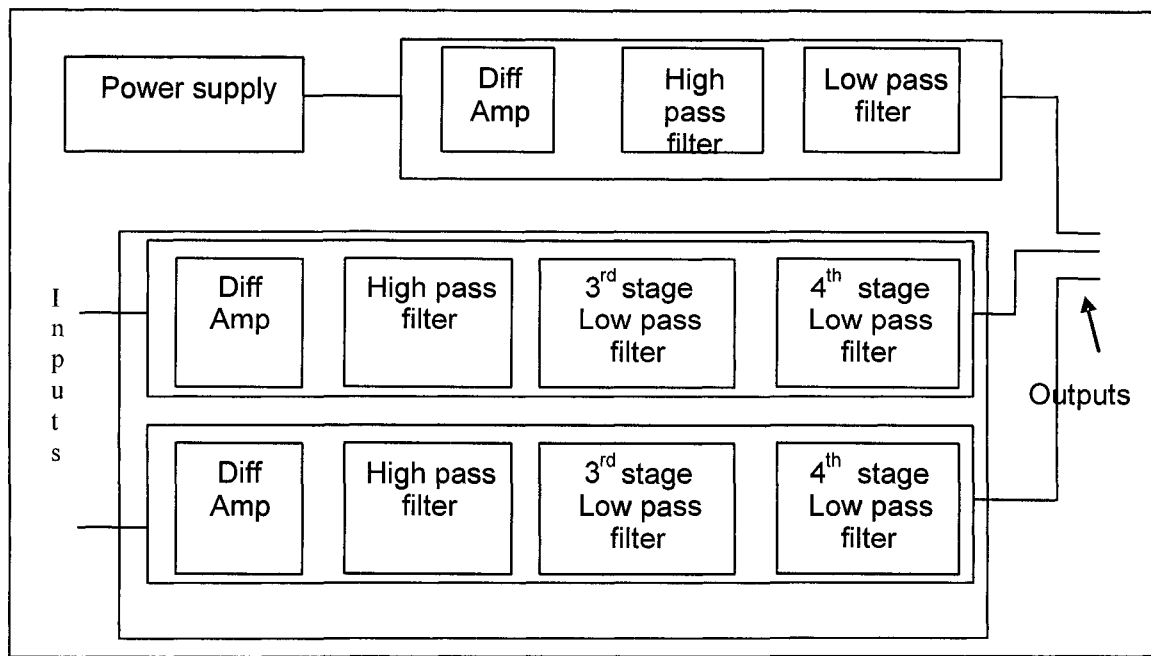


Figure 49 Block diagram of three-channel amplifier system.

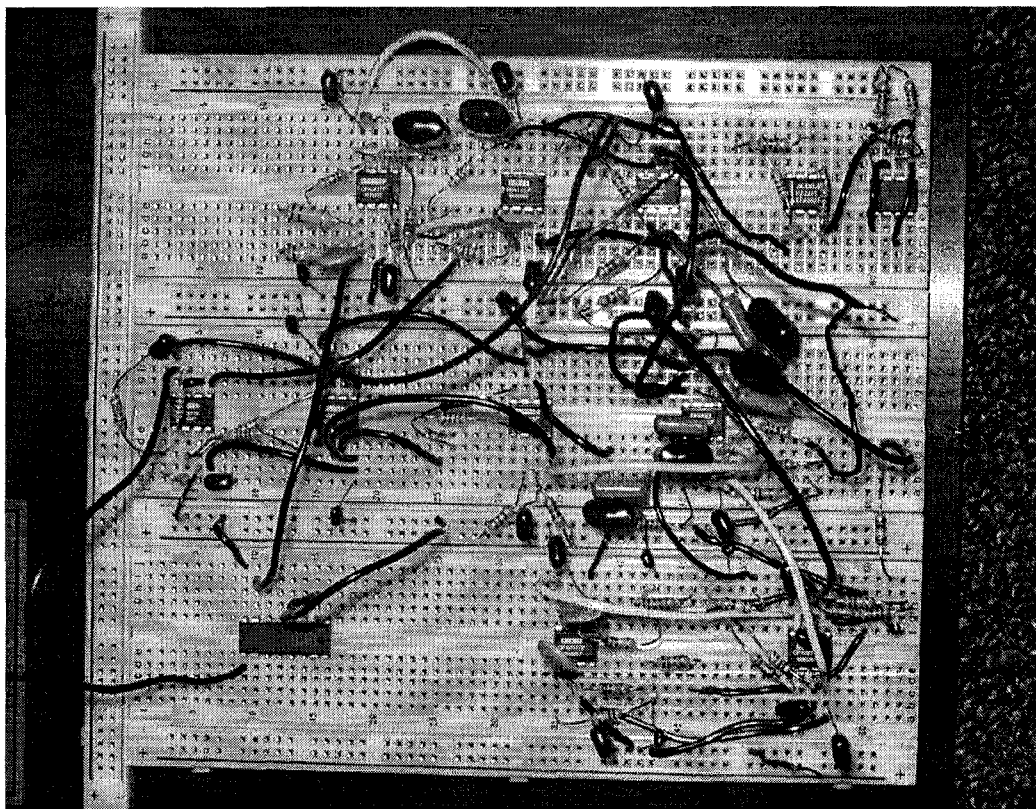


Figure 50 Three-channel amplifier system built on the breadboard.

4.6.3 Development of 15-channel LEEG System

The three-channel amplifier system was increased to accommodate 15-channels. The 15-channel amplifier system had one LECG channel along with 14 LEEG channels. Each two LEEG channels were used for recording LEEG signals from a single tri-polar concentric ring electrode. The 15-channel amplifier system accommodated seven tri-polar electrodes along with a LECG channel. The 15-channel amplifier system again was assembled with two boards. One main board or Amp board contains the four-stage amplifiers for all the 14 LEEG channels and a three-stage amplifier for the LECG channel and another board, Notch-Isolation board. The whole LEEG system was divided in to two boards to simplify troubleshooting and the design. The outputs from the Amp board are passed to the Notch-Isolation board along with the DC power supplies. The block diagram for the 15-channel Amp board is shown in Figure 51. This block diagram is really an expansion of the previously shown three-channel block diagram which is shown in Figure 49. The Capture Schematic circuit for the 15-channel Amp board is shown in Figure 52. All the inputs are shown on the left side and outputs are shown on the right hand side of the board. The Amp board was built on two sided printed circuit board as shown in Figure 53 and 54. Figure 53 shows the front side and Figure 54 shows the back side of the Amp board. Figure 55 shows the Amp board with all the surface mount components along with connectors. The Amp board has circuitry for seven tri-polar electrodes, 14 LEEG channels, power supply and one ECG channel.

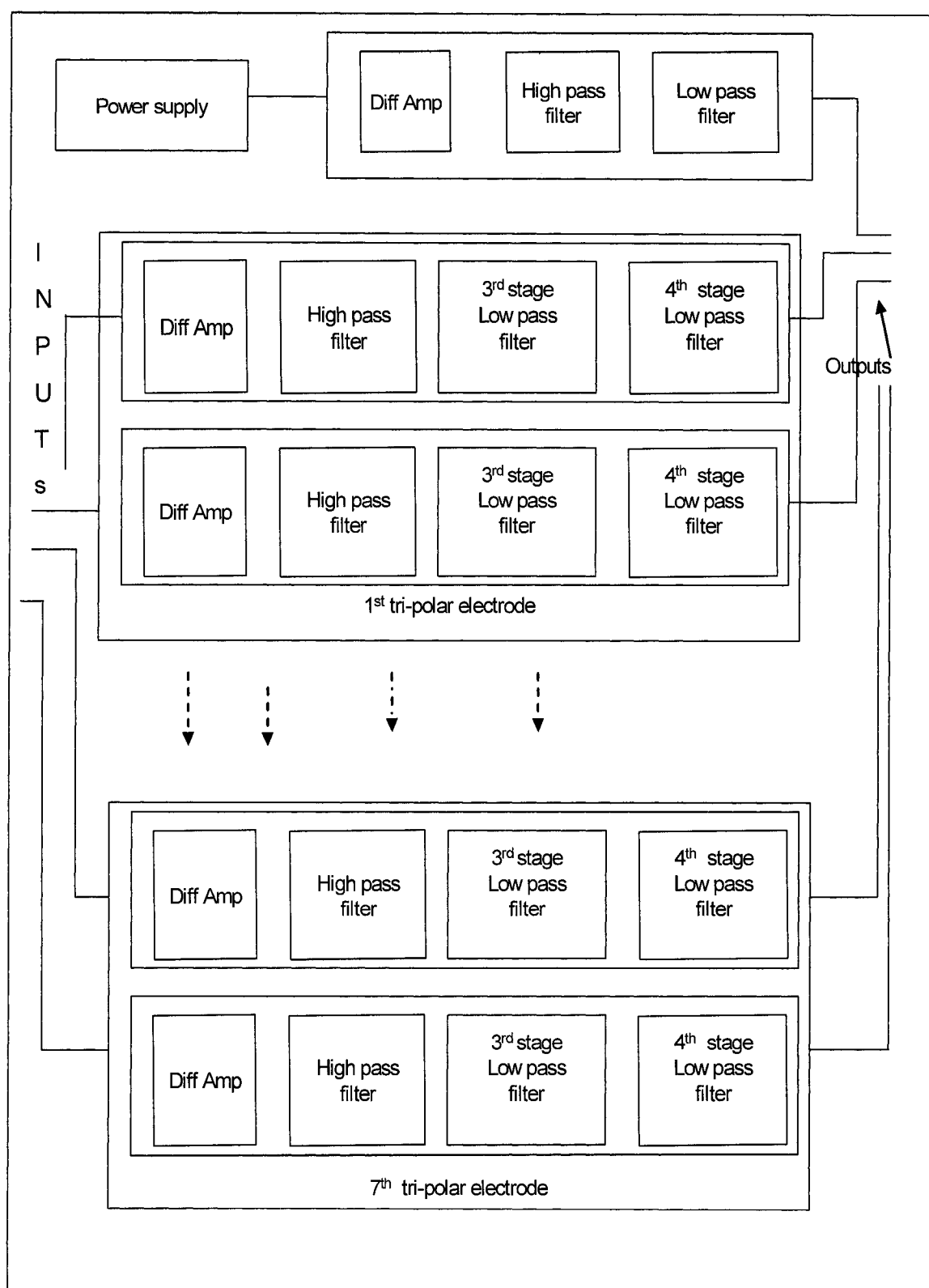


Figure 51 Block diagram of 15-channel amp board.

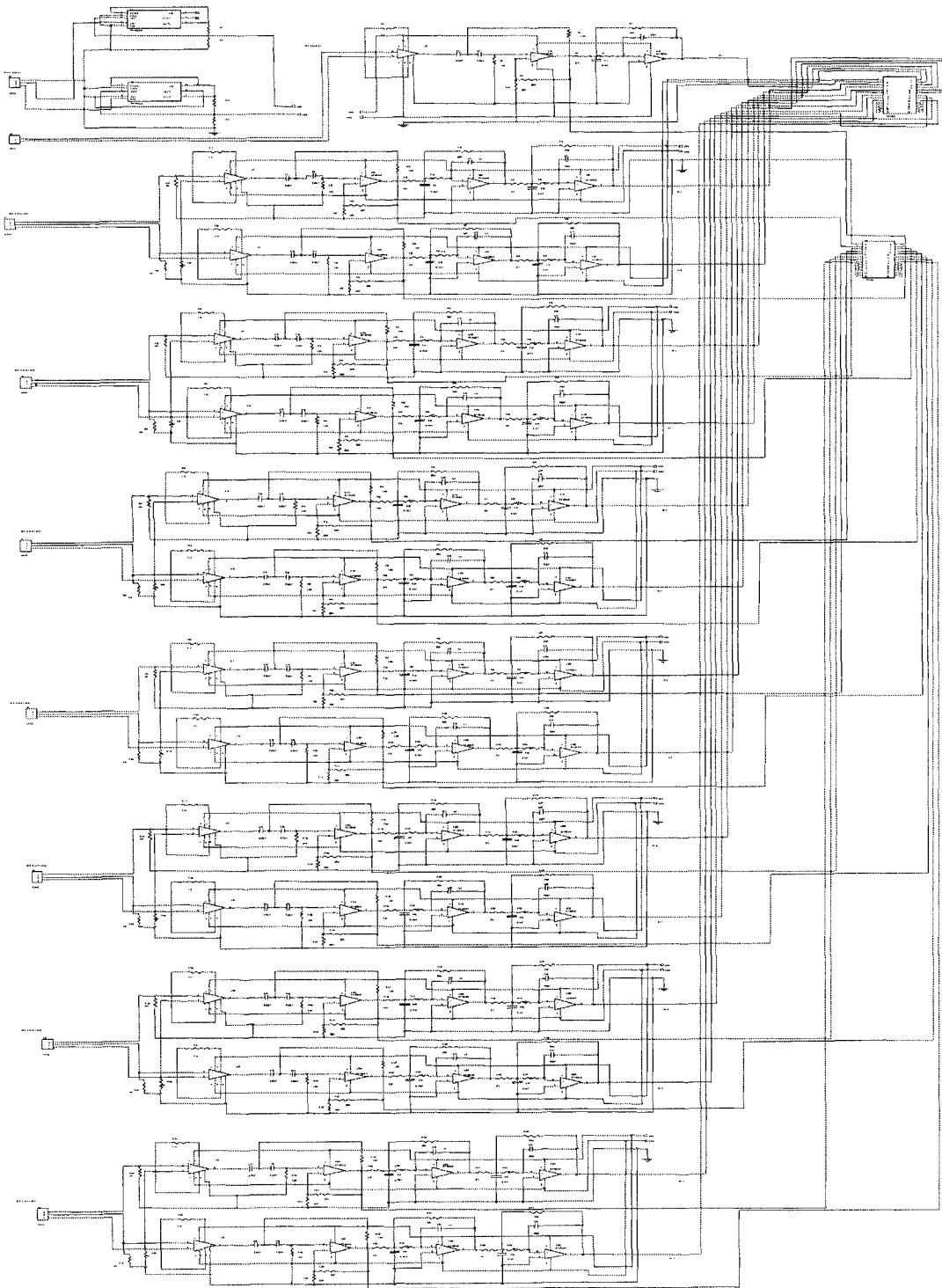


Figure 52 15-channel amp board circuit from Orcad Capture.

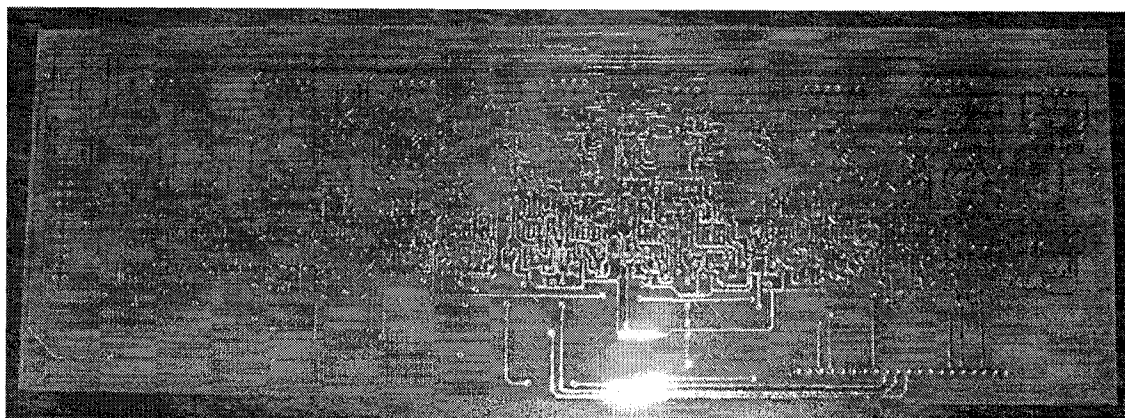


Figure 53 Front side of the 15-channel amp board.



Figure 54 Back side of the 15-channel amp board.

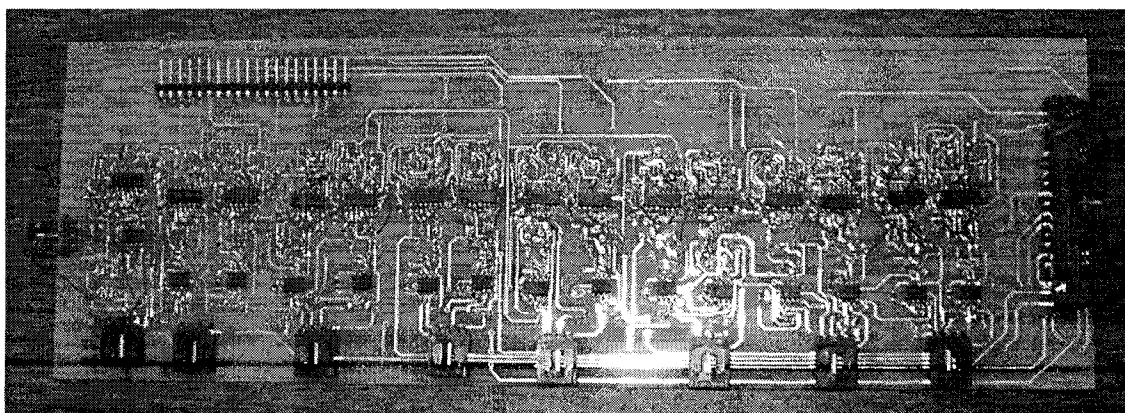


Figure 55 15-channel amp board with all the components.

The Notch-Isolation board has 15-channels of 60 Hz notch filters and 15 isolation amplifiers. The 60 Hz notch filters are necessary to remove the 60 Hz noise even though most of the 60 Hz noise is canceled by the differential amplifiers. The notch filter was designed using two op-amp Fliege topology. This topology has unity gain. The advantage of using the Fliege topology for designing a notch filter over Salle-Key and other topologies is (i) it has good control over tuning, Q and style of the filter; (ii) it uses less components; (iii) it has a symmetrical response over the middle frequency or 60 Hz; (iv) less number of components were critical for setting the Q. The outputs from the Amp board are connected to the inputs of the 60 Hz notch filters and then the outputs from notch filters were connected to the isolation amplifiers. The ISO122 amplifiers from TI (Texas Instruments Incorporated, Dallas, TX) were used for isolation. The advantage of the ISO122 amplifiers was they were low-cost and high precision unity gain isolation amplifiers. The Notch-Isolation board has separate power supply for the outputs of isolation amplifiers. The outputs from the isolation amplifier were connected to a DB37 connector. The DB37 connector was connected to the DI 720 data acquisition system via a ribbon cable.

Figure 56 shows the Notch-Isolation board with only the power supply assembled; Figure 57 shows the Notch-Isolation board with all the components and DB37 connector. The power supply on the 15-channel amplifier system was changed from Max 663, 664 to LM317 and LM337 (National semiconductor, Santa Clara, California, USA) adjustable linear regulators. This power supply change was made to accommodate the necessary current required for the 15-channel LEEG system. Figure 58 shows the power supply circuit used for the 15-channel amplifier system. Figure 59 shows the entire

15-channel LEEG system with power supplies, DB37 connector, and custom-made seven tri-polar electrode strap. The custom-made tri-polar electrode strap had seven tri-polar electrodes placed 1 cm apart. Troubleshooting the 15-channel LEEG system is explained in Appendix-F.

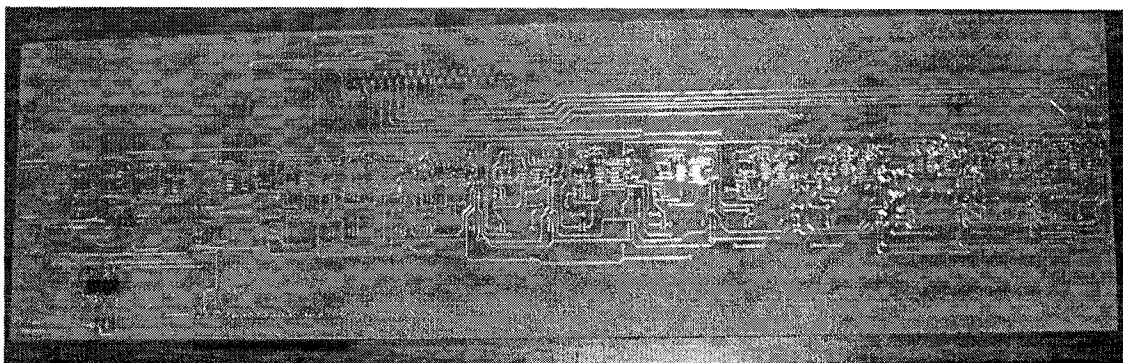


Figure 56 Notch-Isolation board with only power supply and with out any components.

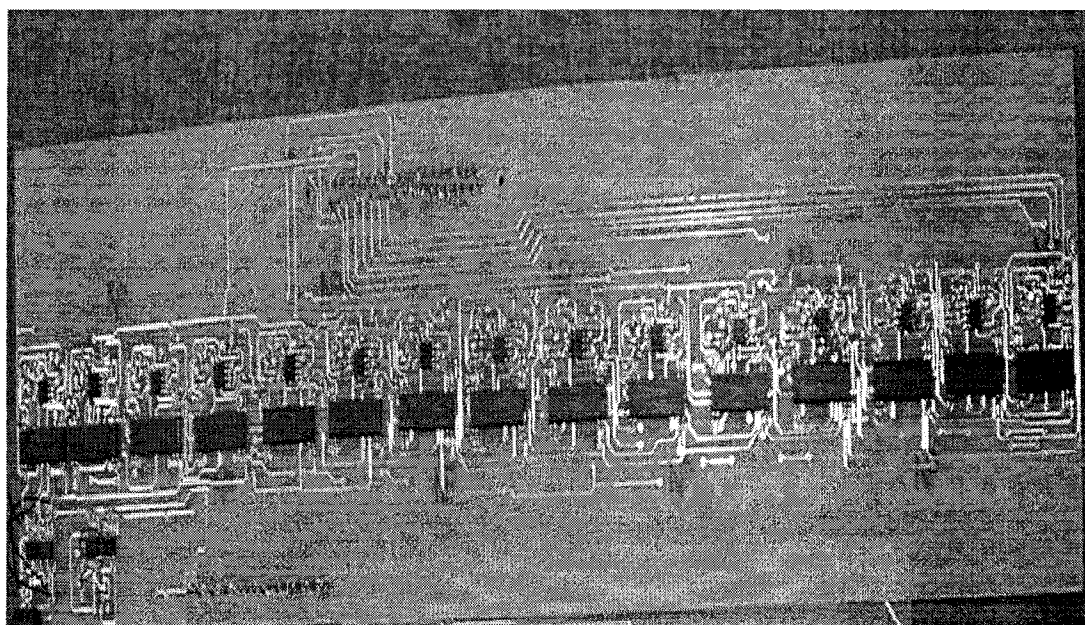


Figure 57 Notch-Isolation board with all the surface mount components.

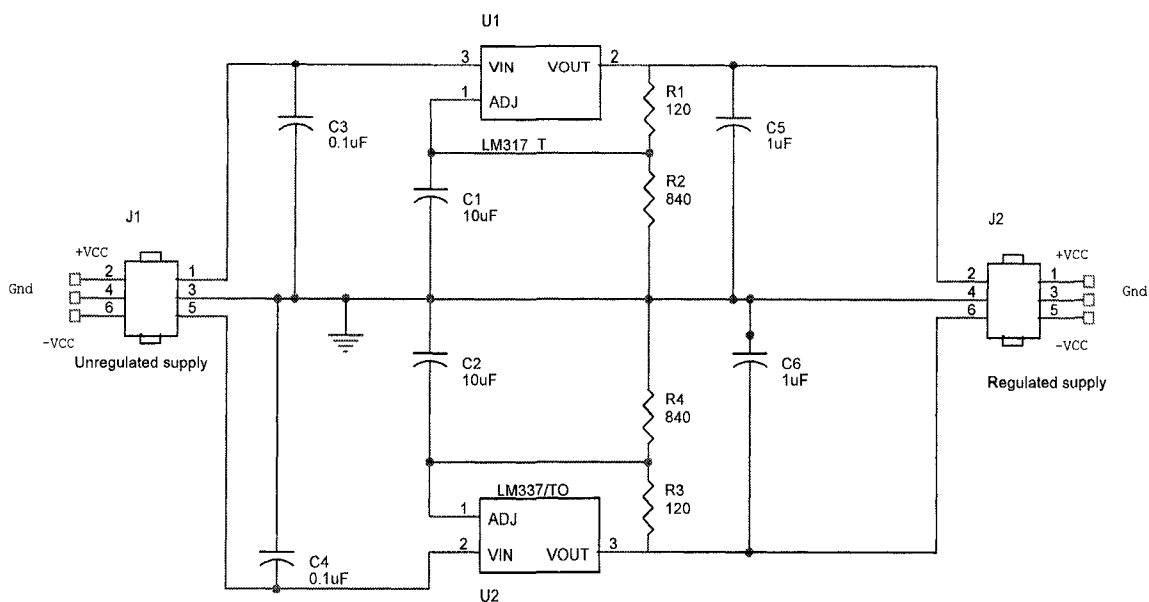


Figure 58 Regulated power supply circuit used for 15-channel LEEG system.

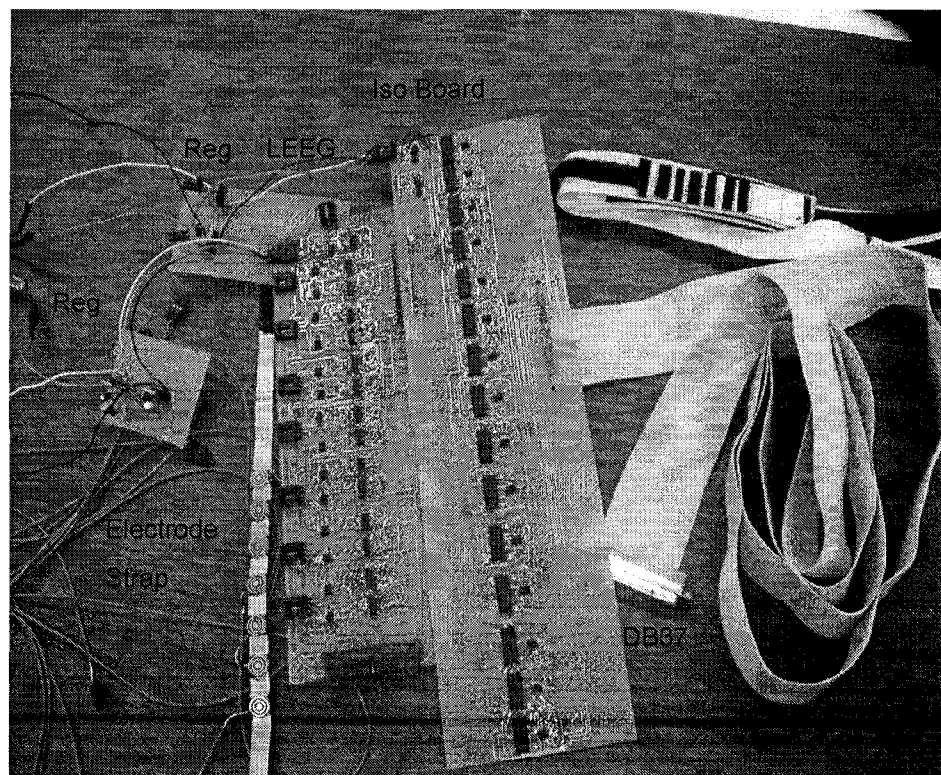


Figure 59 The 15-channel LEEG amplifier system with custom-made seven electrode strap and DB37 cable to connect to the data acquisition system.

4.7 Comparison of SNR of Multi-Channel MRP Recordings

The signal-to-noise ratio was calculated using Equation (3.5) and the results are shown in Table 2. For comparison the SNR was calculated for MRP signals recorded from CZ for all three electrode configurations. The MRP signals recorded from the CZ location are shown in Figure 60 for a typical subject. The post-movement peak [29] was observed at 150 ± 17 ms after the micro-switch closure signifying the index finger movement. The SNR data were analyzed using a single-factor ANOVA and Bonferroni tests. The SNR of the tri-polar concentric ring electrodes showed significant ($p=1.078 \times 10^{-6}$) improvement over bipolar concentric ring electrodes and conventional disc electrodes.

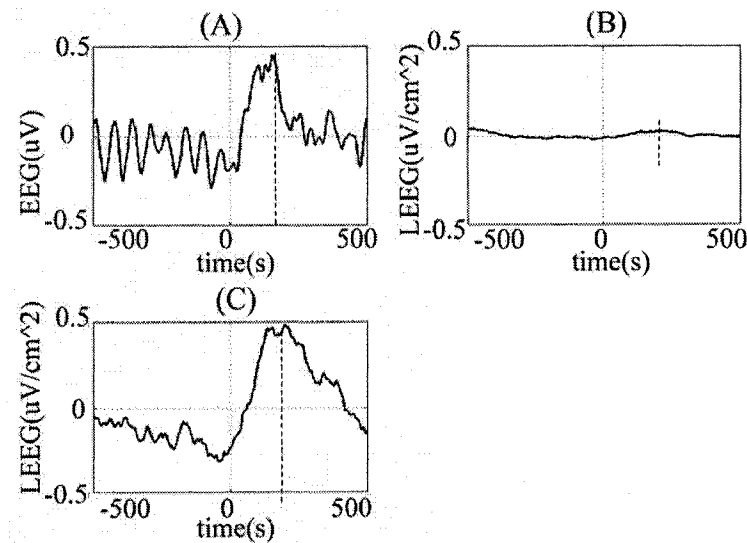


Figure 60 MRP signals recorded from the same subject at CZ location using three different electrode configurations. Positive peak was marked at 150 ms after rising edge of micro switch.

Table 2 SNR for multi-channel MRP signals at location CZ

	<i>Disc</i>	<i>Bipolar</i>	<i>Tri-polar</i>
Subject1	1.661	2.086	5.899
Subject2	1.808	2.961	5.793
Subject3	2.073	2.602	4.136
Subject4	1.299	3.537	5.534
Subject5	0.430	2.961	5.793
<i>Average</i>	<i>1.454</i>	<i>2.829</i>	<i>5.431</i>

4.8 Comparison of Spatial Selectivity

The potentials measured from conventional disc electrodes were processed using a custom Matlab program. The MRP signals were analyzed by taking a window of one second. The window size was selected by taking 499 ms before the switch reference positive pulse edge and 500 ms after the switch reference pulse. The 2-D map of MRP signals were plotted according to their electrode positions and are shown in Figure 61.

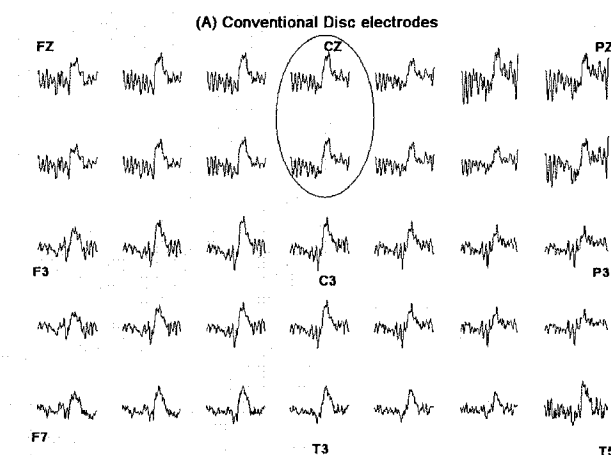


Figure 61 2-D map for the MRP signals recorded from conventional disc electrodes placed on the left hemisphere of the head for multi-channel MRP recordings.

The Laplacian potentials recorded from the concentric ring electrode array were processed in Matlab with a custom program. The recordings were taken as the difference between outer ring and disc, middle ring and disc. These potentials were further processed to calculate the Laplacian potentials for each concentric ring electrode system using Equation (2.18) for tri-polar concentric ring electrodes. The Quasi-bipolar electrode concept was not used in this analysis as it had too low of SNR for MRP signals recorded from FP1 location. The 2-D maps for bipolar and tri-polar concentric ring electrode systems for the corresponding electrode locations were plotted and are shown in Figure 62 and Figure 63, respectively.

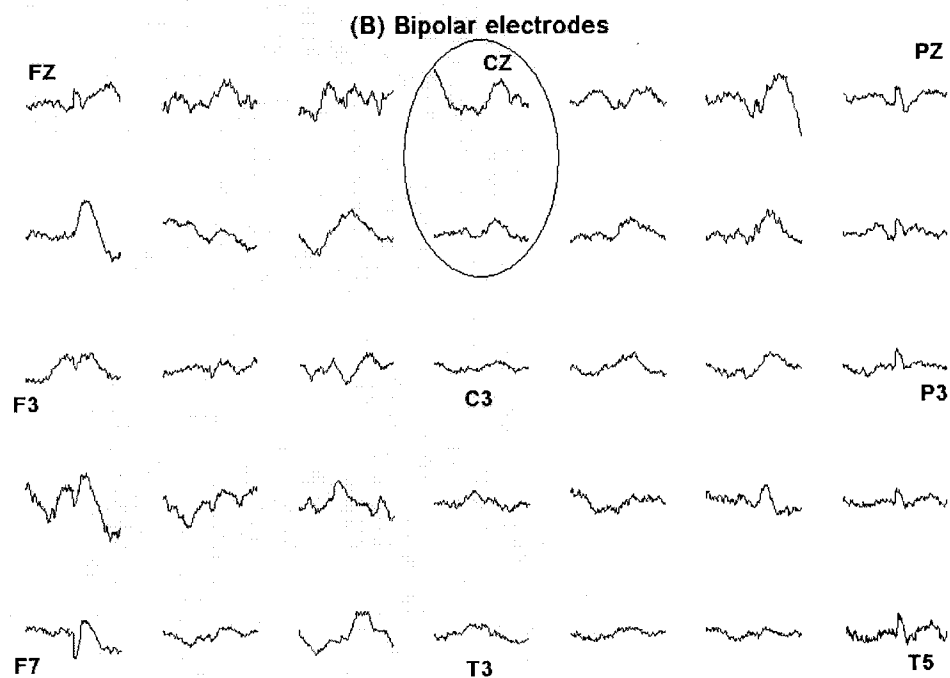


Figure 62 2-D map of MRP signals recorded for bipolar electrode configuration from multi-channel MRP recordings.

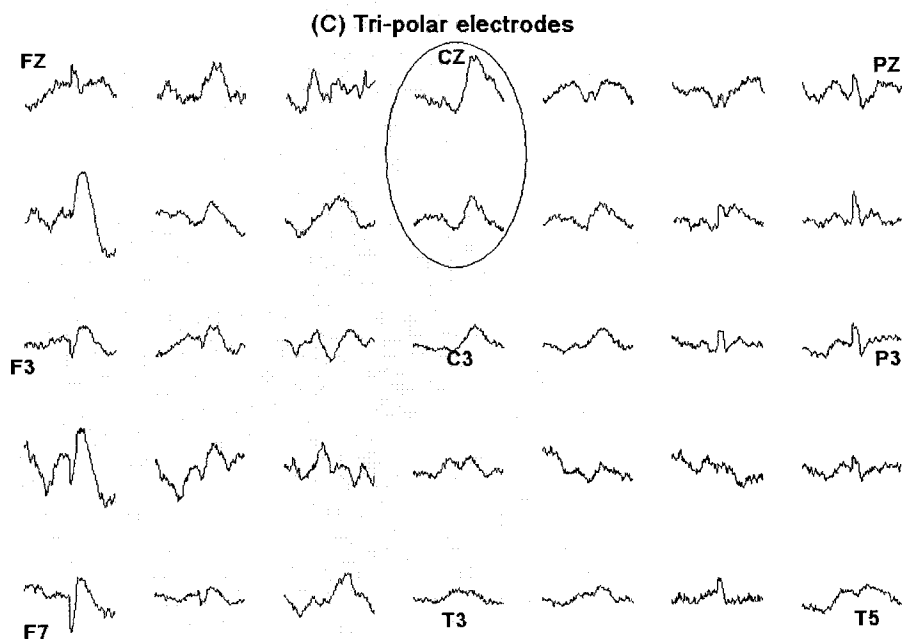


Figure 63 2-D map of MRP signals recorded for bipolar electrode configuration from multi-channel MRP recordings.

The calculated peak ratios for different electrode systems for all the subjects at the location CZ are shown in Table 3. The average peak-to-peak ratio was 1.204 for conventional disc electrodes, 1.539 for bipolar concentric electrodes, and 3.091 for tri-polar concentric ring electrodes. The Bonferroni tests showed there was significant improvement ($p=1 \times 10^{-5}$) of peak ratios obtained from tri-polar concentric ring electrodes over those obtained from conventional disc and bipolar concentric ring electrodes. The increased peak-to-peak ratio illustrates the higher spatial attenuation for off-center signals from tri-polar concentric ring electrodes over bipolar concentric ring electrodes and conventional disc electrodes. The increased spatial attenuation of off-center signals or global signals will increase the spatial selectivity of the tri-polar concentric ring electrodes to sources below the center of the electrode.

Table 3 Peak ratios of MRP signals for comparing spatial selectivity

	Disc	Bipolar	Tri-polar
Subject1	1.331	1.789	3.558
Subject2	1.146	1.409	7.716
Subject3	1.275	2.113	3.559
Subject4	1.201	1.672	2.918
Subject5	1.001	1.409	2.515
Average	1.191	1.678	4.053

4.9 Comparison of Mutual Information

Mutual information between each channel for the three electrode systems were calculated with a custom Matlab program using Equation (3.9). The grand averages of the MI for each electrode system were shown in Table 4. The MI data were analyzed using a single-factor ANOVA, and Bonferroni tests were also performed. The MI for tri-polar concentric ring electrodes was significantly ($p=0.0164$) less than the MI of bipolar concentric ring electrodes and conventional disc electrodes.

Table 4 Mutual information values for three electrode systems

	<i>Disc</i>	<i>Bipolar</i>	<i>Tri-polar</i>
Subject1	0.226	0.050	0.017
Subject2	0.307	0.061	0.022
Subject3	0.217	0.062	0.022
Subject4	0.307	0.093	0.024
Subject5	0.272	0.062	0.021
<i>Average</i>	<i>0.266</i>	<i>0.066</i>	<i>0.021</i>

4.10 Seizure Recordings Using the Tri-polar Electrode

4.10.1 Penicillin-G Seizure Model

Prior to the penicillin-G injection LEEG recordings were initiated to obtain baseline measurement of the normal rat LEEG. The baseline was acquired to verify the frequency components in the rat LEEG before the seizure was induced. A baseline bipolar LEEG recording taken from one of the rat experiments for which the recording was taken with four 5.0 mm concentric ring electrodes is shown in the Figure 64 and is representative of others. Figure 64 shows the recordings for bipolar concentric electrode configuration. These data were again processed in custom Matlab program to calculate the tri-polar electrode LEEG using Equation (2.18). Figure 65 shows the LEEG for the tri-polar electrode configuration from the same experimental data. These signals were again analyzed in frequency domain to determine the frequency content during the baseline recording. The frequency spectrum for LEEG during baseline is shown in Figure 66. The frequency spectrum shows the signals mainly in the frequency range 0.5 Hz to 20 Hz which is normal EEG frequency with no spike or any particular frequency dominant.

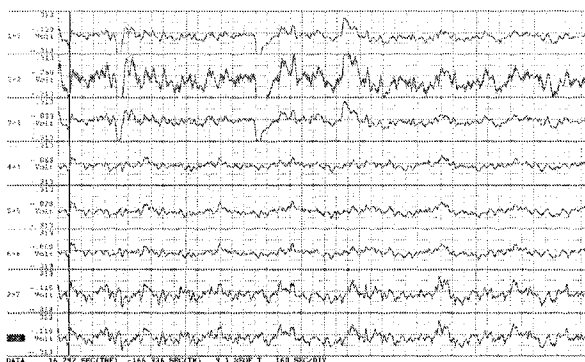


Figure 64 A typical baseline LEEG recording taken during a rat experiment.

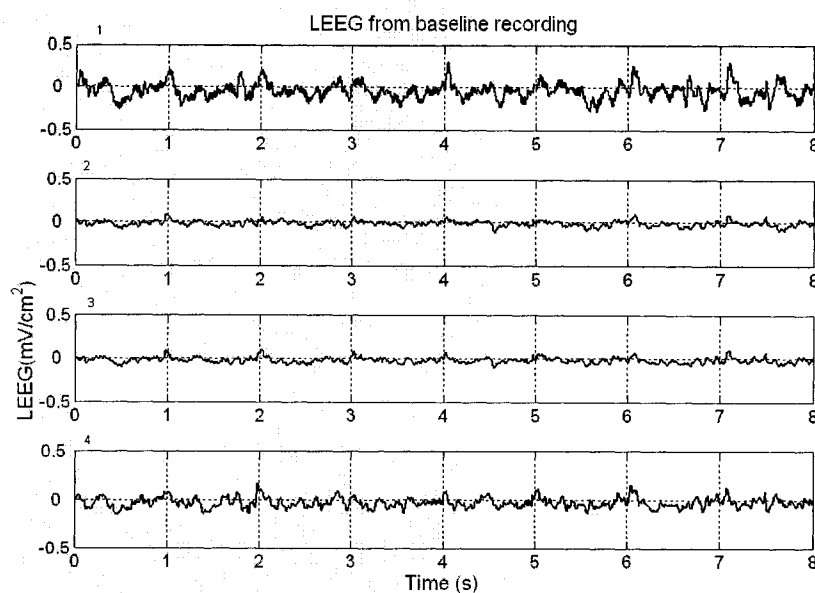


Figure 65 Tri-polar concentric electrode configuration LEEG during baseline recording.

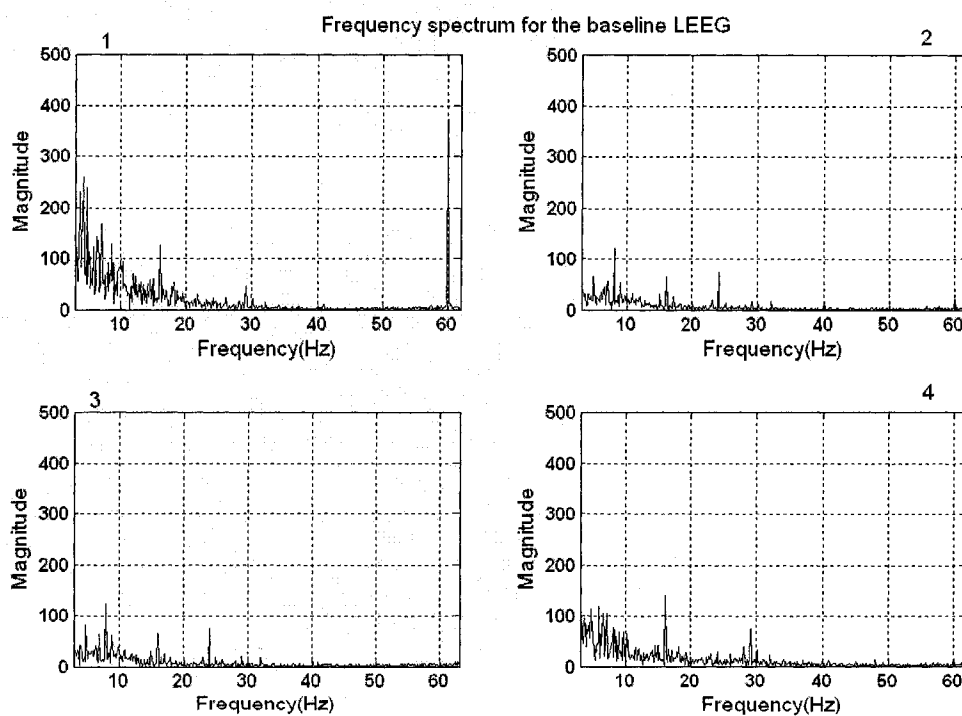


Figure 66 Frequency spectrum of a typical rat LEEG signals taken during baseline recording for tri-polar concentric electrode configuration.

Figure 67 shows a typical recording taken just after penicillin-G was injected and during the seizure activity. The seizures started typically one to two minutes after the penicillin-G injection. The seizure signals can be differentiated from the baseline recordings with spike and sharp wave activity. This spike and sharp wave activity is the typical form of EEG signals during seizures. The frequency of spike and sharp wave activity was observed to be between 1 Hz and 5 Hz. These signals were further processed with a custom Matlab program to calculate the tri-polar LEEG and analyzed the main frequency components during the seizure. The signals recorded during the seizure show higher 1 Hz to 5 Hz range frequencies than the baseline signals. Figure 68 shows the seizure signals and Figure 69 shows the frequency content of the LEEG signals from the tri-polar electrode configuration.

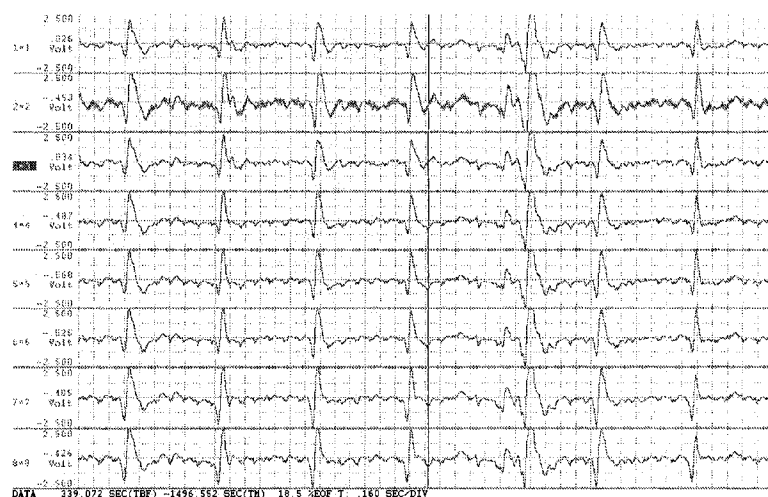


Figure 67 The LEEG signals recording during the seizure.

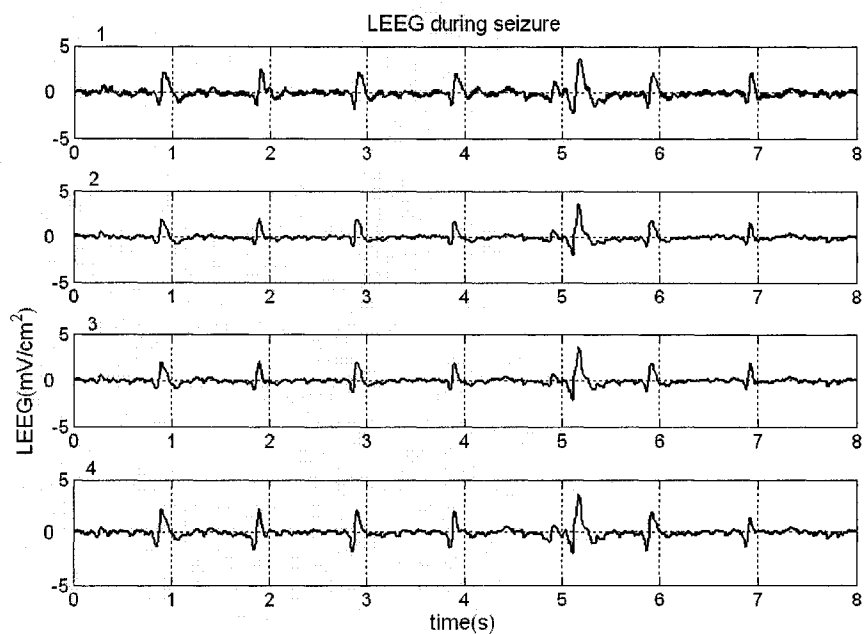


Figure 68 Spike and sharp wave activity during seizures with tri-polar electrode configuration.

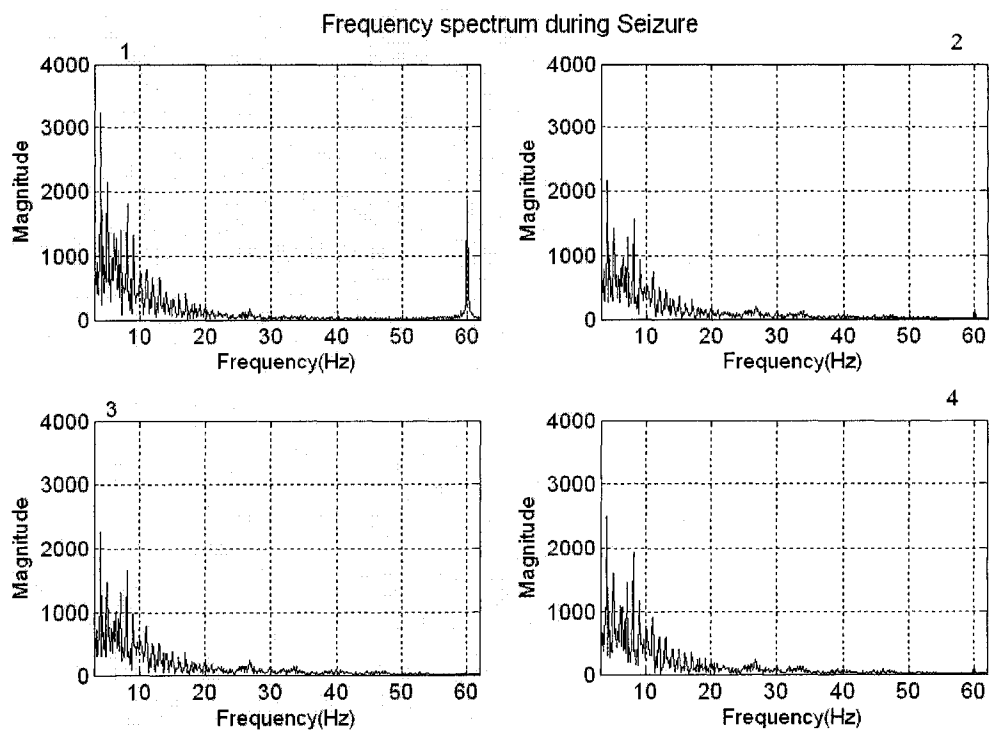


Figure 69 Frequency spectrum of the spike and sharp wave activity during penicillin seizure model.

Figure 70 shows penicillin-induced seizure signals recorded during another rat experiment. In this experiment a 1.0 cm tri-polar concentric ring electrode was placed at CZ and two conventional disc electrodes (1.0 cm dia. gold disc) were placed at C3 and C4. Panel (A) shows the signals from the conventional disc electrodes, Panel (B) from a bipolar concentric ring electrode and Panel (C) from a tri-polar concentric electrode configuration. The vertical scales were kept similar for all the panels to ease the comparison. The tri-polar concentric electrode configuration shows the clear spike and slow waves that correspond to activity from the conventional disc electrodes during the penicillin seizure model. Spike and slow waves are not as evident with bipolar concentric electrode configuration.

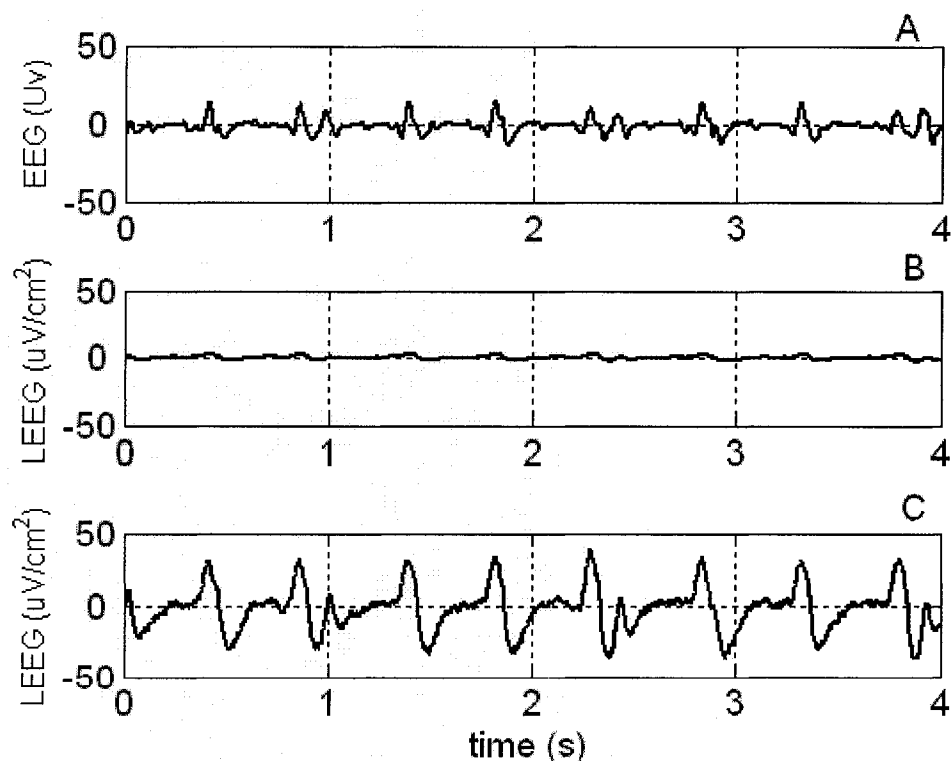


Figure 70 Spike and sharp waves recorded from a penicillin seizure model animal experiment. Panel (A) conventional disc, Panel (B) bipolar concentric electrode, and (C) tri-polar concentric electrode.

4.10.2 Pilocarpine Seizure Model

Ten rats were in the pilocarpine seizure recordings with Protocol 2. Each experiment was video taped for later review. Notes on behavioral and electrographic activities were kept during the experiments. Behavioral seizures usually were observed starting 3 to 6 min after the pilocarpine injection. Behavioral seizures started with chewing and rearing and falling. The rats were observed to enter status epilepticus (SE) on average 19 min after the pilocarpine was administered. For these experiments 30 seconds of continuous spiking activity was considered the start of SE [42]. During the initial stages of status epilepticus, the rats showed more motor activity. Rearing and falling was seen initially after the onset of SE. Different stages of LEEG electrographic activity during the pilocarpine induced seizures were observed and recorded.

The electroencephalographic signals recorded during different stages of SE along with the baseline signals recorded before the pilocarpine injection are shown in Figures 71 to 76 for rat number three, which is typical for all 10 control rats studied with this protocol. The time scales were the same as Treiman *et al.* [36-37] to make the comparisons easier. For rat number three, only two electrode locations are used for recording. They are CZ and C4, as shown in Figure 21. Figure 71 shows the signals during the baseline. The electrographic signals do not show any spiking activity. The signals show a consistent nearly flat background without any dominant spiking activity. In Figure 71 direct concentric bipolar signals are recorded from tri-polar concentric ring electrodes for differentially. Figure 72 shows the signals during the onset of SE. It has 40 sec of continuous spiking activity which is beyond the 30 sec limit considered as SE. Figure 73 shows the discrete seizures with nearly flat background between spiking

activity. These signals look like continuous spiking activity but have breaks in activity in between the spikes. Figure 74 shows signals during the waxing and waning stage. In this stage the electrographic activity does not appear to stop and the amplitude and frequency waxes and wanes. Figure 75 shows continuous spiking activity without any gaps. This activity typically continued for a long time before converting to periodic epileptiform discharge (PED) activity with in frequent spikes on a flat background like baseline which is shown in Figure 76.

Figure 77 shows the progression of the different stages from the onset of SE. These progressive stages are in accordance with Treiman *et al.* Two minutes after the onset of SE discrete seizures were observed. These discrete seizures show continuous electrographic spiking but end abruptly in all channels and then the electrographic spiking activity starts again. At five minutes after the onset of SE nine of the rats were in the discrete seizures and one rat was observed to be in waxing and waning stage. In this stage the epileptiform activity waxes and wanes in frequency and amplitude [36]. Ten minutes after the onset of status epilepticus, nine rats had entered the continuous spiking and one rat in waxing and waning stage. At 15 min after the onset of SE all the rats entered to continuous spiking activity stage and remained in it for a long time. On average five hours after the onset of status epilepticus, continuous electrographic signals were replaced by PED signals. The average survival rate was 15 h after the pilocarpine injection.

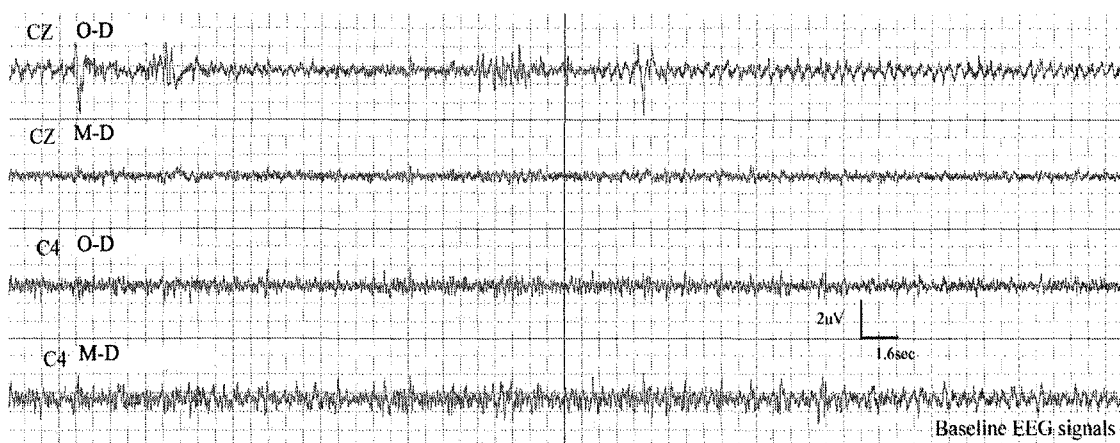


Figure 71 Baseline recording taken during the pilocarpine seizure experiments for rat3.

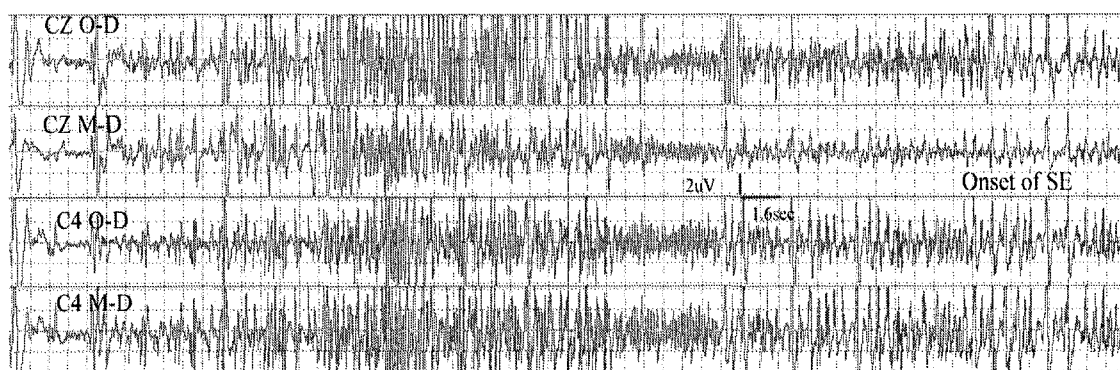


Figure 72 Onset of SE during the pilocarpine seizure experiments for rat3.

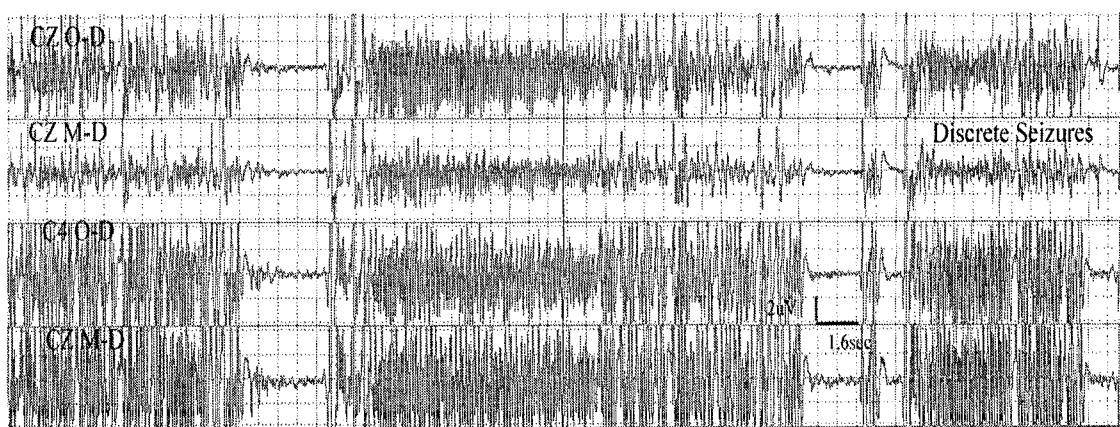


Figure 73 Discrete seizures observed during pilocarpine seizure experiments for rat3.

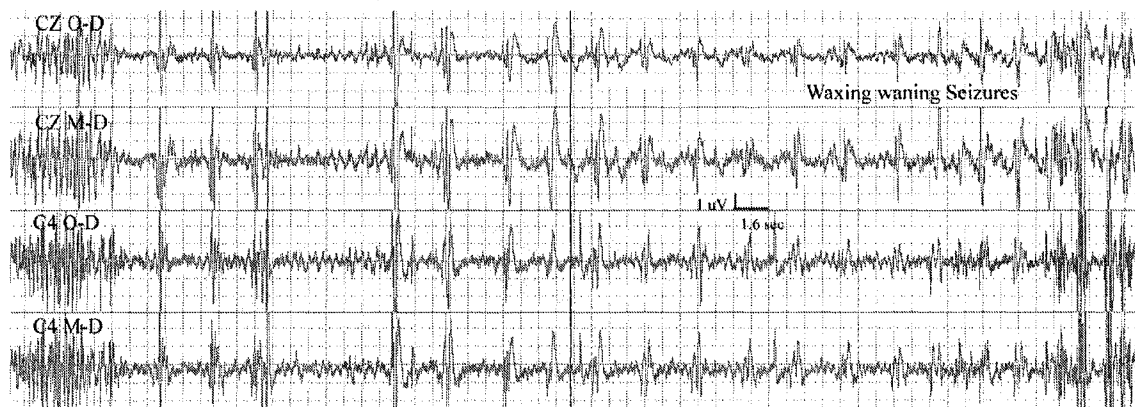


Figure 74 Waxing-waning observed during pilocarpine seizure experiments for rat3.

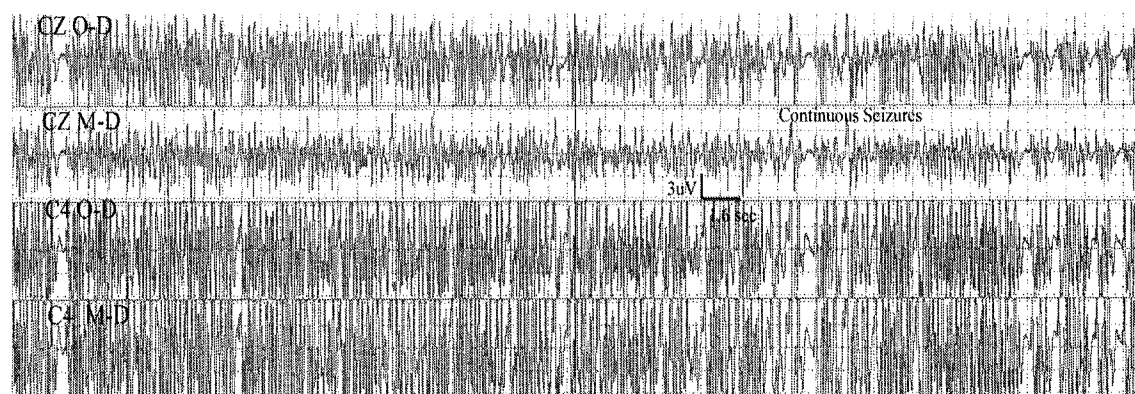


Figure 75 Continuous spiking activity observed during the pilocarpine seizure experiments for rat3.

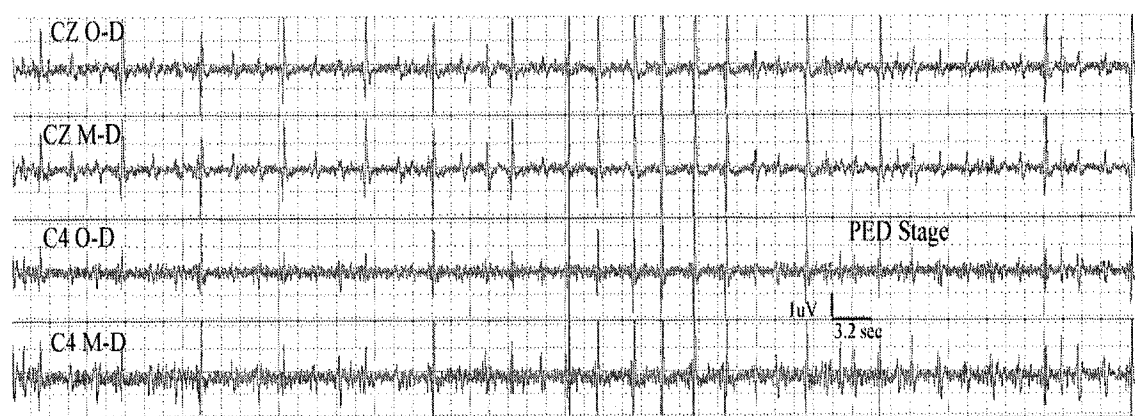


Figure 76 Periodic epileptic discharges observed during the pilocarpine seizure experiments for rat3.

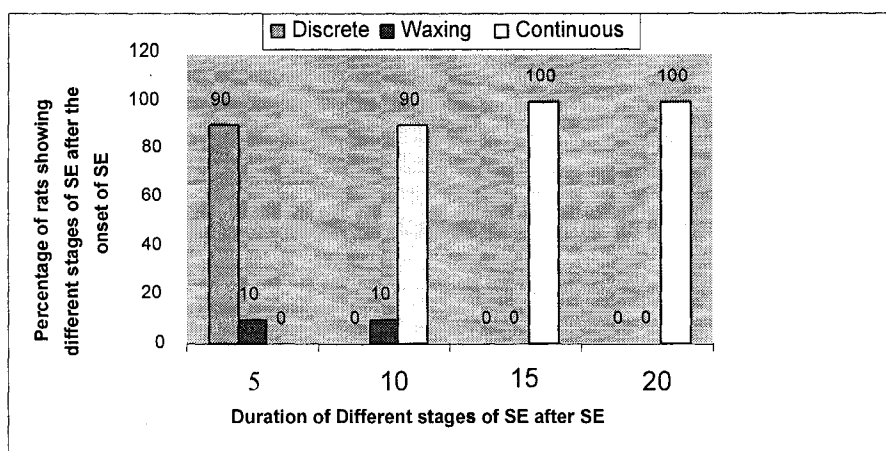


Figure 77 Percentage of rats showing different stages of pilocarpine induced seizures with Protocol 2 after the onset of SE.

Figure 78 shows the spike and slow wave activity observed during one of the pilocarpine seizure experiments. The time scale is set similar to the time scale used for regular EEG recording from conventional systems. This spike and slow wave activity is similar to the seizure patterns observed during regular EEG from a subject suffering with seizures. Figure 78 Panel (A) shows the spike and slow wave activity from a bipolar electrode configuration and Panel (B) shows the spike and slow wave activity from a tri-polar electrode configuration. The spike and slow wave activity is not evident in the bipolar concentric ring electrode electrographic activity as that from the tri-polar concentric ring electrode activity.

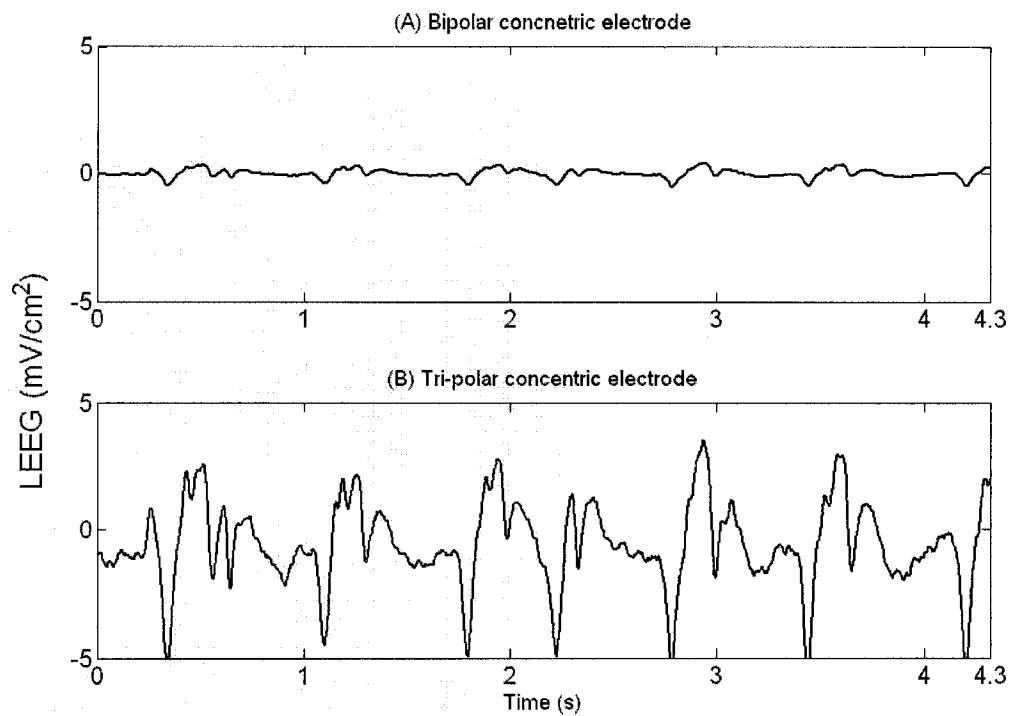


Figure 78 Spike and slow wave activity observed during pilocarpine seizure model.

CHAPTER 5

DISCUSSION

The results from the tank experimental data and the simulated data are in good agreement. After performing analysis on the measured tank experimental data and the simulated data of the 2.0 cm diameter concentric ring electrode, it was determined that the tri-polar electrode had a greater localization capacity than the bipolar and quasi-bipolar concentric electrode configurations and conventional disc electrodes. As illustrated in Figure 26, Figure 27 and Figure 29, without/with noise sources respectively, the tri-polar traces show the greatest attenuation for off center sources. This is confirmed by the results of Bonferroni t-tests. This finding substantiates that the attenuation is greatest for the tri-polar electrode configuration when compared with bipolar, quasi-bipolar concentric electrode configurations and conventional disc electrodes tested for global sources such as noise. It also demonstrates that the tri-polar electrode configuration is more sensitive to local signals as compared with the other configurations analyzed.

An evaluation of the attenuation traces in Figure 29 and Figure 30 highlights that the shapes of the attenuation of off center sources for the three configurations in the computer modeled data are very similar (correlation coefficient= 0.82 ± 0.1) as compared with the measured data from the tank experiments [41]. Since a unity dipole was used as the source of the computer model, a direct magnitude comparison between

the computer model and the tank experiments are not possible. Use of a more realistic dipole source could help enhance these findings. Another experimental improvement is to use multi-conductivity models, both for computer modeling and physical verification experiments. The different conductivities will alter the potentials calculated and measured, decreasing them. This reduction should be relative to each electrode type though and should not alter the outcome that tri-polar concentric electrode was best.

Other possible reasons still exist for the difference between the simulated and measured values. This difference can be justified by a scaling factor, which originates from negligence in the computer model of conductivity for saltwater and permittivity of the printed circuit board material between the two thin discs of copper used to construct the dipole. The tank experiments exposed that there are also ambient noise sources, and non-ideal alignments of electrodes and dipoles that alter signals from the ideal conditions of the computer model. More accurate computer models and higher precision mechanisms for positioning the dipoles and concentric electrodes in the tank experiments can remedy these shortcomings.

Figure 35 shows that the tri-polar concentric electrodes can be used to record regular EEG rhythms and is substantiated by the change in alpha wave rhythm. The change in the mean of the alpha rhythm during eyes open ($7 \mu\text{V}$) to eyes closed ($15 \mu\text{V}$) confirms that these electrodes can be used to record brain waves from the occipital lobes. When the eyes are closed the alpha rhythms should increase as they did in this case.

The LEEG recordings taken during the index finger movement i.e. the MRP signals illustrated in Figure 42 show that the tri-polar concentric electrodes can be used to record more localized brain activity than the other electrode systems namely,

conventional disc electrodes, bipolar and quasi-bipolar concentric ring electrodes. The recording with these small concentric electrodes was possible by use of highly accurate low noise precision pre-amplifiers. The tri-polar concentric ring electrode shows the recording of more localized activity even under the normal conditions i.e. with out any special shielded rooms, which are typically used by other researchers.

A further comparison between tri-polar concentric ring electrodes, bipolar concentric ring electrodes and conventional disc electrodes were performed in my research. In each of three measures of comparison used, SNR, spatial selectivity, and MI, the results from tri-polar concentric ring electrodes were significantly better than the bipolar concentric ring electrodes and conventional disc electrodes.

The significant improvement in SNR was expected as the (NPM) and tri-polar concentric ring electrode estimate the Laplacian significantly better than the other electrodes tested [43-44]. The tri-polar concentric electrodes perform higher spatial sampling than bipolar concentric and disc electrodes. The tri-polar concentric ring electrodes have higher attenuation of global signals, and this attenuation improves the spatial selectivity which sharpens the peaks of the MRP signals, which increases the SNR. The SNR measure used peak signal-to-noise ratio. Even though only the SNR at location CZ was shown in tabular form, the SNR at all locations were calculated and signals from tri-polar concentric ring electrodes have significantly higher SNR than the signals from the other electrodes.

The increase in spatial selectivity can be observed by viewing the MRP signal maps shown in Figures 61, 62, and 63. The MRP signals recorded with tri-polar concentric ring electrodes have sharper peaks and higher peak ratio than the bipolar

concentric ring electrodes and conventional disc electrodes. MRP signals obtained with tri-polar concentric ring electrodes show more spatial selectivity than the bipolar concentric ring electrodes and conventional disc electrodes [45].

The Bonferroni statistical tests on MI showed a significant decrease in MI of MRP signals recorded with tri-polar concentric ring electrodes as compared with other electrode systems tested as shown in Table 4 [45]. The decrease in MI increases the total information by pooling of data from all independent electrodes. The increase in information from the tri-polar concentric ring electrodes can be achieved without increasing the number of electrodes and complexity of the system. By decreasing mutual information, classification should be improved, and brain computer interface (BCI) systems can be improved without a significant increase in cost.

The results from the signals recorded during animal seizure experiments confirm that these tri-polar electrodes can be used for recording EEG during seizures [46-47]. This spike and slow wave activity in the tri-polar concentric ring electrode activity in Figures 70 and 78 may be due to the significant improvement in SNR. With increased SNR and higher spatial selectivity, the seizure activity or seizure foci can be localized and the origin of seizure can be found easily.

CHAPTER 6

CONCLUSIONS

Time and time again in each method used to compare tri-polar concentric ring electrodes to bipolar and quasi-bipolar concentric ring electrodes as well as conventional disc electrodes the tri-polar electrodes were significantly better. The tri-polar (NPM) configuration results in significantly more accurate approximations to the analytical Laplacian than the bipolar (FPM), quasi-bipolar (QBM), and (CNPM) configurations. The tri-polar configuration is also significantly superior for attenuating global sources than the bipolar and quasi-bipolar configurations and is shown evident with results from computer simulations and tank experiments. This property will be beneficial in localizing sources and rejecting global signals such as artefact due to muscle activity from eyes while recording EEG signals. By detecting differences on the concentric electrode elements, it is possible to measure the potentials due to localized brain activity with extremely high attenuation of global noise. The tri-polar LEEG system has also shown to be beneficial for detecting seizure electrographic activity.

CHAPTER 7

FUTURE WORK

Further work is necessary for a more complex model with realistic source magnitudes which would be more accurate in predicting potentials measured with the electrodes. Including multi-conductive layers would increase the accuracy. With a more integrated model using Neurocal, Matlab, and Femlab we would be able to better understand the properties of tri-polar concentric ring electrodes.

Development of instrumentation for recording 20 tri-polar electrodes in 10/20 International EEG system format is necessary to help understand more about spatial selectivity and mutual information.

Application of tri-polar electrodes for a particular BCI application must be tested in the future and advantages of tri-polar electrodes needs to be exploited. More detailed study is necessary to understand the application of tri-polar electrodes for recording the LEEG signals during seizing conditions and more experiments necessary to differentiate the tri-polar concentric ring electrodes with other electrode configurations.

APPENDIX A

**INTERNAL REVIEW BOARD APPLICATION
AND HUMAN CONSENT FORM**

DEPARTMENT HEAD APPROVAL FORM

TO: Project Directors

FROM: Barbara Talbot, Office of University Research
btalbot@latech.edu
318-257-5075 phone
318-257-5079 fax
<http://research.latech.edu/>

SUBJECT: HUMAN USE COMMITTEE REVIEW

DATE:

Please submit this page signed by your Department Head or Dean when submitting a proposal to the Human Use Committee for expedited approval. Their signature is stating that they are aware of this proposal and/or survey that are being conducted.

(print or type below)

Department

Department Head Name

Signature
(Actual original signature required)

Date

STUDY/PROJECT INFORMATION FOR HUMAN SUBJECTS COMMITTEE

Describe your study/project in detail for the Human Subjects Committee. Please include the following information.

TITLE: Comparison of Concentric Ring Electrodes with Conventional Disc Electrodes for Recording EEG Signals.

PROJECT DIRECTOR(S): Walter G. Besio, Ph.D.

EMAIL: Walterb@latech.edu

PHONE: 318-257-4562

DEPARTMENT(S): Biomedical Engineering

PURPOSE OF STUDY/PROJECT: Our goal is to develop a better EEG system with concentric ring electrodes. For this purpose we will be recording EEG signals from healthy subjects with no known neurological disorders. This study will allow us to develop a better EEG system for diagnosing brain related problems.

SUBJECTS: Louisiana Tech University students, faculty, and staff, healthy people

PROCEDURE: Several subjects will be tested in the following manner:

The scalp will be prepared with Nuprep, a mild cleanser used in EEG work and conventional disc electrodes will be coated with a thin film of electrode paste and placed in an array on the head. The subjects will be asked to press a micro-switch with their right index finger while the EEG signals related with movement of index finger are recorded. They will be given a cue from a metronome at approximately once every three seconds and asked to press the micro-switch whenever the cue is given.

The process of recording EEG while the subjects press the micro-switch will be continued for approximately 1h to 90minutes.

INSTRUMENTS AND MEASURES TO INSURE PROTECTION OF CONFIDENTIALITY, ANONYMITY:

Names of subjects will not be released. All reporting of data will refer to subjects in a general manner.

RISKS/ALTERNATIVE TREATMENTS: There are no risks associated with this study.

BENEFITS/COMPENSATION: The subjects will have a measure of their EEG during right index movement. There is no form of compensation.

SAFEGUARDS OF PHYSICAL AND EMOTIONAL WELL-BEING:

Subjects will be electrically isolated from wall power during the recording of EEG signals. This is due to the EEG pre-amplifiers being powered by batteries. These pre-amplifiers are commonly utilized by researchers for recording physiological signals from humans and animal subjects. The input impedance of the pre-amplifiers is greater than 100 mega ohm. The input bias current for the amplifier is 10 nano amps. This is an imperceptible amount of current that the subjects will not be able to feel or be harmed by. Due to the added skin to electrode impedance, this current will be further reduced. The EEG will be recorded from various locations including the standard 10-20 international standard locations with location CZ utilized as the reference.

A laptop computer will be used for acquiring the data. It will be powered via its battery. A data acquisition system (DataQ Instruments DI 720) digitizes the analog signals from the EEG amplifiers. The analog input impedance of the DataQ is 100 Gig ohms and has an input bias current of 100 pico amps. The DataQ system connects to the EEG amplifier and does not directly connect to the subject.

No subject names will be used in the reporting of data. The subjects will be treated cordially.

<p>Note: Use the Human Subjects Consent form to briefly summarize information about the study/project to participants and obtain their permission to participate.</p>
--

HUMAN SUBJECTS CONSENT FORM

The following is a brief summary of the project in which you are asked to participate. Please read this information before signing the statement below.

TITLE OF PROJECT: Comparison of Concentric Ring Electrodes with Conventional Disc Electrodes for Recording EEG Signals.

PURPOSE OF STUDY/PROJECT: Our goal is to develop a better EEG system with concentric ring electrodes. For this purpose we will be recording EEG signals from healthy subjects with no known neurological disorders. This study will allow us to develop a better EEG system for diagnosing brain related problems.

PROCEDURE: Several subjects will be tested in the following manner:

The scalp will be prepared with Nuprep, a mild cleanser used in EEG work and conventional disc electrodes will be coated with a thin film of electrode paste and placed in an array on the head. The subjects will be asked to press a micro-switch with their right index finger while the EEG signals related with movement of index finger are recorded. They will be given a cue from a metronome at approximately once every three seconds and asked to press the micro-switch whenever the cue is given.

The process of recording EEG while the subjects press the micro-switch will be continued for approximately 1h to 90minutes.

INSTRUMENTS: Instruments used to collect data include EEG preamplifiers, amplifiers, filters, an isolated laptop computer, a data acquisition system and software controlling the acquisition.

RISKS/ALTERNATIVE TREATMENTS: There are minimal risks associated with participation in this study. Participation is voluntary.

BENEFITS/COMPENSATION: You may see your EEG signals.

I, _____, attest with my signature that I have read and understood the following description of the study, " _____",

and its purposes and methods. I understand that my participation in this research is strictly voluntary and my participation or refusal to participate in this study will not affect my relationship with Louisiana Tech University or my grades in any way. Further, I understand that I may withdraw at any time or refuse to answer any questions without penalty. Upon completion of the study, I understand that the results will be freely available to me upon request. I understand that the results of my survey will be confidential, accessible only to the principal investigators, me, or a legally appointed representative. I have not been requested to waive nor do I waive any of my rights related to participating in this study.

Signature of Participant or Guardian

Date

CONTACT INFORMATION: The principal experimenters listed below may be reached to answer questions about the research, subjects rights, or related matters.

Dr. Walter Besio (257-4562)

Members of the Human Use Committee of Louisiana Tech University may also be contacted if a problem cannot be discussed with the experimenters:

Dr. Les Guice (257-3056)

Dr. Mary M. Livingston (257-2292 or 257-4315)

APPENDIX B

DIFFERENT RHYTHMS OF REGULAR EEG

EEG recorded from awake adults contains 4 different frequency bands or rhythms namely Delta (0.1Hz -3 Hz), Theta (4Hz – 7 Hz), Alpha (8Hz- 13Hz) and Beta (14Hz- 30Hz) rhythms. Usually there will be a dominant rhythm present in EEG. For adults during awake it is alpha rhythm.

During sleep we can see mainly two different stages. NREM (Random Eye Movement) and REM stages. Figure 79 shows the different stages of NREM sleep along with EEG signals during awake and duration of time also.

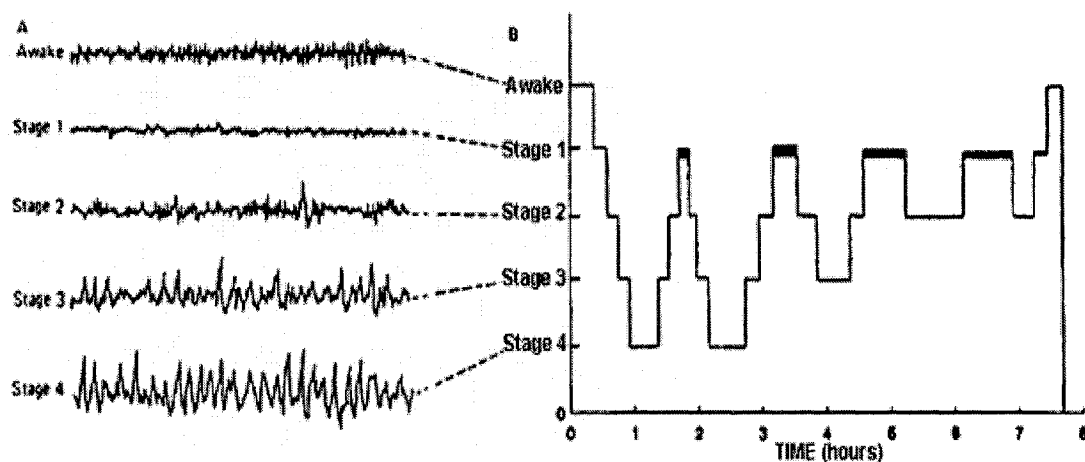


Figure 79 Different stages of NREM sleep along with signals during awake.

NREM stage is again divided into 4 stages. They are

Stage1 NREM: As soon as the person sleeps he enters in to stage1. Brain waves become smaller, slower, and somewhat irregular characterized by a low-voltage fast EEG.

Stage2 NREM: Stage 2 is an intermediate stage of sleep. It initially lasts about twenty minutes.

Stage3 NREM: Stage 3 is the beginning of deep sleep, occurring about thirty to forty five minutes after the person fall asleep.

Stage4 NREM: The deepest sleep occurs in Stage 4.

REM sleep: Brain suddenly becomes more active. EEG shows low-amplitude, mixed frequency waves called theta waves, with some alpha waves. REM stage sleep is shown in Figure 80.

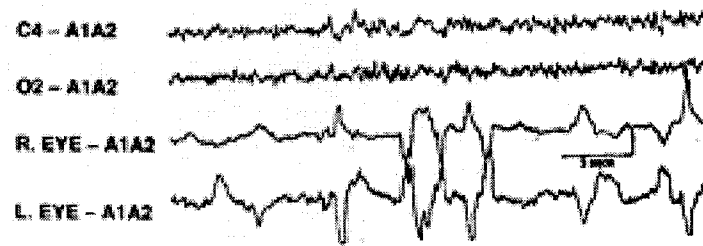
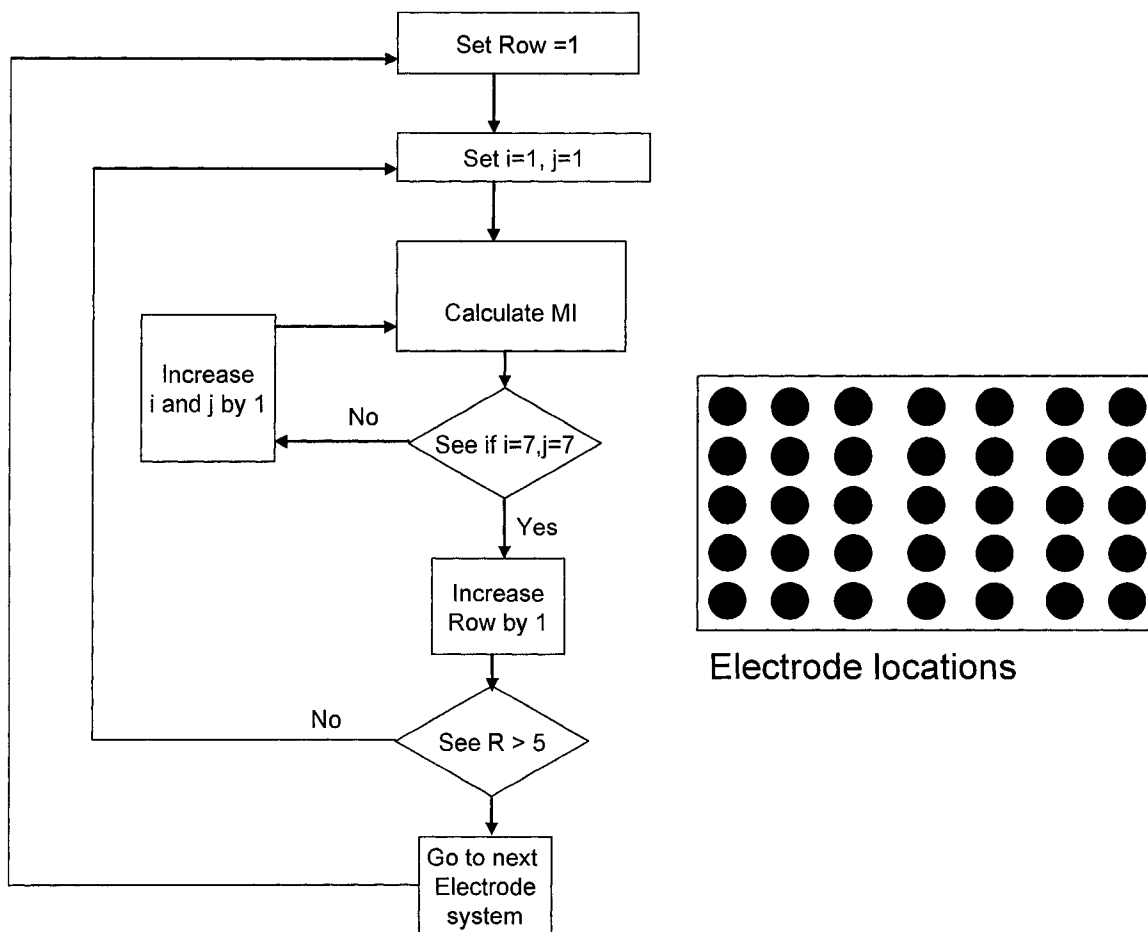


Figure 80 REM sleep stage signals along with EOG signals.

APPENDIX C

Flow Chart for Calculating Mutual Information



APPENDIX D

Classification of Seizures and Different Forms of Seizure Signals

The EEG with seizure can be distinguished from general EEG by the pattern it makes. EEG with seizures shows more spike and sharp waves, spike and sharp waves followed by slow wave. Spike and sharp wave patterns are shown in Figure 81 and Figure 82 and spike and slow wave form is shown in Figure 83.

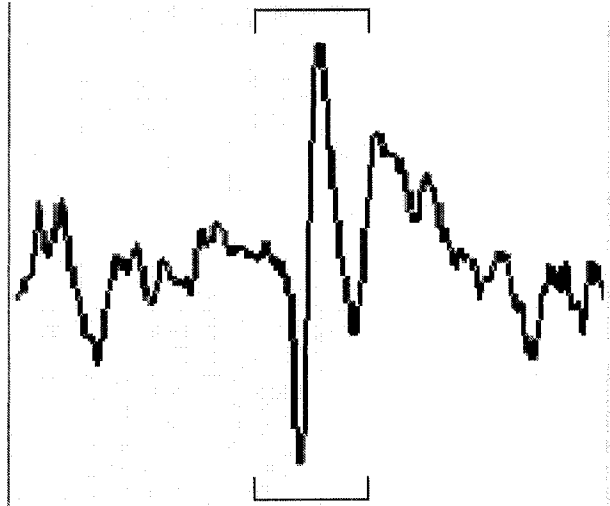


Figure 81 Spike and sharp wave seen during seizure activity.



Figure 82 EEG signals showing spike waveforms.

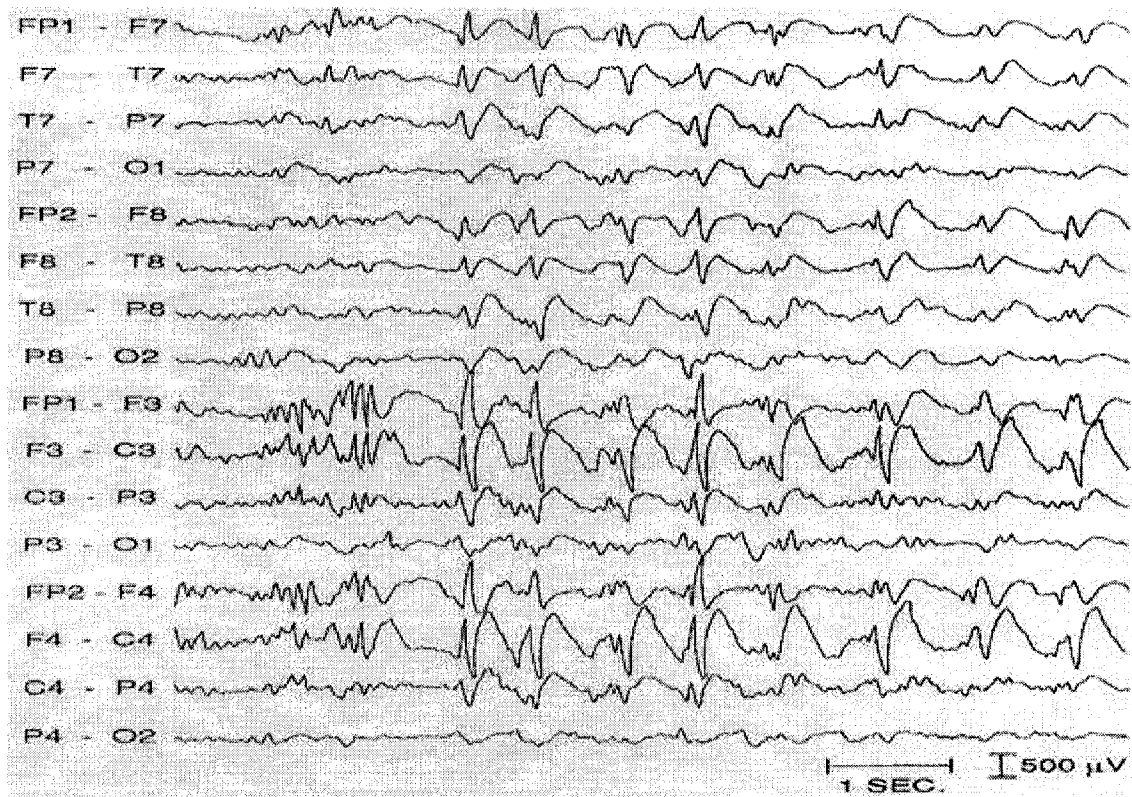


Figure 83 Spike and slow wave form of seizure signals.

Seizures are generally classified into primary generalized seizures and focal seizures. Primary generalized seizures begin with a widespread electrical discharge that involves both sides of the brain at once. Focal seizures begin with an electrical discharge in one limited area of the brain. Some are related to head injury, brain infection, stroke, or tumor, but in most cases the cause is unknown. EEG signals with primary generalized seizures are shown in Figure 84 and with focal seizures are shown in Figure 85. In primary generalized seizures the burst activity can be seen in all the channels whereas with focal seizures the activity is seen only in the right anterior temporal region.

Primary general seizures are again divided into...

1. Absence seizures
2. Atypical absence seizures
3. Myoclonic seizures
4. Atonic seizures
5. Tonic seizures
6. Clonic seizures
7. Tonic-clonic seizures

Focal seizures are divided into...

1. Simple focal seizures
2. Complex focal seizures, and

3. Secondly generalized seizures.

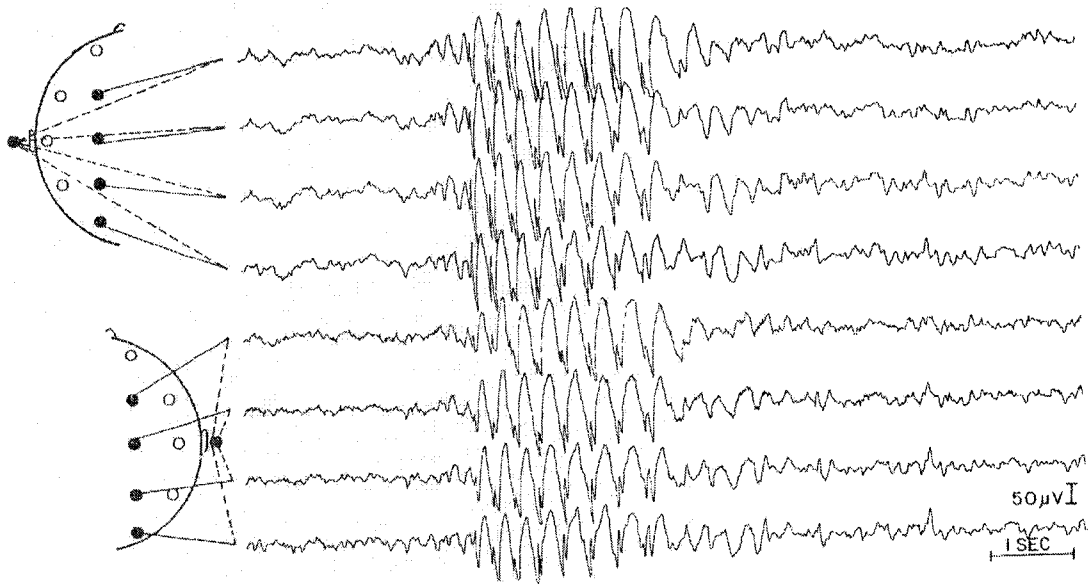


Figure 84 Primary generalized seizures. 3 Hz spike and wave activity can be seen in all the channels.

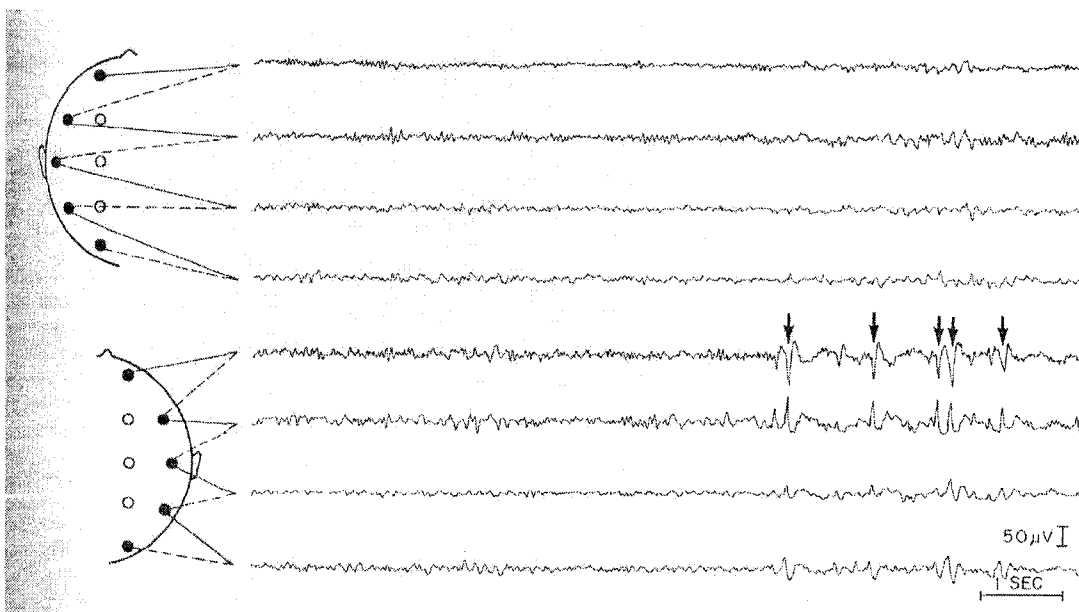


Figure 85 Focal sharp waves in the right anterior temporal lobes. The sharp activity is shown with arrow marks.

APPENDIX E

IACUC Application Form

ANIMAL USE INFORMATION

In order to use vertebrate animals in research or instruction at Louisiana Tech University, you must have the approval of the Institutional Animal Care and Use Committee. Please complete this questionnaire. If the animals are to be housed in the Animal Care Facility, please review your needs with the Facility Director, Dr. James Spaulding, in order to schedule facility use and to prepare a budget. After obtaining the signature of the Facility Director, send the form to Dr. Terry McConathy, Dean of Graduate School & University Research. If you will not be housing animals, send the form directly to Dr. McConathy. She will convene a meeting of the IACUC. Your proposal will be reviewed. You will receive notice of approval or recommendations for changes required for approval.

Project Title: Seizure defibrillator

Proposal Number _____

Project Directors Walter G. Besio, Ph.D. _ Telephone 257-4562 _____

Emails_walterb@latech.edu Performance Period _____4/1/2004 – 5/1/2005_____

Granting Agency _____ Date Due _____

Alterations:

- 1) 50mg/ml ketamine hydrochloride (2.0 ml/kg) will be administered, the animals head will then be shaved and electrodes will be glued on with dental cement.
- 2) The next day (approx. 21 to 24 hours later) scopolamine 1mg/Kg will be administered 30 minutes prior to the pilocarpine to reduce secretions.
- 3) The electrodes will be connected to the amplifiers with extended wires and the animals will be allowed to roam in their cage.
- 4) Pilocarpine 340mg/Kg administered IP will be used to generate seizures.
- 5) EEG will be recorded and at specific intervals after the onset of status epilepticus electrical stimulation will be applied (no stimulation for the control experiments) to determine the effectiveness of the electrical stimulation to control seizures.

- 6) **Stimulation will also be applied at experimental levels in nonseizing unanesthetized rats to test the safety of the stimulation. Histological analysis will be performed on the scalp tissue to test for damage.**
- 7) **Once a penicillin induced seizure is initiated, pancuronium bromide (0.4mg/kg – 2.0mg/kg) will be administered IV to block muscle artefact temporarily.**

Information for the Animal Care Committee

- A. Description of the proposed experiment or laboratory exercise. Attach relevant pages from grant proposal or laboratory exercise. Include literature review and citations:**

The main objective of this protocol is to treat seizure activity in an animal (rat) model by using a “seizure defibrillator” which is being developed by a combined effort between the principal investigators and team for this project. Recent data from our laboratory has shown, in a rat intracisternal penicillin model, that the brain can be “defibrillated” out of a seizure (along with inciting various other responses, such as seizure modulation) – please see attached manuscript detailing this work. Our goal is to develop the technology to sense and deliver electrical current for seizure control, and assess its generalizability in an animal model which can subsequently be extrapolated to human care.

For the majority of human patients, seizures can be controlled by using medications and, in some of the more severe cases, surgical resection of brain tissue must be done to stop the seizures. Clearly, an alternative to this treatment is needed. There has recently been an article (Griesemer et al, Neurology, 1997) in which two children with otherwise unstoppable seizures were controlled using a technique called “electroconvulsive therapy” or ECT. Presently, ECT is mostly used for treatment of depression, and is effective in many cases.

When the heart goes into an abnormal rhythm which is life-threatening, one alternative in certain cases is to “shock the heart back into rhythm.” Similarly, when the brain goes into an unusual electrical rhythm (which is what a seizure really is), it may be able to be “shocked back into rhythm.” The longer a seizure goes on, the more brain damage it can cause. Contrary to popular belief, a quick “defibrillating” ECT shock to the brain very rarely has long-term side effects in the patients who undergo this treatment for depression.

Even though ECT has been tried and used successfully as a “last possible effort” in human children, the method is not completely proven in terms of safety, ideal ECT stimulation parameters, and success rate. For this purpose, an animal study is required; following the appropriate scientific process, if this technique is shown effective

at particular settings in animals, then it can eventually be used in humans for those rare cases in which nothing else seems to help.

B. Statement supporting the need to use animals in the proposed research or laboratory exercise:

Despite a comprehensive literature search, we were not able to find a single animal study (other than our own) that shows the effectiveness of ECT in a comprehensive animal trial. Although ECT has been used in humans, only a handful of patients have been tried, and as noted, several have had positive but not necessarily convincing results. The effectiveness of ECT in controlling seizure activity has been established previously by us in an animal model to a limited, promising extent; specifically, the following questions need to be answered: (1) How frequently can a seizure be both detected and stopped by ECT-type defibrillation?; (2) What is the best setting of defibrillation for stopping seizures?; (3) What are the side effects associated with defibrillation, and how can these be minimized?

The rat is the most appropriate model since it is the smallest animal from which seizure activity can be practically recorded and the brain stimulated, under simultaneous conditions. In addition, a good model of rat epilepsy (using intracisternal penicillin injection) has been developed by our own laboratory, which can be used. ECT has also been performed in rats, and hence this is known to be feasible.

The first few rats will be used to determine effects of stimulation following assessment of ability to sense a seizure. It was noted in our prior study that as a baseline of seizure duration without spontaneous cessation, in the absence of intervention we can determine the effects of direct stimulation. Then the remaining rats will be used to fine-tune this method by varying parameters of frequency, current magnitude, and pulse width.

C. Brief description of the methods used on the animals. Include specific steps taken to minimize pain and suffering.

Aseptic technique will be applied to all animal surgeries listed below.

(1) Animal preparation for experiment, including anesthesia: Animals will be anesthetized using xylazine (5-10 mg/kg) and Ketamine (75-100 mg/kg) combo, intraperitoneally administered. Specifically, a rat will be placed in the supine position on a heated operating table, with body temperature maintained at between 37-39 degrees Celsius. With the aid of a dissecting microscope, a tracheotomy will be performed via a midline skin incision on the neck; the trachea will be intubated. The animal will be mechanically ventilated with a mixture of oxygen and air.

Alteration: urethane 1.25g/Kg administered subcutaneously will be used for anesthesia.

(2) Induction of seizure: Seizure activity will be induced by administering penicillin G (2.5 – 5.0 MU/kg) intracisternally. Approximately 13 minutes thereafter (according to our work, unpublished data, 2003)) seizure activity will result, which will be recorded by electroencephalography (EEG) recording.

Alteration: Pilocarpine 340mg/Kg or Kainic acid 15mg/Kg administered IP will be used to generate seizures. Scopolamine 1mg/Kg is used to reduce secretions.

(3) EEG recording: A modified EEG recording apparatus which is the basis of our work, capable of recording electrical activity from rat brain, will be positioned on the rat's scalp. This will continuously record baseline, spike, and seizure activity.

(4) Control animals: Each animal will serve as its own control, with varying times until intervention: these animals will all receive intracisternal penicillin, and the seizure duration in each will be monitored. By determining the average duration of individual seizures, "baseline seizure duration" will be established, which will be useful in determining whether seizure duration was shortened using ECT (as will be performed in the non-control, or ECT-administered group).

Alteration: For a control, stimulation will be applied at safe levels in unanesthetized rats to test the safety of the stimulation.

(5) Electroconvulsive therapy (ECT) administration: ECT will be induced via electrodes placed in bilateral external auditory mean; specific settings will be 50 mA, 0.5 second, 50 Hz (as described by Madsen et al, Biol Psychiatry 47:1041-1049, 2000). These settings will be varied (e.g. range from 10-70 mA, 0.25-1.0 seconds, 10-500 Hz,) to determine whether one setting has better capability of stopping a seizure versus another. The stimulation will be limited well below the 300mJ level that is considered safe.

(6) Post-procedure care: Animals will be monitored for post-operative neurological status (to ensure that ECT did not cause them to lose movement), ability to feed, and whether they become excessively somnolent for a long period of time. While some somnolence in the post-ictal state will be expected, it is important to determine that ECT did not cause irreversible brain damage

resulting in obvious behavioral manifestations. The tracheotomy hole will hence be closed by a suture, and the animal will be gradually and comfortably awakened as best possible, to resume activity as tolerated. The tracheotomy wounds will be inspected closely until healed (approximately 1 week). In general, the rats do leave the incision site alone and do not aggravate it. Analgesia (Nalbuphine (0.1-0.5mg/kg, s.c.) is administered daily for relief of pain and inflammation, for a period of three days following surgery; as rats return to normal function, euthanasia will be administered.

- D. Does the research require surgery? yes no**
If yes, what anesthetic will be used, in what dosage? If this is not the anesthetic used normally, justify its use.

Animals will be anesthetized using xylazine (5-10 mg/kg) and Ketamine (75-100 mg/kg) combo, intraperitoneally administered. This is the anesthetic used normally.

- E. Will animals be killed at the conclusion of the research? yes no**

If yes, describe the method of euthanasia to be used?

As mentioned, rats will be allowed to awaken from their procedure to facilitate assessment of ECT-related post-procedure effects upon normal functions (such as walking, feeding, and level of sustained somnolence). Time to return of normal function will be recorded; thereafter, Animals will be euthanized according to our IRB protocol injecting potassium chloride intracardially. According to the Panel on Euthanasia of the American Veterinary Medical Association, use of a supersaturated solution of potassium chloride injected intravenously or intracardially in an animal under general anesthesia is an acceptable method to produce cardiac arrest and death.

If no, what will be done with the animals?

- F. Are pathogens or hazardous substances associated with this research?**
 yes no

If yes, explain precautions to be taken to prevent spreading to other animals and personnel.

If no university animal care facilities are required, skip to section IV. If animals are to be housed at Louisiana Tech, you must meet with the Animal Facility Director, Dr. James Spaulding (318-257-4573), to complete sections II and III.

We will house the rats at CyBERS on the 3rd floor.

Animals and Facilities Required:

- A. Species and strain required:** Sprague-Dawley
- B. Commercial supplier:** _____
- C. Number of animals required and length of time in facility:**
1. **Initial number ; Age/Size: Initial** Adult, >250 g.; **Maximum:** _____
 2. **Type of housing required:** _____
 3. **Maximum number of animals in the facility at any time:** _____
 4. **Date of initiation is** _____; **Date of termination is** _____

PLEASE NOTE! If the above dates change, please notify the Facility Director. Every effort will be made to schedule your changes. The sooner you request a schedule modification, the more likely it can be accommodated.

- D. Date of Grant Notification or date when funds will be committed:** after
04/2004

- E. Special requirements: If any of the following apply, please explain in the space provided.** None

1. **Veterinary care**
2. **Work or storage space**
3. **Surgical space**
4. **Access to the facility other than weekdays 8am-5pm.**
5. **Do you want the facility personnel to perform any procedure other than feeding, watering, and cleaning the cages of your animals? If so, please describe the procedure in detail and estimate the number of hours per day required. You may attach an additional sheet.**

Costs: To complete this section you must meet with the Animal Facility Director
(318-257-4573)

A. Total number of animals to be housed 60

B. Number of days each animal will be housed _____

C. Number of Animal Days (A X B) _____

D. Cost for 1 animal/day \$ _____ X animal days
\$ _____

E. List Special Services Requested of facility personnel: None

Cost/hour _____ X Hours needed _____ = _____

F. Cost of Animals (if supplied by Tech, see cost sheet)

Species, Sex, and Age of Animals

Cost per animal (see cost sheet) _____ X number needed _____ = _____

G. Special supplies (list with price) None

Total cost of special supplies = 0

H. Special equipment needed (list) None

Total cost of special equipment = 0

I. Total to be paid Animal Facilities Account = \$

Enter the above costs in the appropriate section of your grant proposal or indicate the source of your funds.

IV. Information on personnel working directly with the animals.

	Name	Where trained	Tetanus
	Immunization Date		
1.	Mesut Sahin, Ph.D.	Case Western Reserve	Current
2.	Walter G. Besio, Ph.D.	LA Tech University	Current (within last 2 yrs)
3.	Ravish V. Patwardhan, M.D.	LSUHSC-Shreveport	Current (within last 2 years)
4.	Kanthaiah Koka	LA Tech University	Current (within last 2 yrs.
5.			

Do you require any Special Immunizations needed for this project? ____yes
 no
 If yes, please list:

If you or your personnel have not received training, you may need to make arrangements to complete the program before beginning the project.

Principal Investigators: Walter G. Besio, PhD

Print or type

Signature

Signature

Signature

3/29/2004

Date

Facilities Director: _____

(James G. Spaulding)

 Date

IACUC Committee Chairman: _____

 Date

 V. Per Diem Rates for Animals Housed in the Animal Facilities at
 Louisiana Tech University

Animal	Code	Housing	Daily Rate
Rat	RW	Wire Bottom Cages	\$0.20 ea
	RWB	Wire with Bedding	0.25 ea
	RS	Shoebox with Bedding	0.20 ea
	RSH	Special Handling	0.30 ea min
Mouse	MS	1/shoebox w/bedding	0.15 ea
	MB	per Box (2-5 per box)	0.30 ea

Unit cost for animals from University Breeding Colonies

Weanling Rats	WR	\$2.00 ea
250g females	FR250	10.00 ea
250g male	MR250	8.00 ea
Weanling Mice	WM	1.00 ea
20g (45 days)	M20	1.50 ea

APPENDIX F

TROUBLE SHOOTING THE 15 channel LEEG AMPLIFIER SYSTEM

1. Working with power supply:

- Make sure the power supply connections are properly connected to the respective $+V_{CC}$ and $-V_{CC}$.
- If the supply IC heats up, there may be wrong connection between $+V_{CC}$ and $-V_{CC}$ or there may be a short circuit between any of the V_{CC} supplies to the Ground.
- Remove the supply as soon as the supply IC's heat up.

2. Checking the each channel of amplifier:

- ECG is the first channel. The inputs are along with the reference. Make sure they are properly connected according to the circuit diagram. If there is any misconnection of ECG input to the reference then there will be lot of ECG in all the LEEG channels.
- After ECG channel, each part of channels are from a tri-polar electrode. They are Outer ring to Disc and Middle ring to Disc.
- Connect very low voltage source (less than 100 μ V) to the channel which needs to be checked. Connect one of the inputs which is going to Disc also to the reference. The ECG generator can be used to check the amplifiers.
- Check the output voltage at each stage, i) After differential amplifier (Gain 5), ii) High pass filter (Gain 2), iii) Third stage low pass filter (Gain 500), and iv) Fourth stage low pass filter (Gain 10).
- If there is any problem at any stage of the amplifier, first make sure the supply to that stage is proper then check the supplies again.
- If output is only one sided, then there may be problem with any one side of the supply.

3. Problems while recording LEEG:

- If there is lots of cross talk, then make sure i) inputs to that channel are connected. ii) electrodes are properly placed on the head. iii) skin-to-electrode impedance is less than 10K. iv) try to decrease the voltage of switch reference or any other channels which are connected directly to the data acquisition system.

REFERENCES

1. R. Srinivasan, "Methods to Improve the Spatial Resolution of EEG," *Journal of Bioelectromagnetism*, vol. 1:102-111, 1999.
2. B. He, J. Lian, and G. Li; "High-resolution EEG: a new realistic geometry spline Laplacian estimation technique;" *Clinical Neurophysiology*, vol. 112: 845-852, 2001.
3. B. He, "Brain Electrical Source Imaging: Scalp Laplacian Mapping and Cortical Imaging," *Critical Reviews in Biomedical Engineering*, vol. 27:149-188, 1999.
4. B. Hjorth, "An On-Line Transformation of EEG Scalp Potentials into Orthogonal Source Derivations," *Electroencephalography and Clinical Neurophysiology*, vol. 39:526-530, 1975.
5. F. Perrin, O. Bertrand, and J. Pernier, "Scalp Current Density Mapping: Value and Estimation from Potential Data," *IEEE Transaction on Biomedical Engineering*, vol. 34:283-288, 1987.
6. S. K. Law, P. L Nunez, R. S. Wijesinghe, "High resolution EEG using Spline Generated Surface Laplacians on Spherical and Ellipsoidal Surfaces," *IEEE Transaction on Biomedical Engineering*, vol. 40:145-153, 1993.
7. F. Babiloni, C. Babiloni, F. Carducci, L. Fattorini, P. Onorati, and A. Urbano, "Spline Laplacian estimate of EEG potentials over a realistic magnet resonance-constructed scalp surface model," *Electroencephalography and Clinical Neurophysiology*, vol. 98:363-373, 1996.
8. F. Babiloni, C. Babiloni, F. Carducci, L. Fattorini, P. Onorati, and A. Urbano, "Performances of surface Laplacian estimators: a study of simulated and real scalp potential distributions," *Brain Topography*, vol. 8:35-45, 1995.
9. B. He and R. Cohen, "Body surface Laplacian electrocardiographic mapping-A review," *Critical Reviews in Biomedical Engineering*, vol. 23(5-6):475-510, 1995.
10. D. Geselowitz and J. Ferrara, "Is Accurate Recording of the ECG Surface Laplacian Feasible?" *IEEE Transaction on Biomedical Engineering*, vol. 46(4):377-381,1999.

11. C. E. Shannon "A mathematical theory of communication," *Bell System Technology Journal.*, vol. 27:379-423 and 623-656, 1948.
12. M. N. Shadlen E. Zohary and W. T. Newsome, "Correlated neuronal discharge rate and its implications for psychophysical performance," *Nature*, vol 370:140–143, 1994.
13. A. Date, "An information theoretic analysis of 256-channel EEG recordings: mutual information and measurement selection problem," *International Conference on Independent Component Analysis and Blind Signal Separation (ICA2001)*, 185-188, 2001.
14. L. Bradshaw and J. Wikswo, "Spatial Filter Approach for Evaluation of the Surface Laplacian of the Electroencephalogram and Magneto encephalogram," *Annals of Biomedical Engineering*, vol. 29:202-213, 2001.
15. W. G. Besio and P. Tarjan, "Atrial Activation Pattern from Surface Laplacian Electrocardiograms of Humans," *International Journal of Bioelectromagnetism*, vol. 4:95-96, 2002.
16. W. G. Besio and P. Tarjan, "Filtering of Surface Laplacian Electrocardiograms From Humans to Produce Atrial Activation Patterns," *Proceedings of 24th Annual International Conference of the IEEE EMBS and Fall Meeting of the BMES 2002*.
17. W. G. Besio, C. Lu and P. Tarjan, "A Feasibility Study for Body Surface Cardiac Propagation Maps of Humans from Laplacian Moments of Activation," *Electromagnetics*, vol. 21:621-632, 2001.
18. W. G. Besio, "A Study of Laplacian Surface Maps from Moments of Activation to Detect Cardiovascular Disease," Ph.D. Dissertation, University of Miami, 2001.
19. D. Farino, and C. Cescon, "Concentric-Ring Electrode systems for Noninvasive detection of single motor unit activity," *IEEE Transaction on Biomedical Engineering*, vol. 48(11):1326-1334, 2001.
20. L. Lapidus, and G. F. Pinder. "Numerical Solution of Partial Differential Equations in Science and Engineering," New York: John Wiley & Sons, Inc., 1st ed., 371-372, 1982.
21. W. F. Ames. "Numerical Methods for Partial Differential Equations," *New York: Barnes & Noble, Inc.*, 15-19, 1969.
22. G. Huiskamp, "Difference formulas for the surface Laplacian on a triangulated surface," *Journal of Computational Physics*, vol. 95(2):477-496, 1991.

23. R. Aakula, "Theoretical Background and Design of Tri-polar Concentric ring Active Sensor" Masters Thesis, Louisiana Tech University, 2004.
24. W. G. Besio, R. Aakula, and W. Dai, "Comparison of Bipolar Vs Tri-polar Concentric Ring Electrode Laplacian Estimates," *Proceedings of 26th Annual International Conference of the IEEE EMBC*, vol. 3:2255-2258, 2004.
25. A. Van Oosterom, and J. Strackee, "Computing the Lead Field of Electrodes with Axial Symmetry," *Medical & Biological Engineering & Computing*, vol. 21:473-481, 1983.
26. M. Kauffer "Multi Ring Sensing Electrodes for Arrhythmia Detection and Classification", Masters Thesis, University of Miami, 1992.
27. J. C. Shaw, "Intention as a Component of the Alpha Rhythm Response to Mental Activity," *International Journal of Psychophysiology*, vol. 24(1-2):7-23, 1996.
28. C. Gerloff, , C. Toro, N. Uenishi, L.G. Cohen, L. Leocani, and M. Hallett. "Steady-state movement-related cortical potentials: a new approach to assessing cortical activity associated with fast repetitive finger movements," *Electroencephalography and Clinical Neurophysiology*, vol. 102:106-113, 1997.
29. B. Kopp, A. Kunkel, G. Muler, W. Muhl nickel and H. Flor, "Steady-State Movement-Related Potentials Evoked by Fast Repetitive Moments," *Brain Topography*, vol. 13:21-28, 2000.
30. F. B. Mark, W. C. Barry, A. P. Michael, "Neuroscience: Exploring the Brain." *Lippincott Williams & Wilkins*. 2nd ed., 208, 2001.
31. C. D. Klug, J. Silny, and G. Rau, "Improvement of Spatial Resolution in Surface EMG: A Theoretical and Experimental Comparison of Different Spatial Filters," *IEEE Transaction on Biomedical Engineering*, vol. 44(7):567-74. 1997.
32. A. Kraskov, S. Harald, and G. Peter. "Estimating mutual information," *Physical Review E*, vol. 28:1-16, 2004.
33. J. R. Hughes, "EEG in clinical practice" *Butterworth-Heinemann publications*, 2nd ed., 1994.
34. R. V. Patwardhan, J. W. Calvert, G. Kusaka, I. Kusaka, "Development of a novel, minimally invasive, quick-onset animal model of epilepsy," *Congress of Neurological Surgeons (CNS) Annual Meeting*, Denver, Colorado, 2003.
35. L. A. Baez, N. K. Eskridge, and R. Schein, "Postnatal development of dopaminergic and cholinergic catalepsy in the rat," *European Journal of Pharmacology*, vol. 36:155-162, 1976.

36. N. Y. Walton, D. M. Treiman “Response of Status epilepticus induced by Lithium and Pilocarpine to Treatment with Diazepam”, *Experimental Neurology*, vol. 101(2):267-75, 1998.
37. D. M. Treiman, N. Y. Walton, C.L. Wickboldt, and C. M. DeGiorgio, “Predictable sequence of EEG changes during generalized convulsive status epilepticus in man and three experimental models of status epilepticus in the rat.,” *Neurology*, vol. 37:244-245, 1987.
38. <http://en.wikipedia.org/wiki/ANOVA>
39. <http://mathworld.wolfram.com/BonferroniCorrection.html>
40. C. E. Bonferroni, "Teoria statistica delle classi e calcolo delle probabilità." *Pubblcazioni del R Istituto Superiore di Scienze Economiche e Commerciali di Firenze*. Vol. 8:3-62, 1936.
41. W. Besio, K. Koka, and R. Patwardhan, “Computer Simulation and Tank Experimental Verification of Concentric Ring Electrode,” *Proceedings of 26th Annual International Conference of the IEEE EMBC*, vol. 3:2243-2246, 2004.
42. H. P. Goodkin, X. Liu, G. L. Holmes, “Diazepam Terminates Brief but Not Prolonged Seizures in Young Naïve Rats,” *Epilepsia*, vol. 44(8):1109-1112, 2003.
43. W. G. Besio, K. Koka, R. Aakula, and W. Dai, “Tri-polar concentric ring electrode development for Laplacian Electroencephalography,” *IEEE Transaction on Biomedical Engineering*, in press 2005.
44. W. G. Besio, R. Aakula, K. Koka, and W. “Dai. Development of a tri-polar concentric ring electrode for acquiring accurate Laplacian body surface potentials.” *Annals of Biomedical Engineering*, in press 2005.
45. K. Koka and W. G. Besio, “Improvement of Spatial Selectivity and Decrease of Mutual Information of Tri-polar Concentric Ring Electrodes,” In Review *Journal of Neuroscience Methods*, 2006.
46. W. G. Besio, K. Koka, R. Patwardhan, M. Sahin “Seizure Frequency Modulation Using Non-invasive Transcutaneous Electrical Stimulation.” *22nd Annual HSEMB Houston Conference*, 26, 2005.
47. W. G. Besio, K. Koka, F. Zhu, and V. Alagiriswamy “Feasibility of Transcutaneous Electrical stimulation for Controlling Pilocarpine Generated status Epileptic Seizures in Rats” *23rd Annual HSEMB Houston Conference*, 169, 2006.